THE RESPONSE OF VERTICAL PILES TO LATERAL LOADING AND MOMENT

This thesis is submitted in accordance with the requirements of the University of Liverpool for the degree of Doctor of Philisophy

by

James N. Fulthorpe, B.Sc. (Hons.)

September 1986

SUMMARY

This thesis presents a study of laterally loaded pile design and theory by centrifugal modelling, existing theoretical approaches and the finite element method.

Centrifugal modelling has been used to determine some of the factors which influence pile behaviour and by back-analysis of the experimental results to assess various theoretical solutions and a finite element method.

Chapter One contains an introduction to the work.

The finite element approach is outlined in Chapter Two and includes the background, theory and computer program formulation to the approach, together with an assessment of its accuracy and limitations, and a comparison with the experimental results.

The experimental procedure and model to prototype parameters are outlined in Chapter Three, together with the historical background and theory of centrifugal modelling.

Chapter Four contains an assessment of the least-squares polynomial and cubic spline methods of analysing the experimental results.

The experimental results have been used in Chapter Five, to determine the factors influencing pile behaviour, in particular the pile deflection at the soil surface and the position and magnitude of the maximum bending moment.

Chapter Six contains the background to, and the theory of, the theoretical approaches used and an assessment of their various merits by back-analysis of the experimental results, and including some finite element results.

Conclusions and suggestions for further work are presented in Chapter Seven.

Appendix A contains a summary of the centrifugal modelling scaling factors for model/prototype conversion. A centrifugal modelling error and its effect in the Liverpool University centrifuge is discussed in Appendix B. Appendix C contains some sample back-analysis calculations of the experimental data to theoretical solutions.

Together with this thesis is a separate document containing listings, data preparation and sample data for the FORTRAN computer program MPAPOLY, Model Pile Analysis by the Polynomial Method and FSP, Fourier Series Pile Finite Element Analysis.

ACKNOWLEDGEMENTS

I would like to thank Dr. G.J.W. King, Senior Lecturer in Civil Engineering, for his supervision and guidance throughout the course of the research.

For his help in preparing and testing on the centrifuge I would also like to thank Mr. A. Moorehouse, Soils Laboratory Technician and other members of the Department of Civil Engineering.

Finally, many thanks to Mrs. B. Lussey for her efficient typing and to Mrs. Barbara Cotgreave for her help in tracing the diagrams.

CONTENTS

NOTATION

A, B	coefficients relating to lateral and moment loading respectively
a, b	dimensions of element with respect to r and z
B	strain shape function
D	elasticity matrix
d	diameter of pile and breadth of footing
E	Young's modulus
E_i	Initial tangent modulus for soil
E_p	Young's modulus for pile
E_s	Young's modulus for soil
e	eccentricity of load
F_ρ , F_θ	yield-displacement and yield-slope factor
f	nodal element force vector
G	shear modulus
G^*	$G(1 + 3\nu/4)$
H_o	shear force at soil surface
H_u	ultimate lateral resistance of pile
I	Influence factor
I'_ρ, $I'_{\rho m}$	elastic influence factors for displacement related to horizontal load and moment
$I'_{\theta H}$, $I'_{\rho m}$	elastic influence factors for slope related to horizontal load and moment
I_p	second moment of area
K	stiffness matrices, matrix of stiffness coefficients and hyperbolic coefficient
K_h	modulus of horizontal subgrade reaction
K_N	flexibility factor
K_p	coefficient of passive earth pressure
k	modulus of subgrade reaction
k_s, k_m	shear and normal stiffness coefficients

L, l	length of pile
M	bending moment
M_o	bending moment at soil surface
m	rate of increase of shear modulus with depth
m*	$m^*(1 + 3\nu/4)$
N	friction element equivalent to strain shape function
N_h	rate of increase of Young's modulus of soil with depth
N_i	shape function
n	number of harmonics and hyperbolic exponent
n_h	rate of increase of K_h with depth
P	loads
p	pressure, soil resistance and load intensity
p_a	atmospheric pressure
R	radius
R_d	relative displacement
r	radial direction
r_o	radius of pile
r_c, z_c	co-ordinates of the centre of an element
r',z'	non-dimensional local co-ordinates
T	characteristic length
u	radial displacement
V	shear force
v	vertical displacement
w	circumferential displacement
y	displacement
y_o	deflection at soil surface
Z	depth coefficient = z/T
z	vertical direction and depth
γ	bulk density

$\gamma_{rz,r\theta,z\theta}$	shear strain in relevant direction
δ	nodal displacement
ε	strain vector
$\varepsilon_{r,z,\theta}$	direct strain in relevant direction
ν	Poisson's ratio
θ	circumferential direction and slope
θ_o	slope at soil surface
ϕ	angle of internal friction (effective stress)
σ	stress vector
$\sigma_{r,z,\theta}$	direct stress in relevant direction
σ_3	minor principal stress
$\tau_{rz,r\theta,z\theta}$	shear stress in relevant direction

CHAPTER ONE
INTRODUCTION

Initially piles were used for overcoming the difficulties of supporting structures in soft soils. However more frequently they have been expected to resist lateral loads and moments for example in harbour and offshore structures, pile supported earth-retaining structures, transmission-towers and structures built in earthquake areas.

In the past design for lateral loading has been based upon empirical information from full-scale lateral load tests. In recent years techniques have been developed to predict pile deformation which include centrifugal modelling, theoretical methods and, most recently, finite element analysis.

The full-scale testing of laterally loaded piles would provide some of the most useful information relating to pile-soil behaviour. However, the cost of such tests is so high as to prevent such testing in sufficient numbers. It is not easy to apply information obtained from one such test to other sites with different loading and soil conditions. It is preferable to carry out a series of model experiments in a centrifuge to determine which parameters affect the pile behaviour.

Centrifugal modelling is not only a low cost technique, but also provides the required amount of control over the soil condition, pile types, sides and loading conditions. The technique allows small scale modelling of a geotechnical structure simulating the same stresses which would occur in the full-scale prototype.

In the theoretical methods of predicting pile deformations which have been developed, two approaches have generally been employed, the subgrade-reaction and the elastic continuum methods.

The subgrade-reaction approach assumes that the pile is supported upon a series of springs, known as the Winkler spring medium. This method ignores the continuum nature of the soil and is simply a relationship between pile reaction and displacement at a point.

The elastic continuum approach relies on separate numerical methods for analysing the pile and the continuum and requires matching of deflection and pressure along the pile/continuum interface using an iterative process. High accuracy is therefore difficult to achieve.

The most recent method for analyses of pile-soil behaviour is the finite element method. This technique is only possible because of the availability of large computers. The method as applied in this thesis considers axisymmetric geometry and material properties subjected to non-axisymmetric loading. Displacement and applied loads are represented by Fourier series.

The main objectives of the research programme described in this thesis were:-

1) to model vertical piles in the centrifuge with various length, diameter, flexural rigidities and load combinations;

2) to determine which of these factors influence the pile displacements and maximum bending moment; and

3) to assess the relative merits of some existing theoretical approaches, and of a finite element approach, by back analysis of the experimental results.

The experimental work was performed using the Liverpool University Geotechnical Centrifuge and the analysis of the experimental data and the finite element modelling were also carried out at Liverpool University using the computer facilities available.

CHAPTER TWO

ANALYSIS BY THE FINITE ELEMENTS METHOD

2.1 INTRODUCTION

The finite element method began as a numerical method of stress analysis. It is the most powerful numerical technique available at present and has been well documented by Zienkiewicz[36], Cook[7], Desai and Abel[12] and many others. Zienkiewicz[36] defines it as a general discretization procedure of continuum problems posed by mathematically defined statements. However, a two-dimensional analysis is limited to plane strain and axisymmetric problems and a full three-dimensional analysis is costly and time consuming even with today's most powerful computers.

The problem presented here is of a vertical pile with axisymmetric geometry and material properties but which is subjected to non-axisymmetric loading. This problem can be analysed by a technique which reduces the three-dimensional problem into two-dimensional analysis by expressing the loads and displacements as Fourier series.

This semi-analytical finite element method was first developed by Wilson[34] for linear elastic analysis and also mentioned by Zienkiewicz and Too[37], Belytschko[4] and furthered by Cheung[6] under the name of the finite strip method. Text book accounts can be found in Zienkiewicz[36] and Cook[7]. It has been further developed by Grose[15] for thermal loading, by Stricklin et al[32] to include circumferentially varying material properties and by Winnick and Zienkiewicz[35] for visco-plastic behaviour.

This approach, described in this thesis, concentrates on linear elastic analysis in which properties can vary in the radial and vertical directions but are kept constant in the circumferential direction, for reasons which are discussed later, Section 2.4.

2.2 METHOD OF ANALYSIS

The axisymmetric geometry of the continuous problem is replaced by a system of axisymmetric elements connected in nodal circles and requiring analysis only in the plane (r,z) at $\theta = 0$.

2.2.1 Harmonic Representation

Let us first validate the use of Fourier series. Assume that the displacements of an arbitrary point in a body are,

$$\begin{aligned} u &= \bar{u}\cos n\theta \\ v &= \bar{v}\cos n\theta \\ w &= \bar{w}\sin n\theta \end{aligned} \tag{2.1}$$

where $\bar{u}$, $\bar{v}$ and $\bar{w}$ are functions of r and z only and n is an integer representing the number of harmonics.

The strain-displacement relationships in polar co-ordinates are represented as

$$\begin{Bmatrix} \varepsilon_r \\ \varepsilon_z \\ \varepsilon_\theta \\ \gamma_{rz} \\ \gamma_{r\theta} \\ \gamma_{z\theta} \end{Bmatrix} = \begin{Bmatrix} \dfrac{\partial u}{\partial r} \\ \dfrac{\partial v}{\partial z} \\ \dfrac{1}{r}\dfrac{\partial w}{\partial \theta} + \dfrac{u}{r} \\ \dfrac{\partial u}{\partial z} + \dfrac{\partial v}{\partial r} \\ \dfrac{1}{r}\dfrac{\partial u}{\partial \theta} + \dfrac{\partial w}{\partial r} - \dfrac{w}{r} \\ \dfrac{1}{r}\dfrac{\partial v}{\partial \theta} + \dfrac{\partial w}{\partial z} \end{Bmatrix} \tag{2.2}$$

The stress-strain relationship is

$$\sigma = D.\varepsilon \tag{2.3}$$

where

$$\sigma = \begin{Bmatrix} \sigma_r \\ \sigma_z \\ \sigma_\theta \\ \tau_{rz} \\ \tau_{r\theta} \\ \tau_{z\theta} \end{Bmatrix} \qquad \varepsilon = \begin{Bmatrix} \varepsilon_r \\ \varepsilon_z \\ \varepsilon_\theta \\ \gamma_{rz} \\ \gamma_{r\theta} \\ \gamma_{z\theta} \end{Bmatrix}$$

and

$$D = \frac{E(1-\nu)}{(1+\nu)(1-2\nu)} \begin{bmatrix} 1 & \frac{\nu}{1-\nu} & \frac{\nu}{1-\nu} & 0 & 0 & 0 \\ & 1 & \frac{\nu}{1-\nu} & 0 & 0 & 0 \\ & & 1 & 0 & 0 & 0 \\ & & & \frac{1-2\nu}{2(1-\nu)} & 0 & 0 \\ & & & & \frac{1-2\nu}{2(1-\nu)} & 0 \\ & & & & & \frac{1-2\nu}{2(1-\nu)} \end{bmatrix} \qquad (2.3a)$$

Substituting the displacements of Eq. (2.1) into the strain-displacement relationship of Eq. (2.2) and combining with Eq. (2.3) gives

$$\begin{aligned} \sigma_r &= \bar{\sigma}_r \cos n\theta & \tau_{rz} &= \bar{\tau}_{rz} \cos n\theta \\ \sigma_z &= \bar{\sigma}_z \cos n\theta & \tau_{r\theta} &= \bar{\tau}_{r\theta} \cos n\theta \\ \sigma_\theta &= \bar{\sigma}_\theta \sin n\theta & \tau_{z\theta} &= \bar{\tau}_{z\theta} \sin n\theta \end{aligned} \qquad (2.4)$$

In which the barred quantities are functions of E,ν,r,z and n but not θ, for example

$$\bar{\sigma}_r = \frac{E(1-\nu)}{(1+\nu)(1-2\nu)} \cdot \frac{\partial \bar{u}}{\partial r} + \frac{\nu}{(1-\nu)} \cdot \left(\frac{\partial \bar{v}}{\partial r} + \frac{n\bar{w}}{r} + \frac{\bar{u}}{r} \right) \qquad (2.4a)$$

The equations of equilibrium in polar co-ordinates are

$$\frac{\partial \sigma_r}{\partial r} + \frac{1}{r} \frac{\partial \tau_{r\theta}}{\partial \theta} + \frac{\partial \tau_{rz}}{\partial z} \quad \frac{\sigma_r - \sigma_\theta}{r} = 0$$

$$\frac{\partial \sigma_z}{\partial z} + \frac{\partial \tau_{rz}}{\partial r} + \frac{1}{r} \frac{\partial \tau_{z\theta}}{\partial \theta} + \frac{\tau_{r\theta}}{r} = 0 \qquad (2.5)$$

$$\frac{1}{r} \frac{\partial \sigma_\theta}{\partial \theta} + \frac{\partial \tau_{r\theta}}{\partial r} + \frac{\partial \tau_{z\theta}}{\partial z} + \frac{2\tau_{r\theta}}{r} = 0$$

as in this problem there are no body forces.

Substituting Eq. (2.4) into Eq. (2.5) yields

$$(- - -) \cos n\theta = 0, \quad (- - -) \cos n\theta = 0, \quad (- - -) \sin n\theta = 0 \qquad (2.6)$$

where $(- - -)$ contain r, z and n but not θ .

These equations must be satisfied for all values of θ and hence the expressions $(- - -)$ must vanish producing three partial differential equations with r and z independent and $\bar{u}$, $\bar{v}$ and $\bar{w}$ dependent variables, therefore reducing the problem to two dimensions.

For the problem considered here the loads and displacements may be expressed as Fourier series.

$$u = \sum_{n=1}^{\infty} \bar{u} \cos n\theta \qquad P_r = \sum_{n=1}^{\infty} \bar{P}_r \cos n\theta$$

$$v = \sum_{n=1}^{\infty} \bar{v} \cos n\theta \qquad P_z = \sum_{n=1}^{\infty} \bar{P}_z \cos n\theta \qquad (2.7)$$

$$w = \sum_{n=1}^{\infty} \bar{w} \sin n\theta \qquad P_w = \sum_{n=1}^{\infty} \bar{P}_\theta \sin n\theta$$

For most practical problems only the first 4 or 5 terms in

the series need be considered. For the problem presented here, as will be discussed in Section 2.4, only the first harmonic n = 1 need be considered for an elastic analysis of a laterally loaded pile.

2.2.2 Finite Element Formulation

Consider the mesh shown in Fig. 2.1. The pile and soil media are represented by 8-node rectangular isoparametric elements, see Fig. 2.2a. The friction elements are represented by a 6-node rectangular isoparametric element, see Fig. 2.2b, similar to that developed by Goodman et al[14] and Desai and Chandrasekaran[12] of which a complete description can be found in Section 2.2.2.3.

2.2.2.1 General Case

Assume the variation of displacement to be represented by

$$u = \sum_{i=1}^{j} \sum_{n=1}^{\infty} N_i \bar{u}_i \cos n\theta$$

$$v = \sum_{i=1}^{j} \sum_{n=1}^{\infty} N_i \bar{v}_i \cos n\theta \qquad (2.8)$$

$$w = \sum_{i=1}^{j} \sum_{n=1}^{\infty} N_i \bar{w}_i \sin n\theta$$

where j is the number of nodes in each element and N_i is the shape function for the ith node in the element and are functions of ξ and η only.

The strain matrix is obtained by substituting Eq. (2.8) into Eq. (2.2) yielding

$$\varepsilon = B\,\delta \qquad (2.9)$$

in which

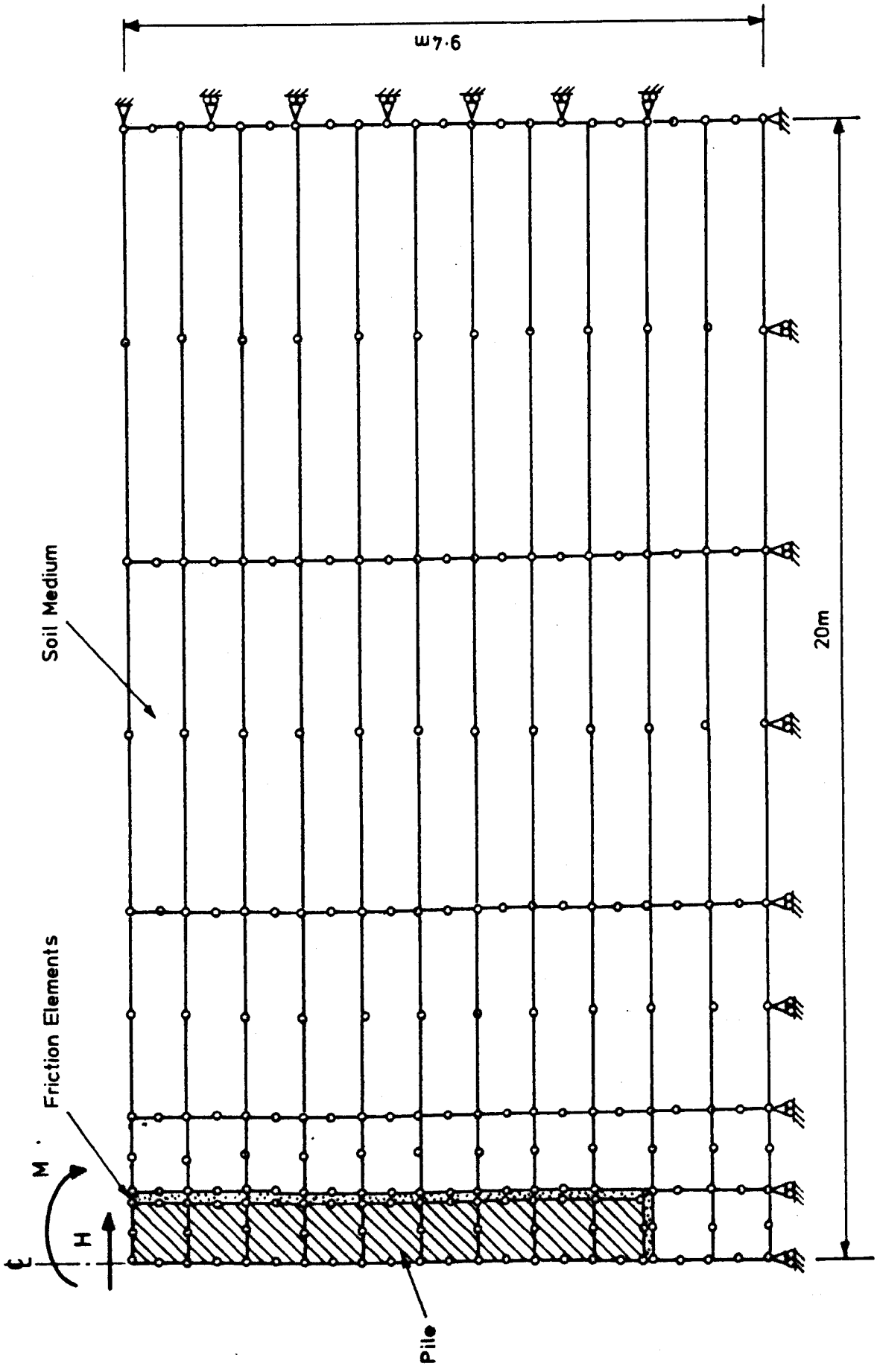

FIG. 2.1. AN EXAMPLE OF THE TYPE OF FINITE ELEMENT MESH USED

$$\delta = \begin{Bmatrix} u_1 \\ v_1 \\ w_1 \\ \vdots \\ u_j \\ v_j \\ w_j \end{Bmatrix} \tag{2.10}$$

and B, the strain shape function, for the ith node is

$$B = \begin{bmatrix} \frac{\partial N_i}{\partial r}\cos n\theta & 0 & 0 \\ 0 & \frac{\partial N_i}{\partial z}\cos n\theta & 0 \\ \frac{\partial N_i}{r}\cos n\theta & 0 & \frac{nN_i}{r}\cos n\theta \\ \frac{N_i}{\partial z}\cos n\theta & \frac{\partial N_i}{\partial r}\cos n\theta & 0 \\ \frac{-nN_i}{r}\sin n\theta & 0 & (\frac{\partial N_i}{\partial r} - \frac{N_i}{r})\sin n\theta \\ 0 & \frac{-nN_i}{r}\sin n\theta & \frac{\partial N_i}{\partial z}\sin n\theta \end{bmatrix} \tag{2.11}$$

The stiffness matrix is obtained using the standard procedure, Zienkiewicz[36]

$$K = \int_v B^T D B \, dv \tag{2.12}$$

$$= \int_0^{2\pi} d\theta \int_A B^T D B \, f(r) \, dr\,dz \tag{2.13}$$

where f(r) is a function of r only and comes from the conversion from Cartesian to polar co-ordinates within the integral.

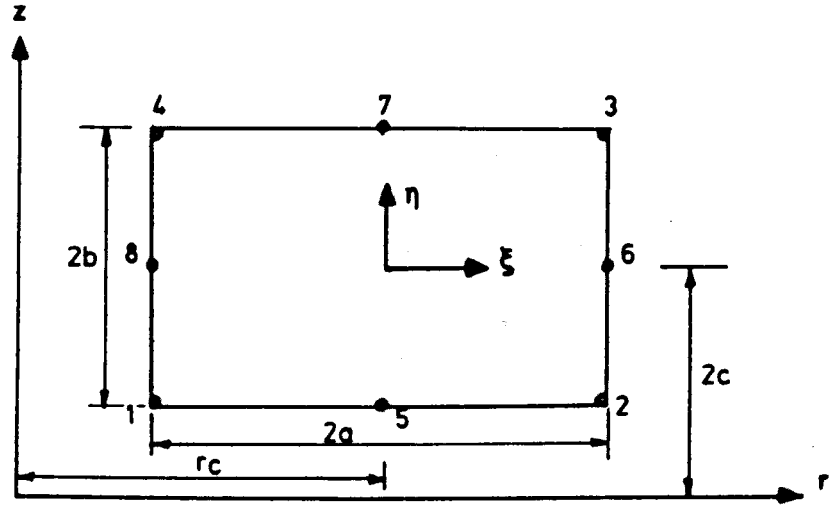

a) Eight Node Isoparametric Element

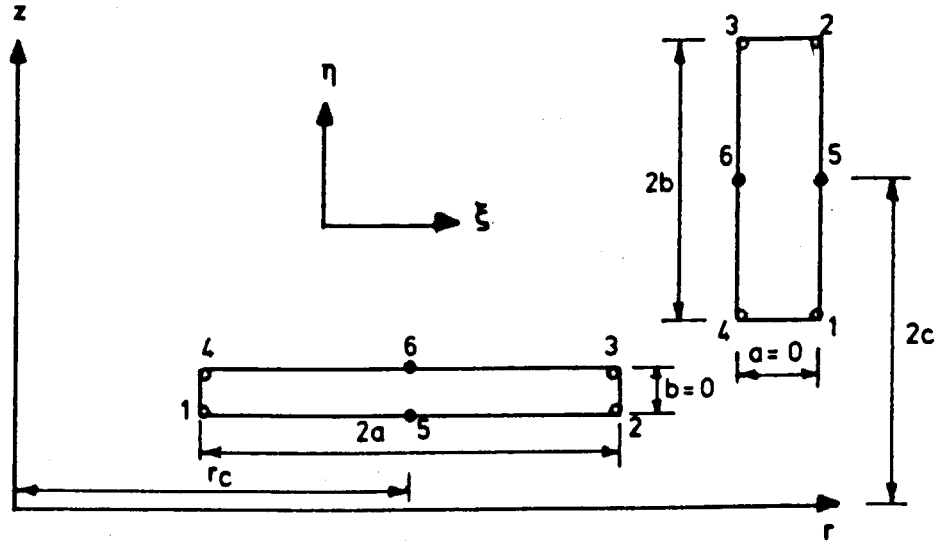

b) Six Node Isoparametric Elements

FIG. 2.2. PILE, SOIL AND FRICTION ELEMENTS

Integrals which appear in Eq. (2.13) include

$$\int_0^{2\pi} \sin m\theta \, \sin n\theta \, d\theta = \begin{cases} \pi \text{ for } m = n \neq 0 \\ 0 \text{ for } m \neq n \text{ and for } m = n = 0 \end{cases}$$

$$\int_0^{2\pi} \cos m\theta \, \cos n\theta \, d\theta = \begin{cases} 2\pi \text{ for } m = n = 0 \\ \pi \text{ for } m = n \neq 0 \\ 0 \text{ for } m = n \end{cases} \qquad (2.14)$$

$$\int_0^{2\pi} \sin m\theta \, \cos n\theta \, d\theta = 0 \text{ for all } m \text{ and } n$$

For the problem presented here $m = n = 1$ hence Eq. (2.13) becomes

$$K = \pi \int_A B^T D B \, f(r) \, dr \, dz \qquad (2.15)$$

The above expression is integrated numerically by Gaussian quadrature, see Cook[7, (pp.103-105)].

The nodal displacements are calculated by solving the system of simultaneous equations

$$K \cdot \delta = f \qquad (2.16)$$

where f is the nodal force vector.

Finally, the stresses are calculated from

$$\sigma = D \varepsilon \qquad (2.17)$$

Since $$\varepsilon = B \delta \qquad (2.18)$$

$$\sigma = DB \delta$$

2.2.2.2 Pile and Soil Media Elements

With reference to Fig. 2.2(a), the shape functions $N_i(\xi,\eta)$ for nodes $i = 1,8$ are

$$N_i = \frac{1}{4}(1 + \xi\xi_i)(1 + \eta\eta_i)(\xi\xi_i + \eta\eta_i - 1) \quad \text{for } i = 1,2,3,4$$

$$N_i = \frac{1}{2}(1 - \xi^2)(1 + \eta\eta_i) \quad \text{for } i = 5,7 \qquad (2.20)$$

$$N_i = \frac{1}{2}(1 + \xi\xi_i)(1 - \eta^2) \quad \text{for } i = 6,8$$

where

$$\xi = \frac{r - r_c}{a}, \qquad \eta = \frac{z - z_c}{b} \qquad (2.21)$$

By following the method outlined in Section 2.2.2.1, it can be shown that the expression for the stiffness matrix becomes

$$k = \pi\, ab \int_{-1}^{+1}\int_{-1}^{+1} B^T D B\, (\xi a + r_c)\, d\xi\, d\eta \qquad (2.22)$$

2.2.2.3 Friction Elements

These are similar to those developed by Goodman et al[14] but instead of 4-nodes they have 6-nodes and are either horizontal or vertical.

Their shape functions and stiffness matrices are developed below.

2.2.2.3.1 Vertical Elements

Referring to Fig. 2.2(b), assume the displacement variation

$$\delta = \alpha_1 + \alpha_2 z + \alpha_3 z^2 \qquad (2.23)$$

Then the displacement functions for each node are

$$\delta_1 = \alpha_1 - \alpha_2 b + \alpha_3 b^2$$

$$\delta_2 = \alpha_1 + \alpha_2 b + \alpha_3 b^2 \qquad (2.24)$$

$$\delta_5 = \alpha_1$$

Solving Eqs. (2.24) yields

$$\begin{bmatrix}\alpha_1\\ \alpha_2\\ \alpha_3\end{bmatrix} = \frac{1}{2b^2}\begin{bmatrix}0 & 0 & 2b^2\\ -b & b & 0\\ 1 & 1 & -2\end{bmatrix} x \begin{bmatrix}\delta_1\\ \delta_2\\ \delta_5\end{bmatrix}$$

and, therefore, δ the displacement of any point is

$$\delta = \frac{1}{2b^2}\begin{bmatrix}1 & z & z^2\end{bmatrix}\begin{bmatrix}0 & 0 & 2b^2\\ -b & b & 0\\ 1 & 1 & -2\end{bmatrix}\begin{bmatrix}\delta_1\\ \delta_2\\ \delta_5\end{bmatrix} \qquad (2.26)$$

$$= \frac{1}{2b^2}\left[\delta_1 z(z-b) + \delta_2 z(z+b) + \delta_5 2(b^2 - z^2)\right] \qquad (2.27)$$

$$= \begin{bmatrix}N_1 & N_2 & N_5\end{bmatrix} x \begin{bmatrix}\delta_1\\ \delta_2\\ \delta_5\end{bmatrix} \qquad (2.28)$$

where N_i for $i = 1,2,5$ are the shape functions for the element, i.e.

$$N_1 = \frac{z(z-b)}{2b^2}, \quad N_2 = \frac{z(z+b)}{2b^2}, \quad N_5 = \frac{(b^2 - z^2)}{b^2} \qquad (2.29)$$

Let $\eta = \dfrac{z - z_c}{b}$ then N_i becomes

$$N_1 = \frac{1}{2}\eta(\eta - 1), \quad N_2 = \frac{1}{2}\eta(\eta + 1), \quad N_5 = (1 - \eta^2) \qquad (2.30)$$

Noting that

$$\delta_i = \begin{Bmatrix}u_i\\ v_i\\ w_i\end{Bmatrix}$$

$$\begin{bmatrix}u\\ v\\ w\end{bmatrix} = \begin{bmatrix}N_1 & 0 & 0 & N_2 & 0 & 0 & N_5 & 0 & 0\\ 0 & N_1 & 0 & 0 & N_2 & 0 & 0 & N_5 & 0\\ 0 & 0 & N_1 & 0 & 0 & N_2 & 0 & & N_5\end{bmatrix}\begin{Bmatrix}u_i\\ v_i\\ w_i\end{Bmatrix} \qquad (2.31)$$

for i = 1,2,5

The relative displacements (right-left) are

$$r = \begin{Bmatrix} r_1 \\ r_z \\ r_\theta \end{Bmatrix} = \begin{Bmatrix} u_r - u_\ell \\ v_r - v_\ell \\ w_r - w_\ell \end{Bmatrix} = N.\delta \qquad (2.32)$$

with

$$\delta = \begin{Bmatrix} u_i \\ v_i \\ w_i \end{Bmatrix}$$

for i = 1 to 6 and

$$N = \begin{bmatrix} N_1 & 0 & 0 & N_2 & 0 & 0 & -N_2 & 0 & 0 & -N_1 & 0 & 0 & N_5 & 0 & 0 & -N_5 & 0 & 0 \\ 0 & N_1 & 0 & 0 & N_2 & 0 & 0 & -N_2 & 0 & 0 & -N_1 & 0 & 0 & N_5 & 0 & 0 & -N_5 & 0 \\ 0 & 0 & N_1 & 0 & 0 & N_2 & 0 & 0 & -N_2 & 0 & 0 & -N_1 & 0 & 0 & N_5 & 0 & 0 & -N_5 \end{bmatrix}$$

Defining the interface stiffness coefficients

$$K = \begin{bmatrix} k_n & 0 & 0 \\ 0 & k_s & 0 \\ 0 & 0 & k_s \end{bmatrix} \qquad (2.33)$$

we have

$$\sigma = k \cdot r \qquad (2.34)$$

in which

$$\sigma = \left[\sigma_r, \ \tau_{rz}, \ \tau_{r\theta} \right] \qquad (2.35)$$

Expressing the displacements as Fourier series

$$\begin{aligned} r_r &= \sum_{i=0}^{\infty} \bar{r}_r \cos n\theta \\ r_z &= \sum_{i=0}^{\infty} \bar{r}_z \cos n\theta \\ r_\theta &= \sum_{i=0}^{\infty} \bar{r}_\theta \sin n\theta \end{aligned} \qquad (2.36)$$

and

$$u_i = \sum_{i=1}^{\infty} \bar{u}_i \cos n\theta$$

$$v_i = \sum_{i=0}^{\infty} \bar{v}_i \cos n\theta \qquad (2.37)$$

$$w_i = \sum_{i=0}^{\infty} \bar{w}_i \sin n\theta$$

Following the usual procedure the element stiffness matrix can be expressed in the two-dimensional r z plane as

$$K = b \int_{-1}^{1} \int_{0}^{2-\pi} \bar{N}^T . K.\bar{N}\, r_r \, d\theta \, d\eta \qquad (2.38)$$

where

$$\bar{N} = \begin{bmatrix} N_1c & 0 & 0 & N_2c & 0 & 0 & -N_2c & 0 & 0 & -N_1c & 0 & 0 & N_5c & 0 & 0 & -N_5c & 0 & 0 \\ 0 & N_1c & 0 & 0 & N_2c & 0 & 0 & -N_2c & 0 & 0 & -N_1c & 0 & 0 & N_5c & 0 & 0 & -N_5c & 0 \\ 0 & 0 & N_1s & 0 & 0 & N_2s & 0 & 0 & -N_2s & 0 & 0 & -N_1s & 0 & 0 & -N_5s & 0 & 0 & -N_5s \end{bmatrix}$$

with

$$c = \cos n\theta \quad , \quad s = \sin n\theta$$

By Eq. (2.14), Eq. (2.38) becomes

$$K = \pi r_c b \int_{-1}^{1} N^T.K.N \, d\eta \qquad (2.39)$$

2.2.2.3.2 Horizontal Elements

The same procedure is followed replacing z,b and η with r, a and ξ yielding shape functions

$$N_1 = \frac{1}{2}\xi(\xi - 1), \quad N_2 = \frac{1}{2}\xi(\xi + 1), \quad N_3 = (1 - \xi^2) \qquad (2.40)$$

Referring to Fig. 2.2(b), the relative displacements (top-bottom)

$$r = \begin{Bmatrix} z_r \\ z_2 \\ z_\theta \end{Bmatrix} = \begin{Bmatrix} u_t - u_b \\ v_t - v_b \\ w_t - w_b \end{Bmatrix} = N\,\delta \qquad (2.41)$$

with

$$\delta = \begin{Bmatrix} u_i \\ v_i \\ w_i \end{Bmatrix}$$

for i = 1 to 6, and

$$N = \begin{bmatrix} -N_1 & 0 & 0 & -N_2 & 0 & 0 & N_2 & 0 & 0 & N_1 & 0 & 0 & N_5 & 0 & 0 & -N_5 & 0 & 0 \\ 0 & -N_1 & 0 & 0 & -N_2 & 0 & 0 & N_2 & 0 & 0 & N_1 & 0 & 0 & N_5 & 0 & 0 & -N_5 & 0 \\ 0 & 0 & -N_1 & 0 & 0 & -N_2 & 0 & 0 & N_2 & 0 & 0 & N_1 & 0 & 0 & N_5 & 0 & 0 & -N_5 \end{bmatrix}$$

The interface stiffness coefficients are now

$$K = \begin{bmatrix} k_s & 0 & 0 \\ 0 & k_n & 0 \\ 0 & 0 & k_s \end{bmatrix} \qquad (2.42)$$

Expressing the displacements as Fourier series and following the usual procedure the element stiffness matrix can be expressed in the two-dimensional r z plane as

$$K = a \int_{-1}^{1} \int_{0}^{2\pi} \overline{N}^{T} . K . \overline{N} (\xi_a + r_c)\, d\theta\, d\xi \qquad (2.43)$$

where

$$\overline{N} = \begin{bmatrix} -N_1^c & 0 & 0 & -N_2^c & 0 & 0 & N_2^c & 0 & 0 & N_1^c & 0 & 0 & -N_5^c & 0 & 0 & N_5^c & 0 & 0 \\ 0 & -N_1^c & 0 & 0 & -N_2^c & 0 & 0 & N_2^c & 0 & 0 & N_1^c & 0 & 0 & -N_5^c & 0 & 0 & N_5^c & 0 \\ 0 & 0 & -N_1^s & 0 & 0 & -N_2^s & 0 & 0 & N_2^s & 0 & 0 & N_1^s & 0 & 0 & -N_5^s & 0 & 0 & -N_5^s \end{bmatrix}$$

with

$$c = \cos n\theta \quad , \quad s = \sin n\theta$$

By Eq. (2.14), Eq. (2.43) becomes

$$K = \pi z_c \, a \int_{-1}^{1} N^T.K.N(\xi_a + r_c) \, d\xi \tag{2.44}$$

2.2.3 Load Vector

As previously mentioned in Eq. (2.7) the loads are expressed as Fourier series

$$\begin{aligned} P_r &= \sum_{i=1}^{\infty} \overline{P}_r \cos n\theta \\ P_z &= \sum_{i=1}^{\infty} \overline{P}_z \cos n\theta \\ P_\theta &= \sum_{i=1}^{\infty} \overline{P}_\theta \sin n\theta \end{aligned} \tag{2.45}$$

2.2.3.1 Horizontal Loading

Consider a uniform load of intensity 'P' applied on the circumference of a pile of radius 'R', as shown in Fig. 2.3(a).

The load acting on the arc $d\theta$ at an angle θ from the centre of the pile is $pRd\theta$. Resolving in the radial and circumferential directions the load components are

$$P_r = pr \cos\theta \, d\theta$$

and (2.46)

$$P_\theta = -pr \sin\theta \, d\theta$$

respectively.

The equivalent nodal force may now be calculated by equating the work done by the nodal force to the work done by the distributed force moving through a distance u_o .

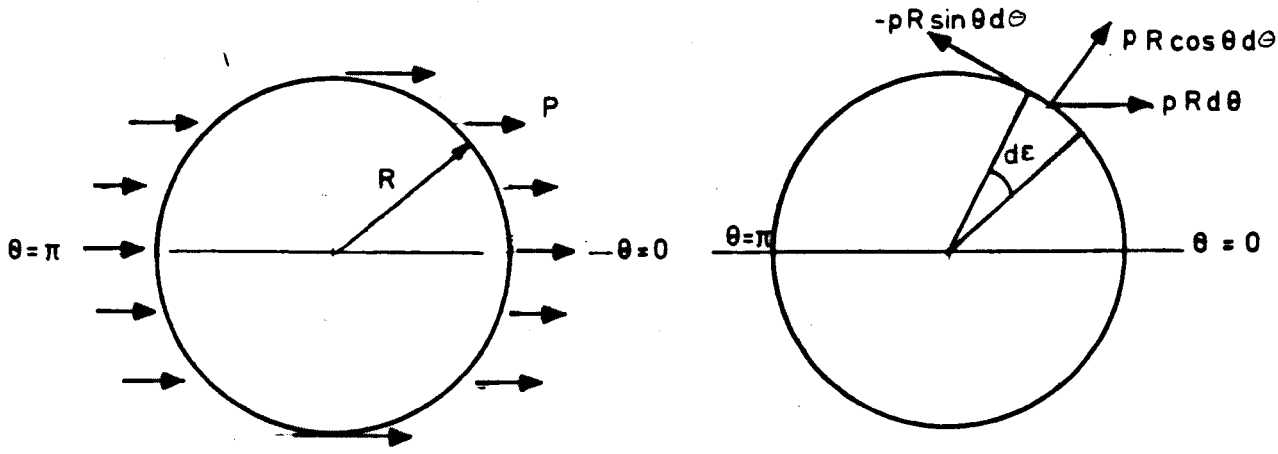

a) Horizontal Loading

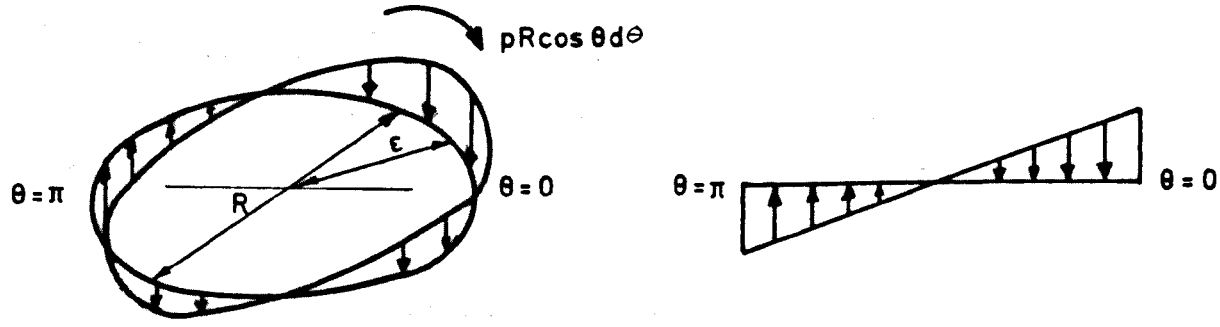

b) Moment Loading

FIG. 2.3. LOADING ARRANGEMENT

$$\frac{1}{2} P_r u_o = \frac{1}{2} \int_0^{2\pi} pR \cos\theta \, d\theta \, u_o \cos\theta$$

$$= \frac{1}{2} \int_0^{2\pi} u_o pR \cos^2\theta \, d\theta \qquad (2.47)$$

Substituting for the uniform load intensity $p = \frac{P}{2\pi R}$

$$\frac{1}{2} P_r u_o = \frac{1}{2} \int_0^{2\pi} \frac{P}{2\pi R} R u_o \cos^2\theta \, d\theta$$

$$\therefore \quad P_r = \frac{P}{2} \qquad (2.48)$$

Similarly, the load component in the circumferential direction can be proved to be

$$P_\theta = -\frac{P}{2} \qquad (2.49)$$

These loads are applied on the circumference of the pile at $\theta = 0$.

2.2.3.2 Moment Load

The moment load is simulated by applying two equal and opposite vertical loads on the circumference of the pile at $\theta = 0$ and $\theta = \pi$.

Consider the pile as shown in Fig. 2.3(b) being acted upon by a vertical load $pR\cos\theta$ on the circumference.

The vertical force acting on an arc length $Rd\theta$ is

$$P_z = pR \cos\theta \, d\theta \qquad (2.50)$$

The moment at the centre of the pile is

$$M = pR \cos\theta \, d\theta \, R \cos\theta$$

$$= pR^2 \cos^2\theta \qquad (2.51)$$

Therefore the total moment acting over the circumference is

$$M = \int_0^{2\pi} pR^2 \cos^2\theta d\theta$$

$$\therefore M = pR^2\pi \qquad (2.52)$$

By equating the work done by the nodal force to the work done by the distributed force moving through a distance ω_o the equivalent nodal force is obtained.

$$\frac{1}{2} P_z \omega_o = \frac{1}{2} \int_0^{2\pi} p \omega_o R \cos^2\theta \, d\theta \qquad (2.53)$$

Substituting for p gives

$$\frac{1}{2} P_z \omega_o = \frac{1}{2} \int_0^{2\pi} \frac{M}{\pi R^2} \omega_o R \cos^2\theta \, d\theta$$

$$P_z = \frac{M}{R} \qquad (2.54)$$

This load is also applied on the circumference of the pile at $\theta = 0$.

2.3 COMPUTER PROGRAM

A computer program was developed to analyse vertical piles subjected to lateral load and moment, using the finite element theory described above. Other features of the program are as follows.

2.3.1 Soil Model

The soil medium was modelled using the power law proposed by Janbu[17],

$$E_i = K p_a \left(\frac{\sigma_3}{p_a}\right)^n \qquad (2.55)$$

By determining K and n experimentally for any particular soil the initial modulus is thus related to the stress level. For elastic analysis this modulus is used to represent the soil for all subsequent loading increments; reasons for this are discussed in Section 2.4.

As stated in Section 2.2.2, the stiffness matrix is calculated by Gaussian quadrature and, therefore, the moduli at the Gauss points have to be assigned. A parabolic variation of the modulus is assumed across the element and from this the moduli at the Gauss points is calculated.

An advantage in using the power law is that it embraces simpler modulus variations with depth which are commonly assumed, i.e. with n = 0 Eq. (2.55) becomes

$$E_i = K\, p_a \tag{2.56}$$

and E_i is then constant with depth, and with n = 1, Eq. (2.55) becomes

$$E_i = K\, \sigma_3 \tag{2.57}$$

and E_i then varies linearly with depth.

2.3.2 Pile-Soil Interface

This is modelled by using the friction elements developed in Section 2.2.2.3 and is achieved by varying k_n and k_s, the normal and shear stiffness coefficients.

2.3.3 Pile Model

Although hollow tubes are used in the centrifugal modelling of piles to scale both size and rigidity correctly, the computer program uses a single element across the radius to model a pile. When analysing a prototype corresponding to an arbitrary model pile this element has the prototype radius but has adjusted modulus to give the correct prototype flexural rigidity.

2.3.4 Computer Output

The displacements of the pile are calculated by solving Eq. (2.16) and the stresses in the pile and soil are then calculated from Eq. (2.19). From the pile displacements the slope at points down the

pile are calculated using finite difference approximations.

The stresses in the pile are used to calculate the bending moments and then the shear forces in the pile are evaluated by finite difference approximations.

2.4 ACCURACY AND LIMITATIONS OF THE METHOD

2.4.1 Accuracy

The accuracy of the Fourier series technique was tested by applying separate horizontal and moment loads at the top of a model cantilever and comparing the results with conventional bending theory.

The cantilever was modelled by fixing the pile at its base, setting Poisson's ratio to a value slightly less than 1.0 and setting the soil modulus very small by letting the power exponent n = 0 and assigning a very small value to the coefficient K.

For horizontal loading only the deflection was found to be o.23% less than expected and for moment loading only 0.1% greater than expected. These results are well within the accuracy of any results expected from experimental data.

Although testing the accuracy by this method is not particularly rigorous, comparison with pile design theories, experimental model tests, or field data cannot be relied upon as their accuracy is undetermined.

2.4.2 Limitations

2.4.2.1 Linear Elastic Analysis

As already mentioned in Section 2.1, the use of Fourier series to express the displacements necessitates the additional conditions of axisymmetric material properties and geometry.

The condition of axisymmetric geometry is acceptable but the

condition of axisymmetric material properties limits the analysis to a linear elastic one with material properties varying in the radial and vertical directions only.

As the pile is loaded the stress levels in the soil change accordingly, i.e. with maximum increase at $\theta = 0$ and maximum decrease at $\theta = \pi$. The modulus of the soil, being dependent upon the stress levels is thus effected by differing amounts around the pile. In a more conventional two- or three-dimensional analysis, soil properties could be allowed to change using non-linear-elastic or plastic models. The condition of constant axisymmetric properties does not allow the use of such models.

Work has been carried out by Winnick and Zienkiewicz[35] and also Barton[3] into visco-plastic behaviour of soils using Fourier series analysis. However, in both studies the elastic modulus was kept constant around the pile and used to calculate plastic strains.

Stricklin et al[32] furthered the method to non-linear elastic analysis. They expressed the modulus and Poisson's ratio for the soil as functions of θ, using another Fourier series. The expression for the stiffness matrix then became a third order triganometric function, involving a combination of sine and cosine terms.

This numerical solution is most complicated and time consuming and, therefore, leads away from the benefit of the simplification provided by the two-dimensional approach.

2.4.2.2 Tension Release

The problem being modelled here is that of piles in sand and it is well known that sands are not capable of holding tensile stresses.

In a conventional finite element analysis, the tension behind the pile could be released by setting the normal stiffness of the

friction element to zero. However, the axisymmetric material properties associated with Fourier series cannot model this type of behaviour.

A possible method of releasing the unrealistic tension is to calculate the tension distribution around the back of the pile and then apply additional load to give the same deflection had there been no tension.

Due to the complexity of the problem and the time involved, this has not been attempted here. This would involve higher order harmonics in the Fourier series and only the first harmonic has been considered.

2.5 APPLICATION OF THE FINITE ELEMENT METHOD

2.5.1 Analysis

The dimensions and properties of the experimental piles are known and, therefore, input directly into the finite element model (Sections 2.3.3 and 2.3.2) assuming a stainless steel pile to be smooth.

The only unknown variables are the subgrade coefficients K and n in Eq. (2.55). The theories of Matlock and Reese[20], Poulos[23] and Randolph[24] assume a linear variation of modulus with depth, i.e. n = 1 and, therefore, Eq. (2.57) has been used in this analysis. As the coefficient, K, is unknown, experimental pile displacements were compared with displacements from the finite element model using a range of values of K. The initial stress at any Gauss point at depth z was evaluated as $\sigma_3 = K_o \gamma z$, with the coefficient of earth pressure at rest $K_o = 0.24$ and specific weight of the soil $\gamma = 16.62$ KNm^{-3}.

The experimental displacements were taken from a typical test on pile No. 1.

2.5.2 Discussion

Figure 2.4 shows displacement against load for the experimental and finite element results for pile No. 1 with embedded length/diameter, $l/d = 11$, and load eccentricity, $e = d$.

The curve represents the experimental data and the straight lines computed with K = 2900, 3500, 3600 and 4000. The corresponding values of parameter N so that $E_s = Nz$ are $N = K(K_o\gamma) = 4\ K$.

It is obviously difficult to obtain a good fit between the linear finite element results and the non-linear experimental results. However, the values of N which yield the experimental displacements at various points are plotted for comparison with Poulos' parameter N_h in Fig. 6.9, (Chapter 6). Figures 2.5 to 2.7 show the results from the finite element analysis, with K = 2900 and with an applied horizontal load and moment of 469 KN and 357 KNm respectively, plotted with the experimental results, with the same applied loads, calculated using a polynomial (Section 4.2) in Figs. 2.5 and 2.7, and in Fig. 2.6 the measured bending moments.

The distributions produced from the finite element analysis are of the expected shape. However, the bending moment distribution, Fig. 2.6, was the only one measured directly from the experiments and these values are higher than that from the finite element analysis. Therefore, from Section 2.3.4 the finite element shear force distribution is doubtful even though it is close to the experimental distribution.

The finite element displacement distribution shows the expected shape but its magnitude cannot be verified because there was no measured displacement down the pile for comparison.

2.5.3 Conclusions

It is possible to select a value of K for a given deflection which represents a rate of increase of soil modulus with depth.

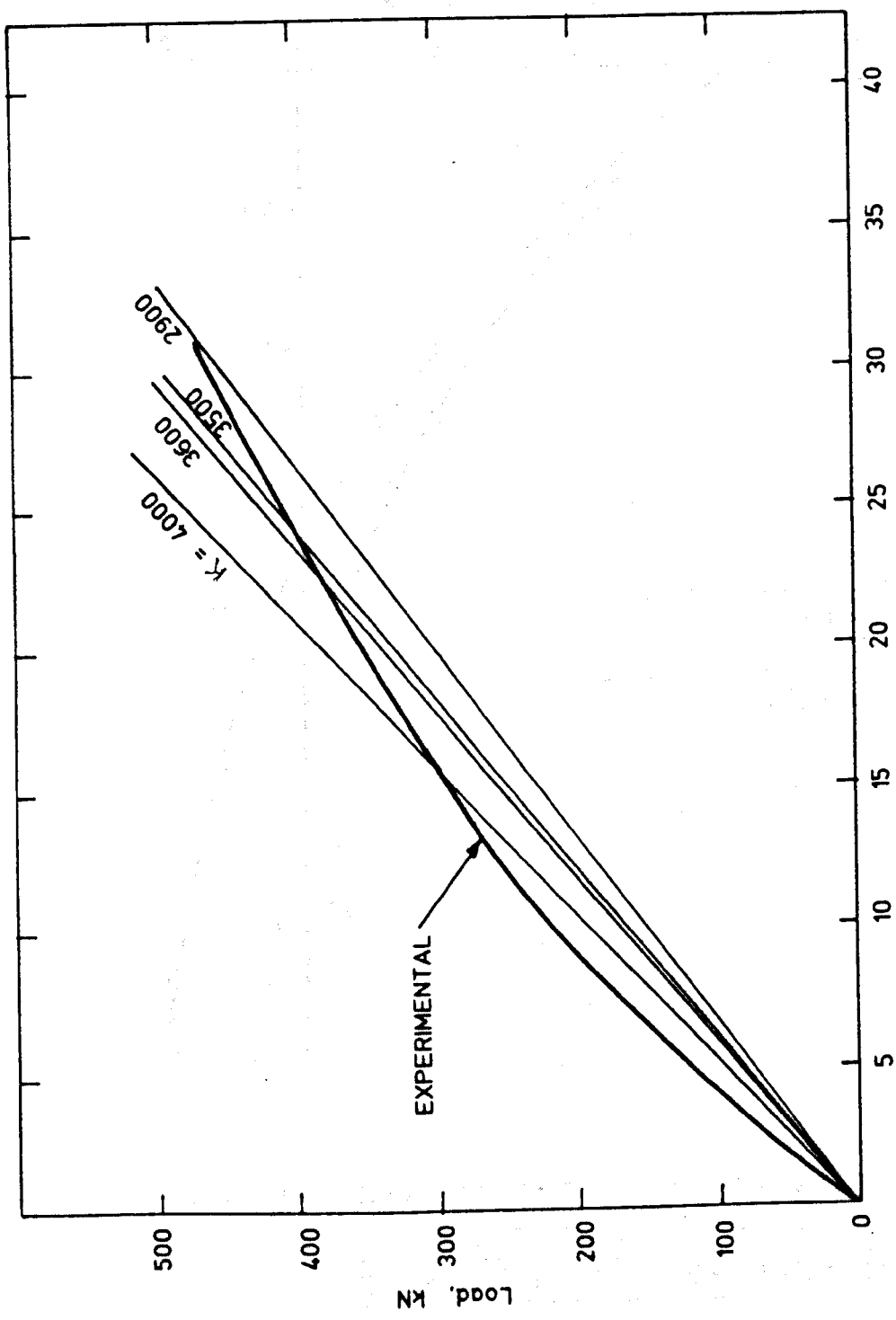

FIG. 2.4. LOAD vs. DISPLACEMENT FOR FINITE ELEMENT AND EXPERIMENTAL RESULTS FOR PILE No. 1 (WITH l/d = 11 and e/d = 1)

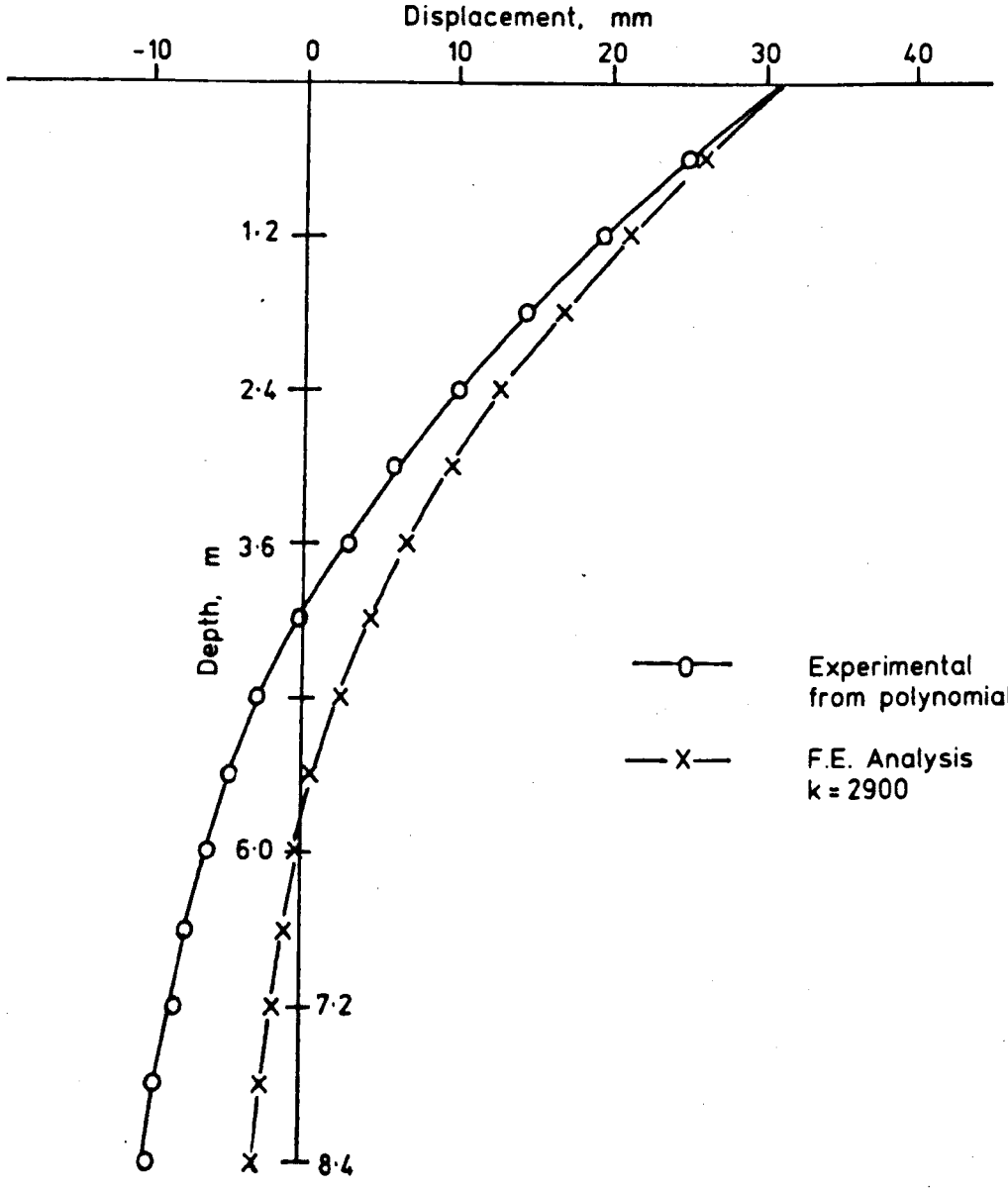

FIG. 2.5. DISPLACEMENT vs. DEPTH FINITE ELEMENT AND EXPERIMENTAL RESULTS PILE No. 1 Experiment No. 1 Load = 469kNm (e = 0·76m)

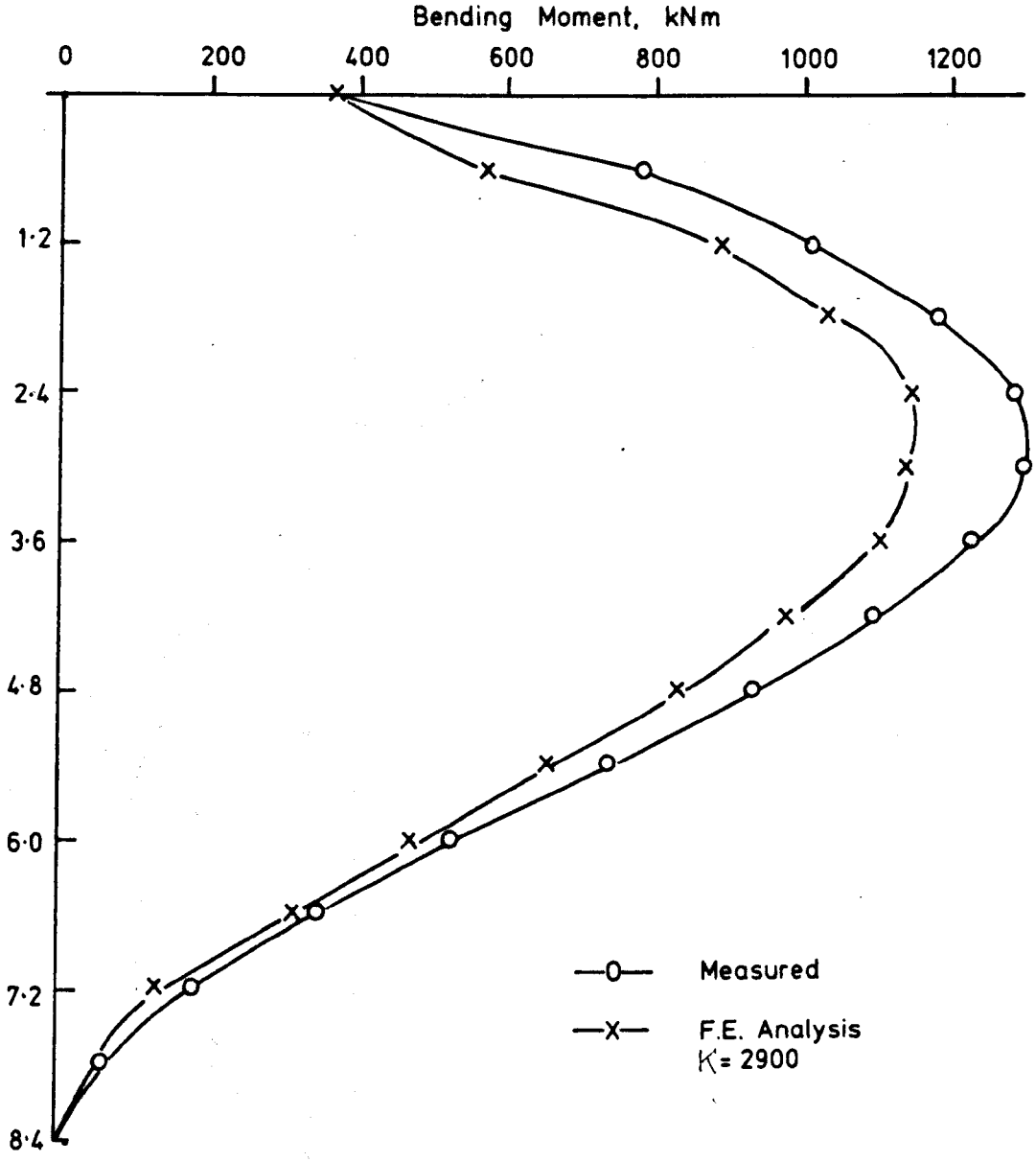

FIG. 2.6. BENDING MOMENT vs. DEPTH FINITE ELEMENT AND EXPERIMENTAL RESULTS
PILE No. 1 Experiment No. 1 Load = 469kN (e = 0·76m)

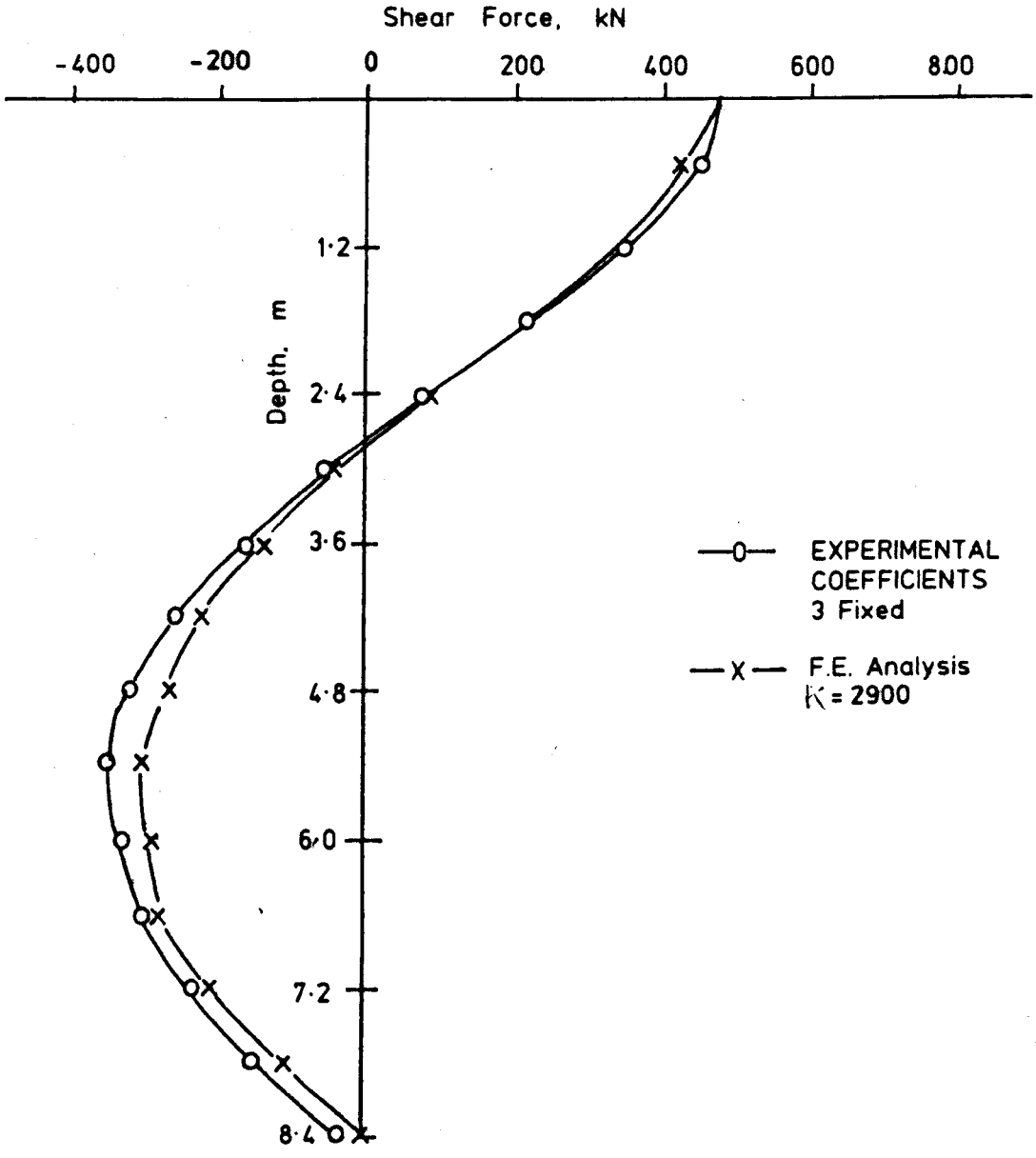

FIG. 2.7. SHEAR vs. DEPTH FINITE ELEMENT AND EXPERIMENTAL RESULTS

PILE No. 1. Experiment No. 1. Load = 469kN (e = 0·76m)

However, from Fig. 2.4 it is not possible to model the load-deflection relationship from the experiments with a single value of K.

This shows that a non-homogeneous medium, such as a soil, cannot be modelled satisfactorily by the simple elastic method used.

The finite element method presented in this thesis is a valid and well proven method for elastic stress analysis, but is of limited use once observed behaviours become non-linear.

A non-linear stress-strain relationship could be included but this would increase the storage and time required by the program as discussed in Section 2.4.2.

For the above reason the finite element model presented here cannot be expected to give close agreement with the centrifuge results. However its merits can be compared with other elastic analyses such as Matlock and Reese, Poulos and Randolph (Chapter 6). In particular back-analysis yields values of N which are appreciably higher than Poulos' parameter N_h at the same pile head displacement.

CHAPTER THREE

EXPERIMENTAL METHOD

3.1 CENTRIFUGAL MODELLING

3.1.1 Introduction

Centrifuge tests were first performed in the 1930's independently in America and Russia and thus the principles of similarity between model and prototype have been recognised for over 50 years.

In the United Kingdom this modelling technique was first pioneered by Avgherinos and Schofield[1] on a hired aerospace centrifuge. This work lead to the building of a geotechnical centrifuge at the University of Manchester, Institute of Science and Technology (UMIST) in 1969, of which a short description is given by Schofield[31].

In 1971, centrifuges were constructed at the University of Manchester, Simon Engineering Laboratories, detailed by Rowe[29] and Craig and Rowe[9], and at Cambridge University, described by Schofield[30].

The Liverpool University geotechnical centrifuge, shown in Plate 3.1 and Fig. 3.1, was completed in 1973, a full description of which can be found in King et al[18].

Although centrifugal modelling will never replace full scale field tests, it does provide a unique method of studying the behaviour of geotechnical structures. It is possible, under these controlled conditions, to study modes of failure that previously were unrecognised and hence formulate new methods of analysis and design.

3.1.2 Basic Principles and Scaling Laws

Centrifugal modelling differs from conventional modelling only by the forced gravitational field induced into the model by the centrifuge.

Provided model and prototype are made of the same materials, a model N times smaller than the prototype but in a gravitational field

PLATE 3. 1. LIVERPOOL UNIVERSITY CENTRIFUGE AND DATA RECORDING EQUIPMENT

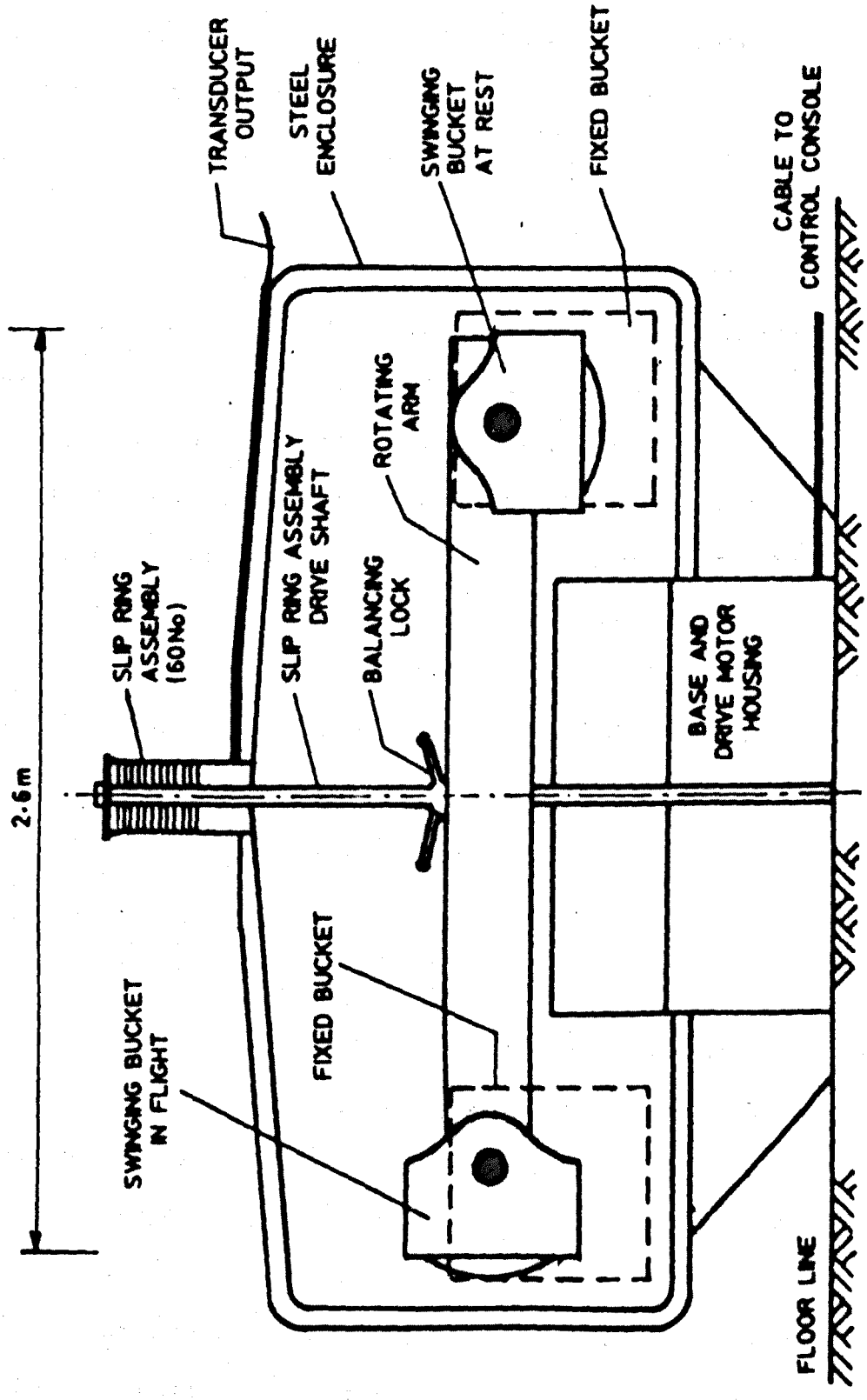

FIG. 3.1. DIAGRAMMATIC REPRESENTATION OF THE CENTRIFUGE.

N times greater the model will experience the same unit stress as the prototype at corresponding points and, because consolidation rates depend on length squared, consolidation in the model will be N^2 times faster than in the prototype.

The remaining scaling laws, listed in Appendix A, follow automatically.

However, the gravitational field created by the centrifuge varies radially and hence over the depth of a model, stresses in model and prototype cannot be matched at all points.

The linear variation of acceleration with depth through the model causes a non-linear variation of stress and it can be shown, Appendix B, that the operating speed can be chosen so that the maximum percentage error in stresses between model and prototype for the maximum depth of model in the Liverpool centrifuge, is less than 3.5%. As this error is small no corrections have been made to experimental or theoretical calculations. All models were run at 176.4 rpm to give an average scaling factor, N = 40.

3.2 TESTING

3.2.1 Model Arrangement

The main features of the Liverpool University centrifuge and a review of previous research topics and test methods have been outlined by King et al.[18]

The test arrangement, used for the experiments described here, is shown in Plates 3.2 and 3.3 and Fig. 3.2.

Load is applied to the model pile by a high torque low-speed AC motor and through a gear system to give a horizontal pull.

The soil used in the experiment was dry Erith sand having an effective size, D_{10}, of 0.16 mm and a uniformity coefficient, C_u, of

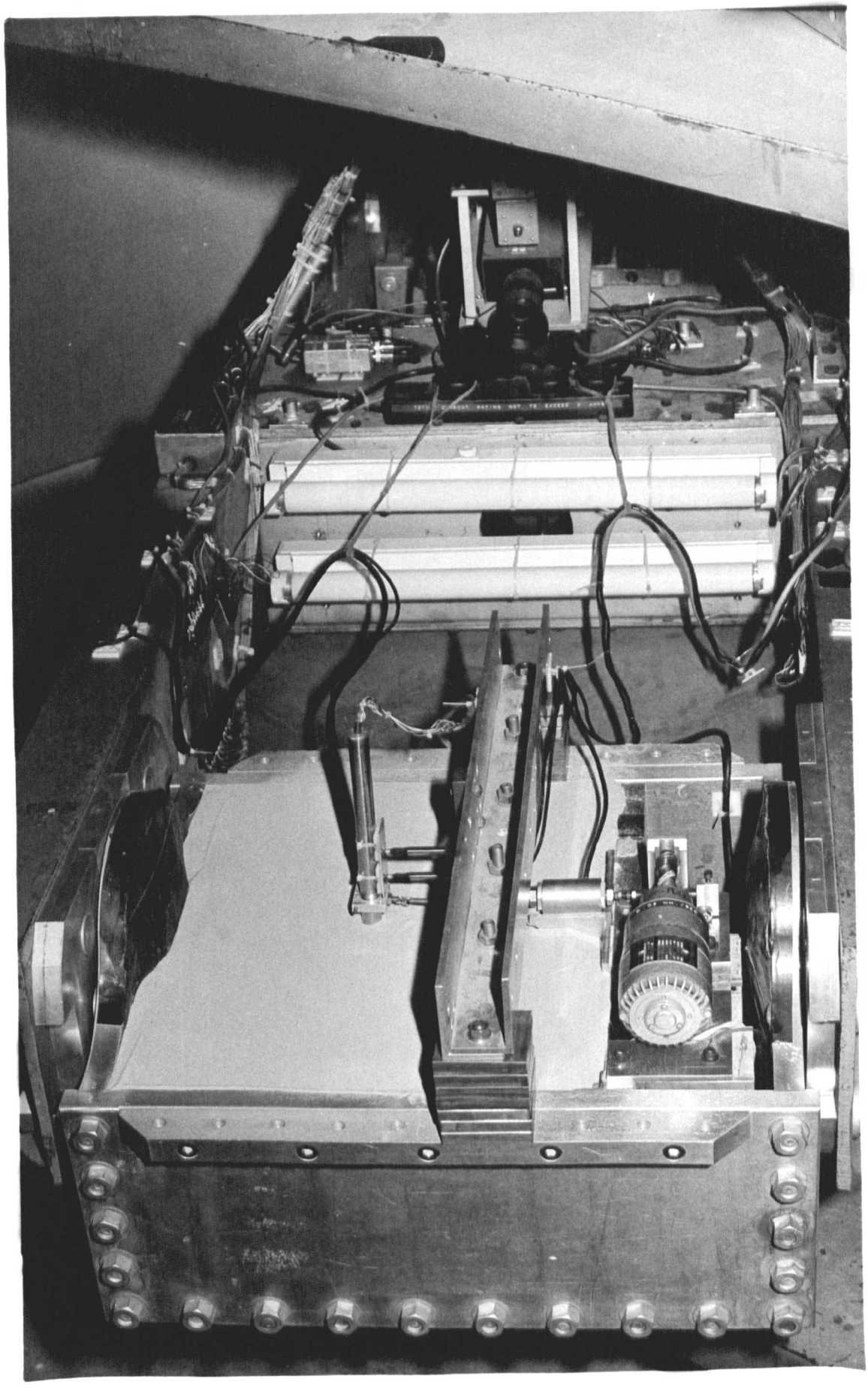

PLATE 3. 2. MODEL ARRANGEMENT

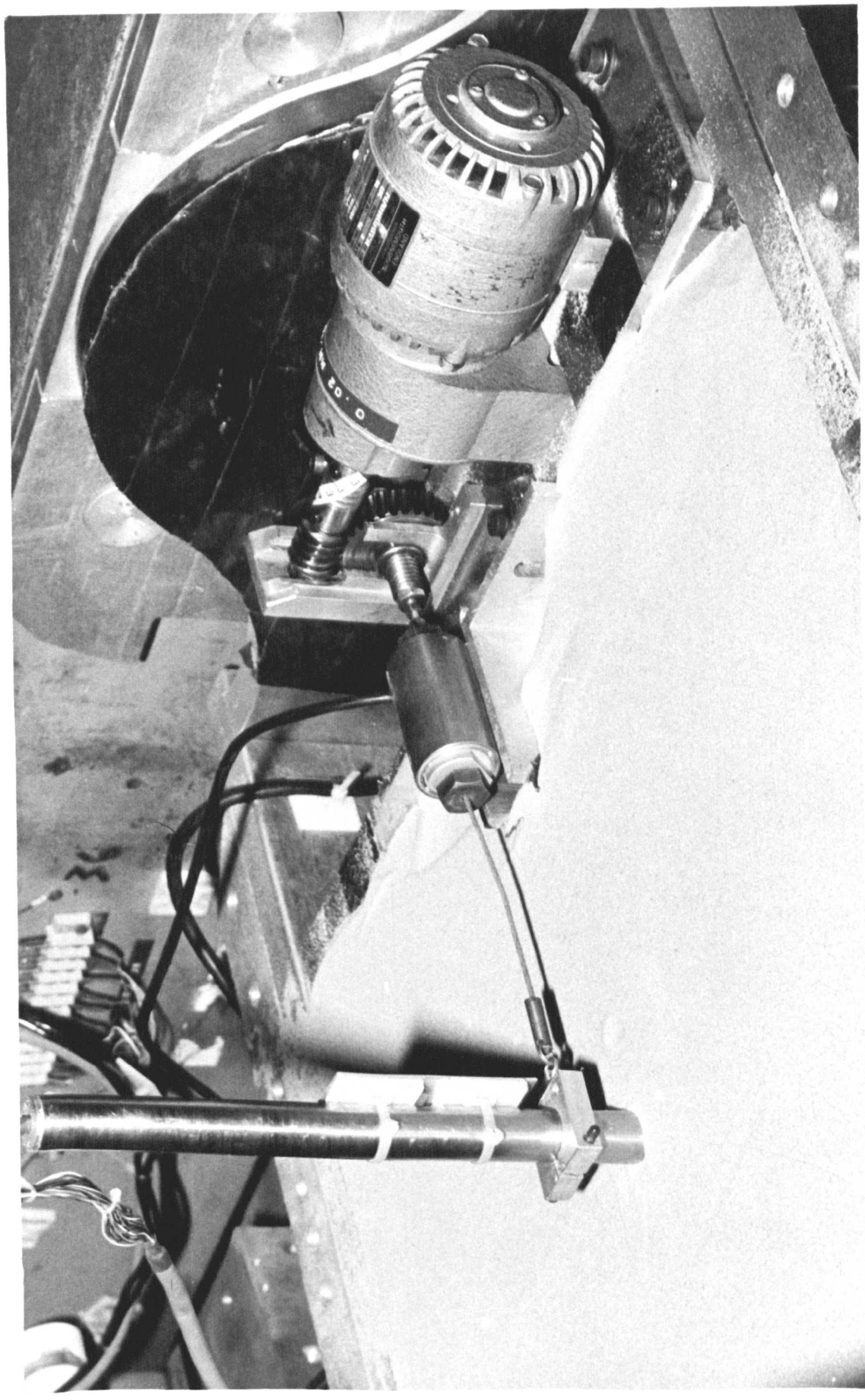

PLATE 3.3. LOADING MECHANISM

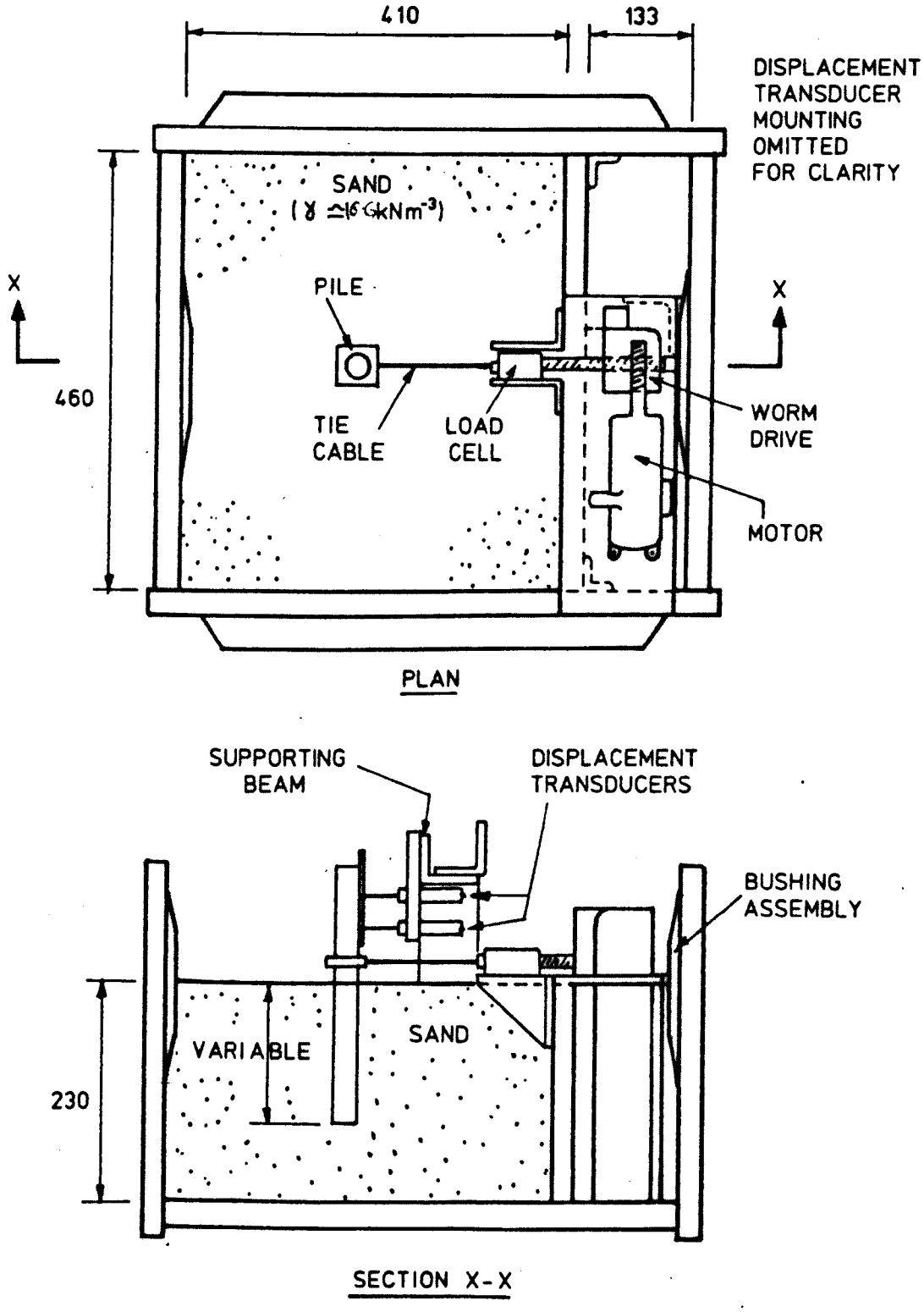

FIG. 3.2. MODEL ARRANGEMENT FOR TESTING SINGLE PILES

of 1.25. The sand was compacted in several layers using a hand vibrator with the model pile held firmly in position. This produced, as determined by taking measurements at random throughout the series of tests, an average bulk density of 16.616 KN/m^3.

3.2.2 The Model Piles

Three model piles were tested. They were made of stainless steel tubing and designed so that there were two with approximately the same diameter and two with approximately the same flexural rigidity. The dimensions and properties of each pile are listed in Table 3.1.

To measure the bending moment in the piles during the tests 14 pairs of strain gauges with a gauge length of 3 mm and a resistance of 120 ohms were fixed to the inner surface of each pile at 15 mm centres and starting 15 mm from the bottom of the pile. Calibration of each pile was by cantilever theory, each pile being supported at the top and loaded at the tip.

The measured strains are shown in Tables 3.2, 3.3 and 3.4, together with average values for flexural rigidity calculated over each strain gauge length.

The average flexural rigidity determined for each pile is included in Table 3.1, together with corresponding values of Young's modulus derived using the measured diameters.

This apparent variation in Young's modulus reflects inaccuracies in the positioning and response of the strain gauges and variations in material properties.

At the tip of the pile a metal insert was made to prevent sand from entering the pile while setting up and running the experiment. It was made to be a loose fit and glued into position with a rubber solution glue so that it would not affect the flexural rigidity of the pile at the tip.

Table 3.1

Dimensions and properties of model and prototype pile.

Pile No.	Scale	Internal Diameter mm	External Diameter mm	Thickness mm	Gauged length mm	Flexural* Rigidity kNm^2	Young's modulus E kNm^2
1	Model	17.93	19.07	0.37	210	0.302	212.885 x 10^6
	Prototype	717.2	762.8	22.8	8400	7.7312 x 10^5	
2	Model	23.98	24.47	0.345	210	0.287	209.807 x 10^6
	Prototype	959.2	978.8	9.8	8400	7.3472 x 10^5	
3	Model	17.93	18.57	0.32	210	0.157	205.479 x 10^5
	Prototype	717.2	742.8	12.8	8400	4.0912 x 10^5	

* see Tables 3.2, 3.3 and 3.4

Table 3.2

Calibration of Model Pile No. 1

Gauge No.	Dist. from load m	Strain x 10^{-6}	Flexural Rigidity kNm^2
1	0.210	311	0.300
2	0.195	289	0.300
3	0.180	262	0.305
4	0.165	240	0.306
5	0.150	222	0.300
6	0.135	200	0.300
7	0.120	177	0.301
8	0.105	155	0.299
9	0.090	135	0.296
10	0.075	193	0.295
11	0.060	89	0.300
12	0.045	68	0.294
13	0.030	45	0.302
14	0.015	20	0.333

Note Load = 49.6 x 10^{-3} KN

Average Flexural Rigidity = 0.302 KNm^2

Table 3.3

Calibration of Model Pile No. 2

Gauge No.	Dist. from load m	Strain x 10^{-6}	Flexural Rigidity KNm^2
1	0.210	250	0.302
2	0.195	236	0.297
3	0.180	223	0.290
4	0.165	199	0.298
5	0.150	185	0.292
6	0.135	168	0.289
7	0.120	144	0.300
8	0.105	129	0.293
9	0.090	109	0.297
10	0.075	94	0.287
11	0.060	75	0.287
12	0.045	60	0.270
13	0.030	40	0.270
14	0.015	22	0.245

Note Load = 30.0×10^{-3} KN

Average Flexural Rigidity = 0.287 KNm^2

Table 3.4

Calibration of Model Pile No. 3

Gauge No.	Dist. from load m	Strain x 10^{-6}	Flexural Rigidity KNm^2
1	0.209	230	0.164
2	0.194	213	0.165
3	0.179	195	0.166
4	0.164	177	0.168
5	0.149	162	0.166
6	0.134	146	0.166
7	0.119	131	0.164
8	0.104	115	0.163
9	0.089	100	0.161
10	0.074	85	0.157
11	0.059	69	0.155
12	0.044	55	0.145
13	0.029	38	0.138
14	0.014	20	0.127

Note Load = 20.2 x 10^{-3} KN

Average Flexural Rigidity = 0.157 KNm^2

3.2.3 Data Collection

Readings taken during each test were :-

(a) Lateral load, measured by a load cell placed between the gear box assembly and the pile cap.

(b) Horizontal deflection at two points above the loading point.

(c) Strain readings at 14 points down the pile.

The readings were fed through a Vishay-Ellis 220 recording system, see Plate 3.1, which is interfaced to a PET computer for immediate processing of results, King et al[18].

3.2.4 Test Procedure

Once the model had been set up and the rotating arm of the centrifuge statically balanced the machine was spun up to a test speed of 176.4 rpm (equivalent to a 40 g acceleration), for about 2-3 minutes. This was done to make sure that the machine was running smoothly and to allow any initial settlement of the pile and sand to take place.

When the centrifuge stopped the strain gauges, load cell and displacement transducers were set to zero and a scan of the output channels taken. This is known as the static zero datum.

The machine was then spun up to speed and another scan of the output channels taken. This is known as the dynamic zero datum.

Load was then applied to the pile by the motor and at any required load, the motor was stopped and a scan of the output channels taken.

The data was recorded in approximately equal increments of load until one of the following limits was reached; (i) maximum allowable load cell reading of 360 N, to guarantee a linear calibration of the load cell, (ii) maximum strain reading of 550 microstrains, to prevent the pile from becoming plastically strained and (iii) maximum

allowable deflection of 6 mm from the upper displacement transducer as it reached the limit of its travel.

When one of the above limits was reached the load was reduced and scans taken at 5 or 6 intervals until the load was removed completely.

3.2.5 Testing Sequence and Objectives

As mentioned in Section 3.2.2, three model piles, two of the same diameter and two of the same flexural rigidity were tested.

In the first series of tests the loading eccentricity was kept constant and the length to diameter ratio varied for each pile.

In the second series of tests two length to diameter ratios from the first series were used with a different loading eccentricity.

The sequence of tests performed is summarised in Tables 3.5, 3.6 and 3.7.

The objectives of the tests was to study the effect on the deflection of the piles at the soil surface, and the value and position of the maximum bending moment in the piles, of independent variations in the length diameter and the flexural rigidity of the piles and of the eccentricity of loading.

Table 3.5

Test sequence for model pile No. 1.

Test No.	Length to diameter ratio	Length of Pile embedded in sand mm	Load eccentricity mm
1	11	210	19
2	10	190	19
3	9	171	19
4	8	152	19
5	7	133	19
6	6	114	19
7	5	95	19
8	10	190	29
9	8	152	29

Table 3.6

Testing sequence for model pile No. 2

Test No.	Length to diameter ratio	Length of Pile embedded in sand mm	Load eccentricity mm
1	8	203	19
2	7	178	19
3	6	152	19
4	5	127	19
5	4	102	19
6	8	203	29
7	6	152	29

Table 3.7

Testing sequence for model pile No. 3

Test No.	Length to diameter ratio	Length of Pile embedded in sand mm	Load eccentricity mm
1	11	204	19
2	10	186	19
3	9	167	19
4	8	159	19
5	7	130	19
6	6	111	19
7	5	93	19
8	10	186	29
9	8	159	29

3.3 METHODS FOR INTERPRETATION OF MEASURED DATA

3.3.1 Introduction

The results were interpreted by two methods of numerical curve fitting through the bending moment, calculated from the strain readings down the pile.

The first method was based on the least-square error procedure, see Cope et al[8], in which a polynomial any order up to m-1 is fitted through the data.

The second method used standard subroutines supplied by the Numerical Algorithms Group (NAG) to fit a cubic spline through the data.

3.3.2 Polynomial Analysis

The method of curve fitting by the least-square error procedure used here is shown in Section 4.2.1.

The known bending moment and shear and the additional assumption of zero soil pressure at the soil surface provide the first three coefficients of the polynomial and successive differentiations of the polynomial yields the shear and soil resistance respectively, at points down the pile.

When successively integrating the polynomial to obtain the slope and deflection respectively at points down the pile, the slope and deflection at the soil surface provide the constants of integration.

The effect of varying the number of known and unknown coefficients in the polynomial will be discussed in Chapter 4.

3.3.3 Spline Analysis

The use of the NAG subroutines is restricted in that it is not possible to include external boundary conditions, as in Section 3.3.2.

The subroutines fit a cubic spline through the bending moments

and differentiate to give shear and soil resistance distribution. Integration to find deflection and slope is not possible.

For a detailed explanation of cubic splines see Cope et al.[8] and for fundamental or B-splines see De Boor[11].

The accuracy of the method can be increased by adding extra known bending moments in the pile above the sand surface and below the loading point.

A cubic spline is comprised of a set of cubic polynomials which meet at predefined points called knots. The number and position of the knots determines the shape and accuracy of the spline. This will be discussed in Chapter 4.

CHAPTER FOUR

INTERPRETATION OF EXPERIMENTAL RESULTS

4.1 INTRODUCTION

In this chapter the optimisation of the polynomial and spline numerical methods, described in Chapter 3, are discussed.

Polynomial optimisation is achieved by varying the number of known and unknown coefficients (Section 3.2.2) in order to obtain the best fit to the experimental observations whereas spline optimisation is achieved by varying the number and position of 'knots' (Section 3.3.3).

4.2 POLYNOMIAL OPTIMISATION

By studying the effect of varying the number of unknown coefficients in the polynomial on the sum of the least squares, the difference in the standard deviation and the mean between the measured bending moments and those calculated from the polynomial, the 'best fit' is obtained.

4.2.1. Analysis

The sum of the least squares is the sum of the square of the difference between the measured and calculated data points defined as

$$\sum_{i=1}^{n} (y_i - p(x_i))^2 \qquad (4.1)$$

where n is the number of points, y_i is the input data and $p(x_i)$ is the calculated values from the polynomial $p(x)$.

The mean of a sample of data is defined as

$$\bar{y} = \frac{1}{n} \sum_{i=1}^{n} y_i \qquad (4.2)$$

and the difference in the means between the measured and calculated values is

$$\frac{1}{n}\sum_{i=1}^{n} y_i - \frac{1}{n}\sum_{i=1}^{n} p(x_i) \qquad (4.3)$$

The standard deviation of a sample of data is defined as

$$S = \sqrt{\frac{1}{n-1}\sum_{i=1}^{n} (y_i - \bar{y})^2} \qquad (4.4)$$

therefore the difference in the standard deviations between the measured and calculated values is

$$\sqrt{\frac{1}{n-1}\sum_{i=1}^{n} (y_i - \bar{y})^2} - \sqrt{\frac{1}{n-1}\sum_{i=1}^{n} (p(x_i) - p(\bar{x}))^2} \qquad (4.5)$$

where $p(\bar{x})$ is the mean of the calculated data.

Tables 4.1 to 4.4 illustrate the variations of the above mentioned values for one model pile at one applied load. The maximum recorded bending moment was 1298.55 KNm. The position of the maximum calculated bending moment was between 2.4 m and 3.0 m below the soil surface.

By considering consecutive polynomial orders and noting when the magnitude and position of the maximum bending moment varies relatively little, Tables 4.1 to 4.2, then the best approximation to these quantities is reached. This value coincides with a low value for the sum of the least squares. However, as shown in Fig. 4.2, the order of the polynomial makes very little visible difference and generally low order polynomials give the best overall fit.

Figures 4.1 to 4.8 illustrate typical displacement moment, shear and soil resistance distributions generated by the polynomials.

The displacement distributions in Fig. 4.1 are almost identical for all variations of known and unknown coefficients. It is, however, impossible to know how realistic this distribution is

Table 4.1

No. of Coeff-icients	Sum of the Least Squares	Difference in Standard Deviations $\times 10^3$	Difference in Means	Max.Bending Moment KNm	Position of Max.Bending Moment m
4	4288.44	15.31	-21.79	1295.49	2.642
5	1889.69	13.86	-20.79	1295.36	2.719
6	1802.65	13.93	-20.79	1298.13	2.724
7	851.38	14.67	-21.47	1292.42	2.787
8	476.40	14.44	-21.47	1296.34	2.829
9	200.85	14.97	-21.97	1301.55	2.811
10	87.71	14.72	-21.96	1301.98	2.793
11	75.96	14.97	-22.21	1300.96	2.766
12	17.31	15.48	-22.24	1303.13	2.750
13	13.66	15.83	-22.48	1303.73	2.752
14	382.45	8.59	-16.45	1308.43	2.664

Summary of optimisation values for polynomial analysis

No. of known coefficients = 0

Table 4.2

No. of Coeff-icients	Sum of the Least Squares	Difference in Standard Deviations x 10^3	Difference in Means	Max.Bending Moment KNm	Position of Max.Bending Moment m
4	4456.57	16.07	-22.72	1294.09	2.627
5	1980.80	13.48	-20.26	1296.30	2.716
6	1947.71	13.44	-20.16	1298.09	2.718
7	874.31	14.51	-21.25	1292.18	2.786
8	480.09	14.37	-21.38	1296.30	2.830
9	201.09	14.96	-21.95	1301.55	2.811
10	87.71	14.72	-21.96	1301.98	2.773
11	75.96	14.97	-22.21	1300.97	2.766
12	20.41	15.43	-22.25	1302.81	2.752
13	13.56	15.84	-22.50	1303.69	2.752
14	13.35	15.95	-22.60	1303.65	2.754

Summary of optimisation values for polynomial analysis

No. of known coefficients = 1.

Table 4.3

No. of Coeffic-ients	Sum of the Least Squares	Difference in Standard Deviations x 10^3	Difference in Means	Max.Bending Moment KNm	Position of Max.Bending Moment m
4	37136.4	74.09	41.88	1081.38	3.258
5	68446.4	13.86	4.43	1278.98	3.123
6	21846.7	12.64	-10.45	1325.84	2.855
7	13485.2	11.21	-13.57	1321.30	2.700
8	8055.24	13.15	-17.14	1299.57	2.623
9	4922.63	12.45	-17.99	1284.97	2.754
10	2675.22	14.39	-20.11	1294.14	2.910
11	1076.92	12.86	-19.66	1306.20	2.852
12	92.36	15.86	-21.94	1306.96	2.744
13	37.44	14.58	-21.12	1304.57	2.727
14	56.35	13.71	-20.57	1304.08	2.717

Summary of optimisation values for polynomial analysis

No. of known coefficients = 2

Table 4.4

No. of Coefficients	Sum of the Least Squares	Difference in Standard Deviations x 10^3	Difference in Means	Max.Bending Moment KNm	Position of Max.Bending Moment m
4	353748.0	-274.13	-234.71	1672.59	4.199
5	69027.3	17.91	7.07	1268.82	3.123
6	65703.7	26.80	11.44	1250.05	3.089
7	43761.6	18.73	-0.27	1305.71	3.031
8	30496.3	12.89	-5.18	1329.61	2.858
9	21214.8	13.64	-10.88	1324.44	2.671
10	15269.9	11.22	-12.42	1302.51	2.556
11	11093.7	14.11	-16.37	1282.24	2.715
12	7754.53	9.94	-15.22	1295.25	2.976
13	3709.07	19.68	-23.87	1316.47	2.858
14	3752.31	19.31	-23.99	1316.61	2.859

Summary of optimisation values for polynomial analysis

No. of known coefficients = 3

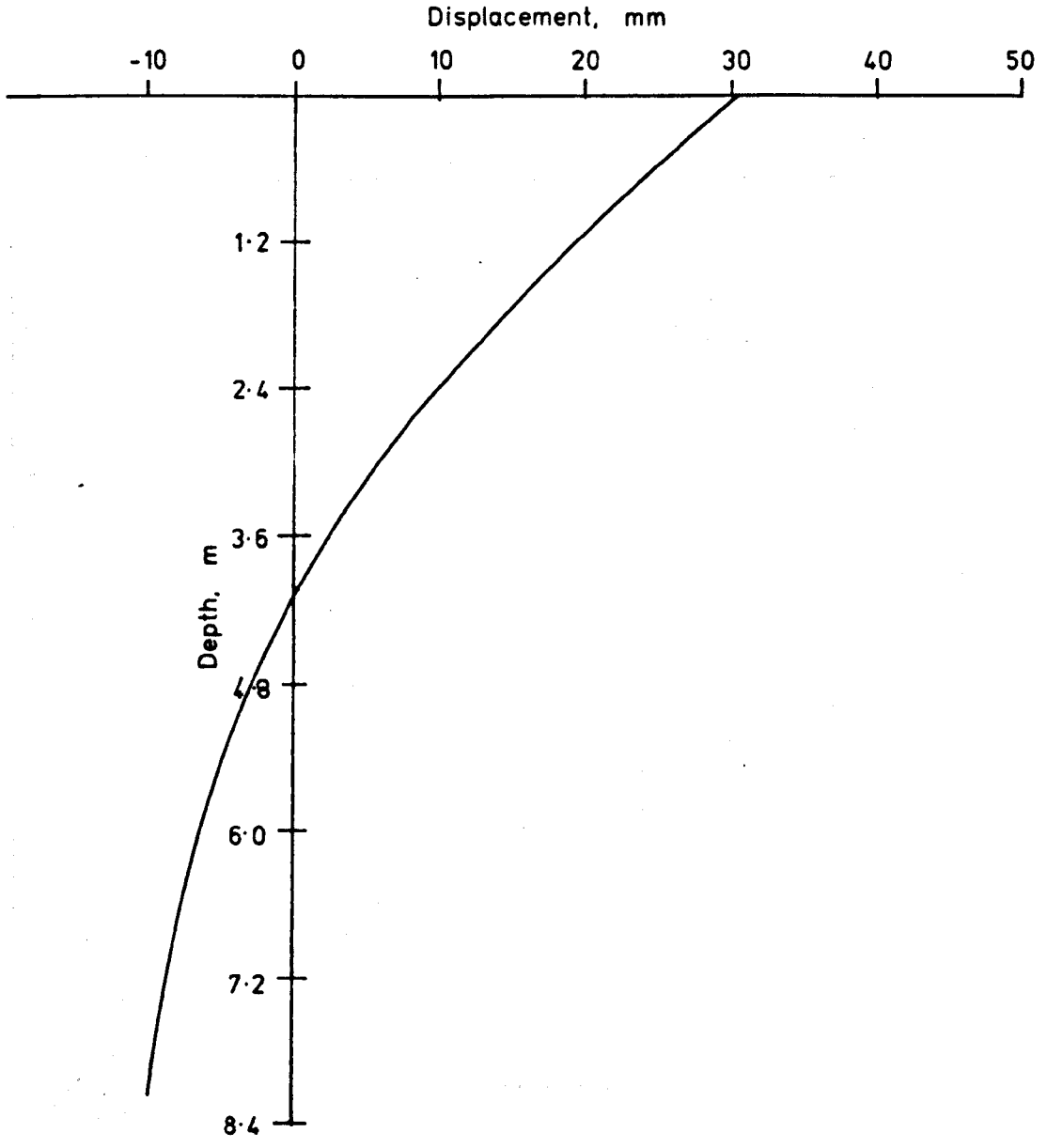

FIG. 4.1. DISPLACEMENT vs. DEPTH FOR VARIOUS COEFFICIENT COMBINATIONS. PILE No. 1

Experiment No. 1 Load = 469kN (e = 0·76m)

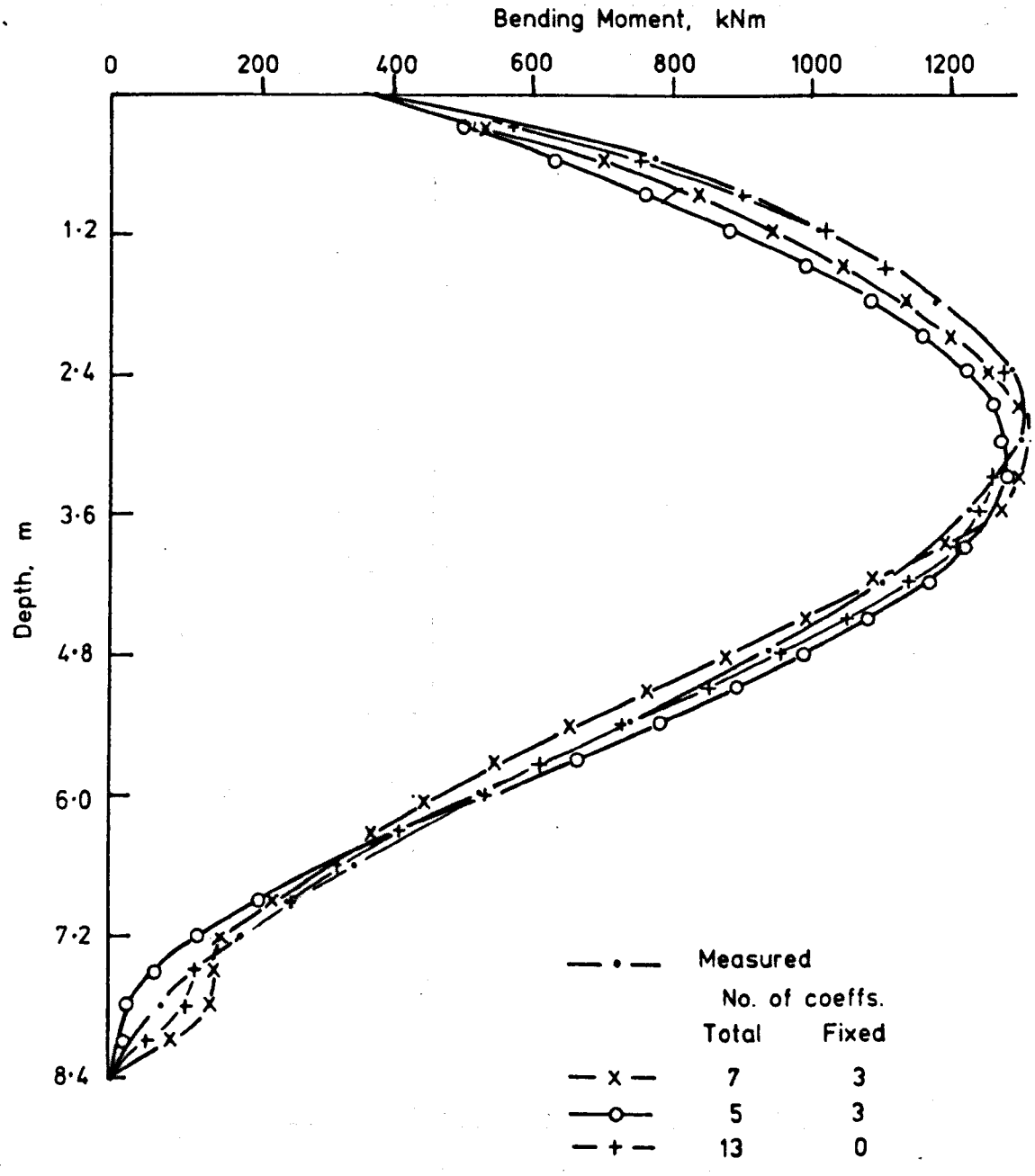

FIG. 4.2. BENDING MOMENT vs. DEPTH FOR VARIOUS COEFFICIENT COMBINATIONS. PILE No. 1

Experiment No. 1 Load = 469kN
(e = 0·76m)

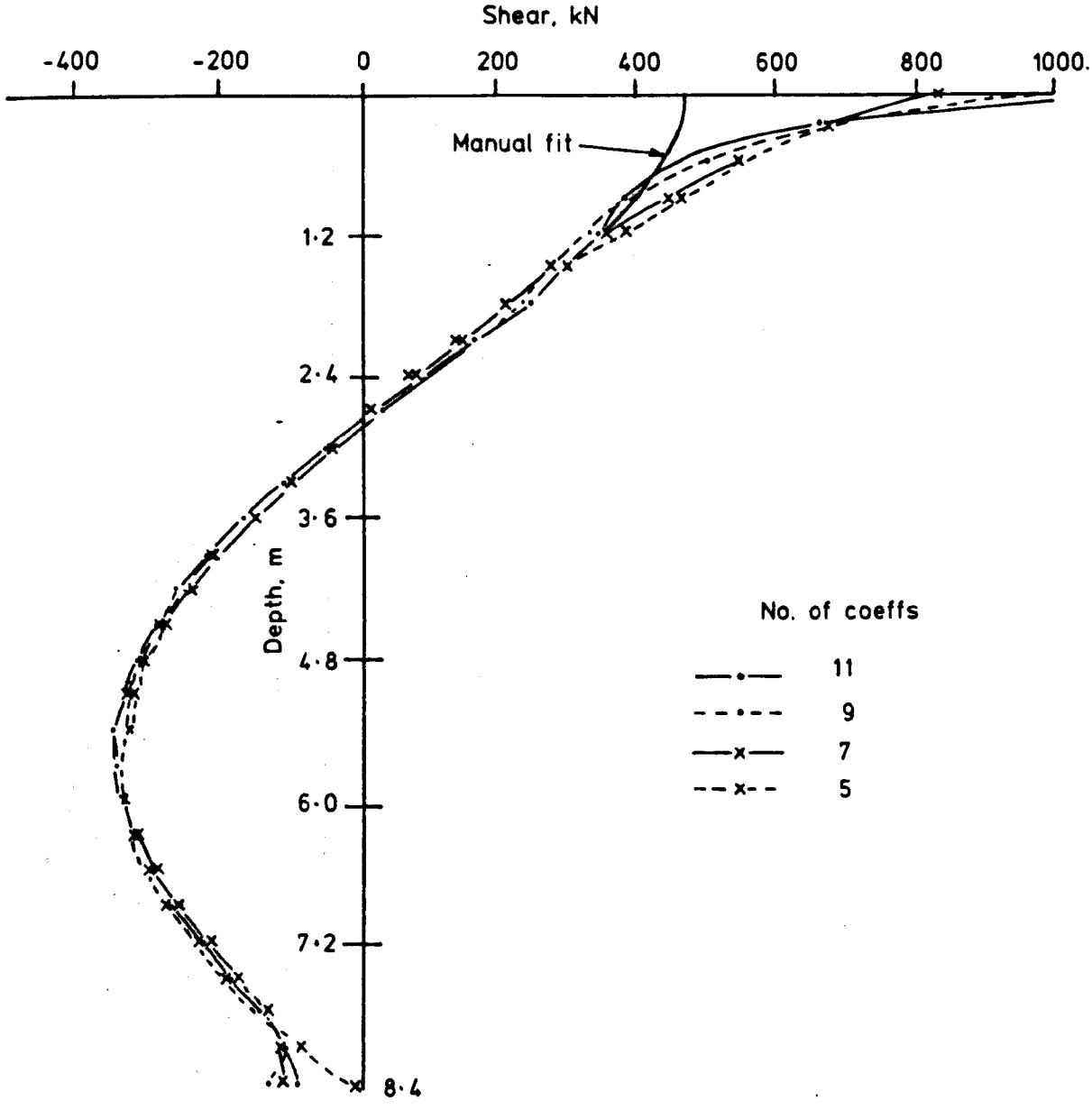

FIG. 4.3. SHEAR vs. DEPTH FOR BOTH 0 AND 1 FIXED COEFFICIENTS. PILE No. 1
Experiment No. 1 Load = 469 kN
(e = 0·76m)

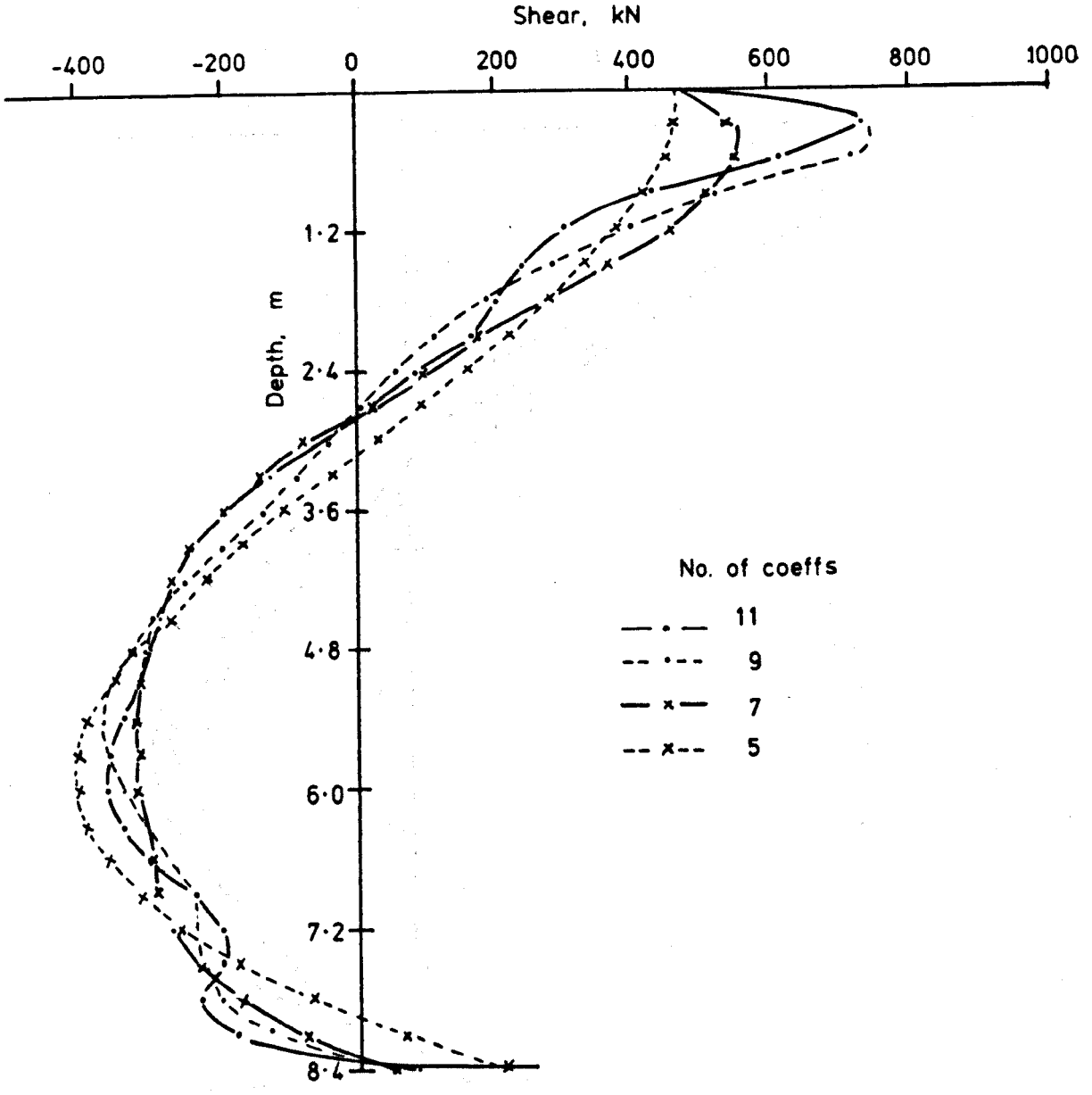

FIG. 4.4. SHEAR vs. DEPTH FOR 2 FIXED AND VARIOUS UNKNOWN COEFFICIENTS. PILE No. 1

Experiment No. 1 Load = 469kN (e = 0·76m)

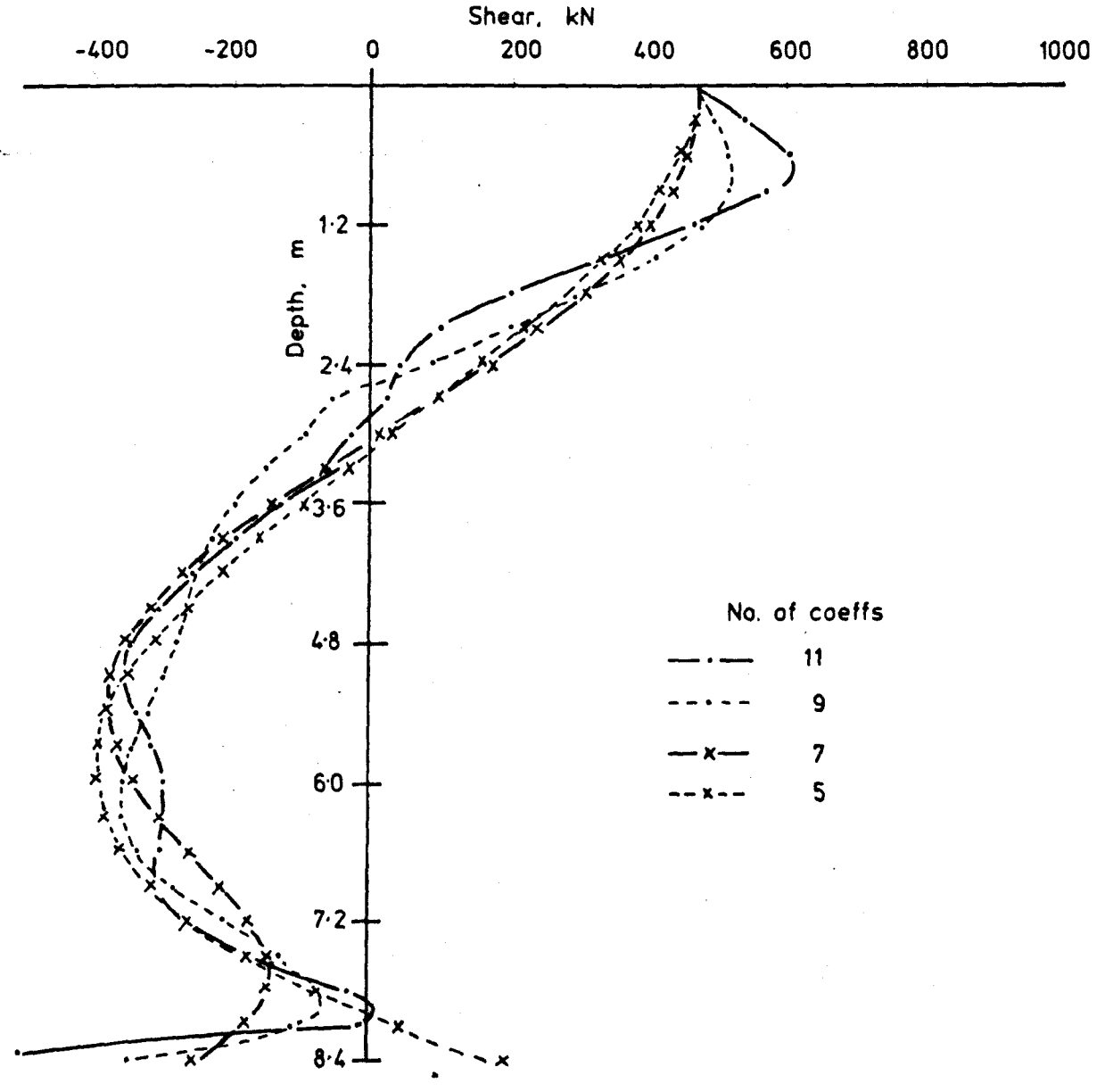

FIG. 4.5. SHEAR vs. DEPTH FOR 3 FIXED AND VARIOUS UNKNOWN COEFFICIENTS. PILE No. 1
Experiment No. 1 Load = 469kN (e = 0·76m)

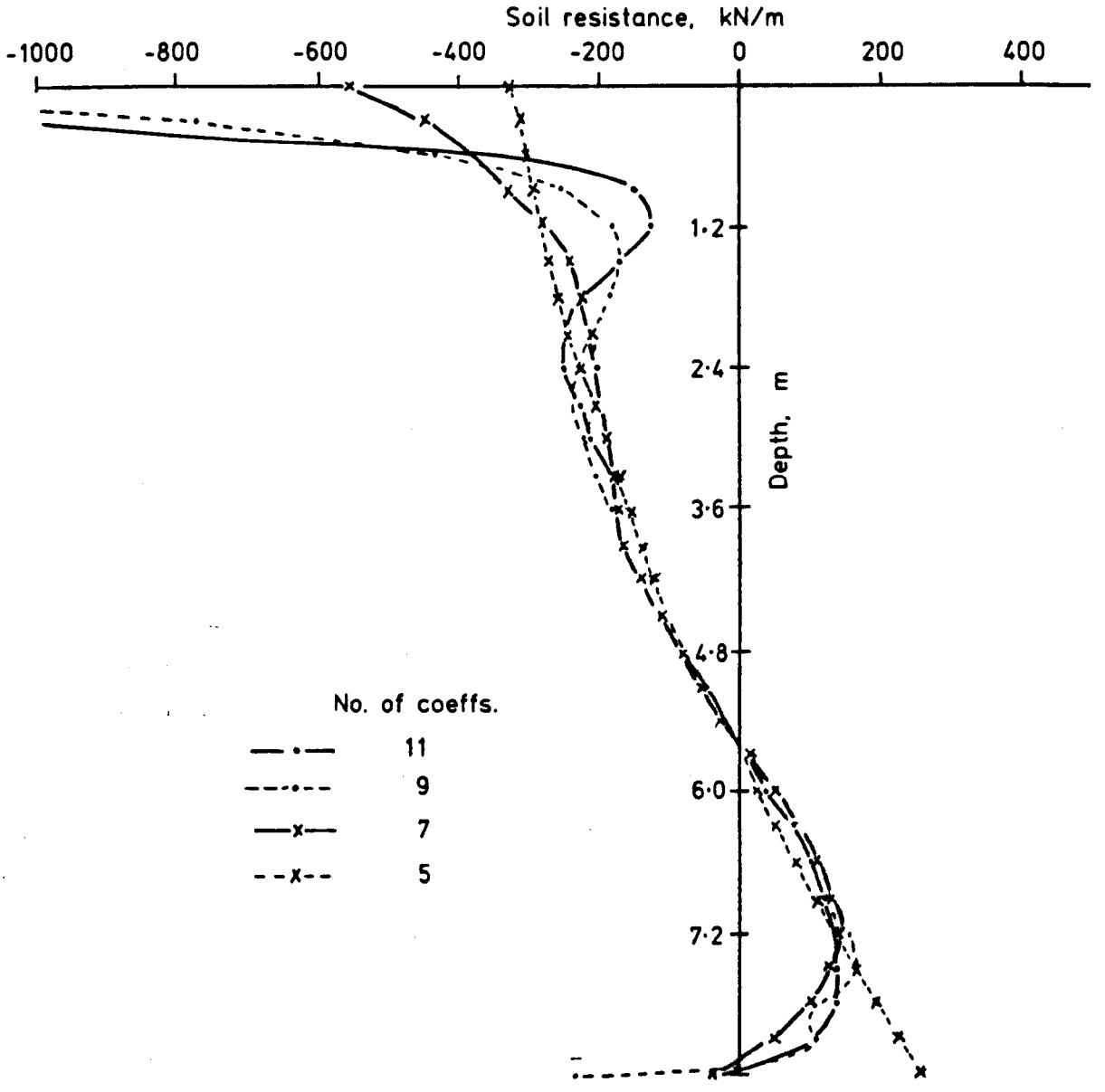

FIG. 4.6. SOIL RESISTANCE vs. DEPTH FOR BOTH 0 AND 1 FIXED AND VARIOUS UNKNOWN COEFFICIENTS

PILE No. 1 Experiment No. 1 Load = 469kN (e = 0·76m)

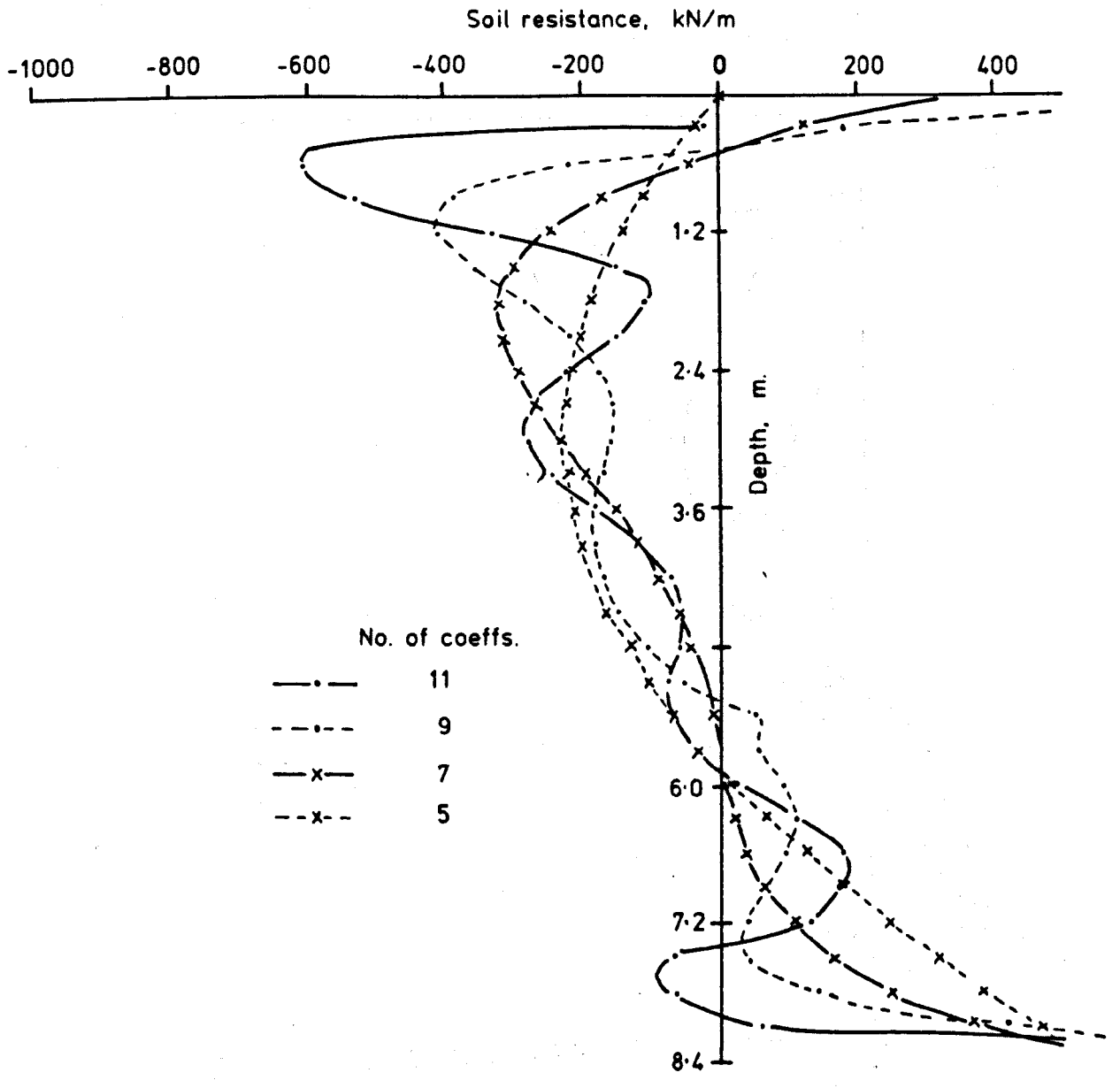

FIG. 4.7. SOIL RESISTANCE vs. DEPTH FOR 2 FIXED AND VARIOUS UNKNOWN COEFFICIENTS PILE No. 1

Experiment No. 1 Load = 469kN (e = 0·76m)

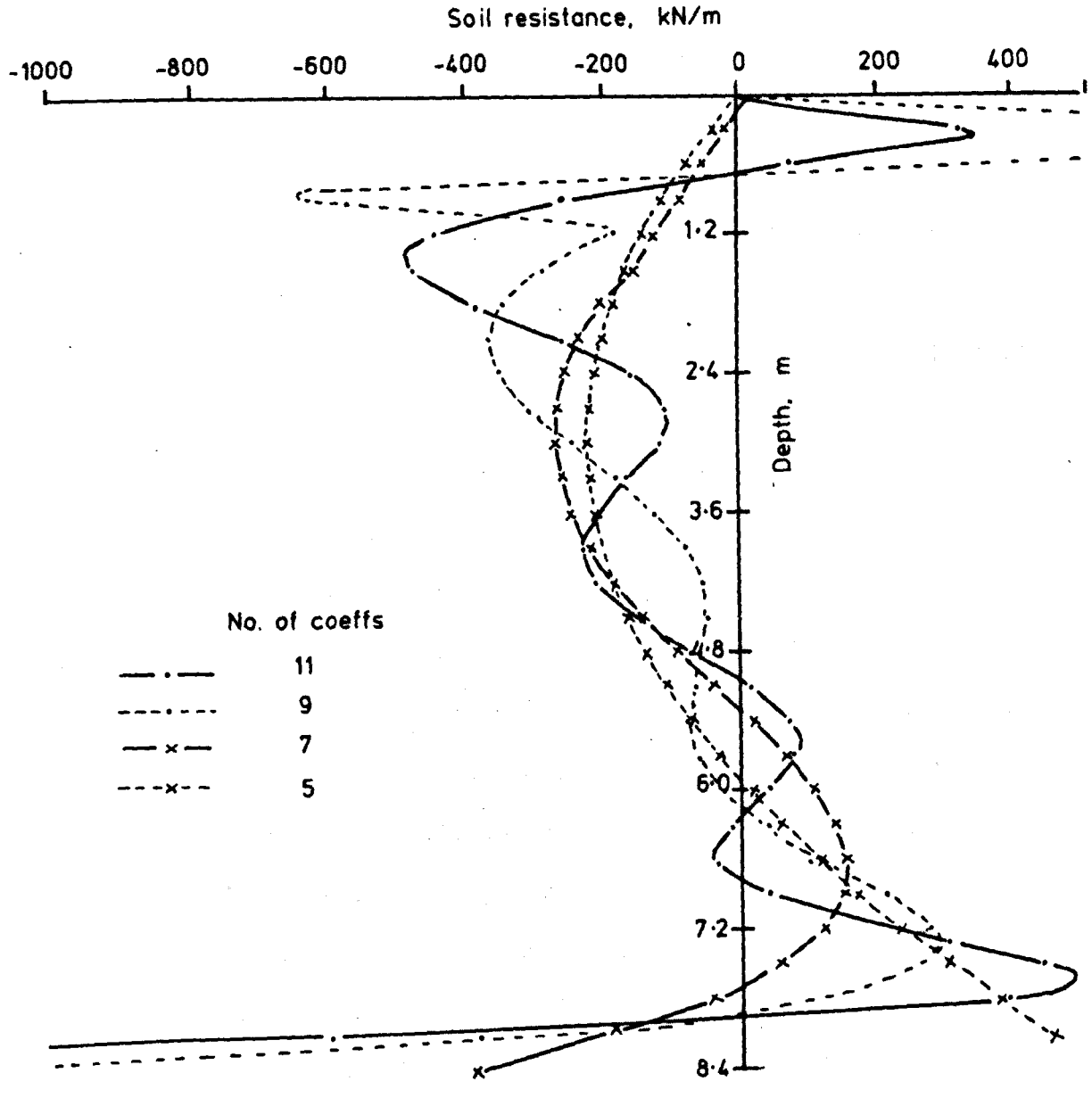

FIG. 4.8. SOIL RESISTANCE vs. DEPTH FOR FIXED AND VARIOUS UNKNOWN COEFFICIENTS. PILE No. 1

Experiment No. 1 Load = 469kN (e = 0·76m)

as no displacement could be measured below the soil surface. Also under the increased gravitational field the operation of the displacement transducers became suspect in that they would stick and bend under their own increased weight.

Figure 4.2 shows the bending moment distributions for various coefficient combinations which all produce reasonable distributions. Comparing Fig. 4.2 with the experimental results, and considering Tables 4.1 to 4.4, that the best overall fit coincides with relatively low order polynomials, i.e. approximately or less than half the number of coefficients as there are data points. This generally corresponds to a low difference of standard deviations.

The shear distributions, shown in Figs. 4.3 to 4.5, illustrate their variations with the number of coefficients. They show that it is not possible to model the complete shear distribution accurately with one polynomial. However, most of the curves give similar distributions over the lower three quarters of the pile. The best looking distributions are given by polynomials with zero or one known coefficient. Although the surface shear is highly over estimated, it is possible, using the known applied horizontal load, to adjust these distributions manually towards the top of the pile.

The soil resistance distributions (Figs. 4.6 to 4.8) show considerable and erratic variation for the higher order polynomials, although the lower order with three fixed coefficients give reasonable distribution in the upper three quarters of the pile.

4.2.2 Discussion

It can be shown that the above behaviour is typical of all the tests performed. It suggests that the best overall fit corresponds with low values for the difference in standard deviation.

However, to determine the position and magnitude of the maximum bending moment high order polynomials, corresponding to the lowest values for the sum of the least squares, appear preferable.

The higher order polynomials behave erratically between data points and when differented yield meaningless distributions. Although the lower order polynomials with two or three fixed coefficients produce smooth curves, they may not yield the correct magnitudes of shear and soil resistance when differentiated.

Although the calculated distributions of displacements are smooth and consistent, their magnitudes may be unreliable due to the sensitivity of the displacement transducers measuring displacement and slope at the top of the pile.

Only the polynomials with a small number of coefficients, including three fixed ones, give reasonably smooth soil resistance distribution, but their magnitudes may not be reliable.

This makes both displacement and pressure distribution doubtful and, therefore, it is not possible to evaluate effective moduli of subgrade reaction with any confidence. Therefore the merits of the p - y method of analysis (Section 6.1) cannot be evaluated from the experimental results.

Values of displacements and pressure calculated from the polynomials will not be discussed further for the above reasons.

4.2.3 Conclusions

The best overall fit is obtained from low order polynomials and is indicated numerically by a low value for the difference in standard deviations.

Using zero or one fixed coefficient yields the best bending moment distributions, using two yields the best shear

distributions and using three yields the best soil resistance distributions.

To determine the magnitude and position of the maximum bending moment it is best to use a high order polynomial and this is indicated numerically by a low value for the sum of the least squares.

The polynomial method is a useful technique for interpreting the results of the test on the model piles. It is limited by the accuracy of the measured data, particularly the pile head displacements.

4.3 SPLINE ANALYSIS

The choice number and position of the knots so as to give the 'best fit' is largely a matter of trial and error, therefore, each stage must be examined graphically. However, in regions where the data is changing rapidly, a concentration of knots is advised. Generally, positioning is not usually critical and equally-spaced knots are often satisfactory.

4.3.1 Analysis

Table 4.5 illustrates the effect of variation in the number of the knots for the pile test considered in Section 4.2.1.

Using the NAG subroutines it is not possible to calculate the exact depth and value of the maximum bending moment. However, Table 4.5 shows that its value varies only slightly with the variation of the number of knots and that it stays within the same depth range.

Figures 4.9 to 4.11 illustrate moment, shear and soil resistance distributions generated by the splines using from 8 to 15 knots.

The bending moment distribution, Fig. 4.9, was not influenced by the number of the knots and is a very close fit to the experimental data.

Table 4.5

No. of interior knots	Sum of the Least Squares	Position of Max. Bending Moment between (m)	Value of Max. Bending Moment not less than (kNm)
15	120.43	2.4 - 3.0	1298.5
14	159.78	2.4 - 3.0	1298.5
13	162.57	2.4 - 3.0	1298.5
12	162.58	2.4 - 3.0	1298.5
11	174.83	2.4 - 3.0	1297.7
10	180.75	2.4 - 3.0	1296.1
9	193.22	2.4 - 3.0	1297.2
8	3369.06	2.4 - 3.0	1289.0

Summary of optimisation values for spline analysis

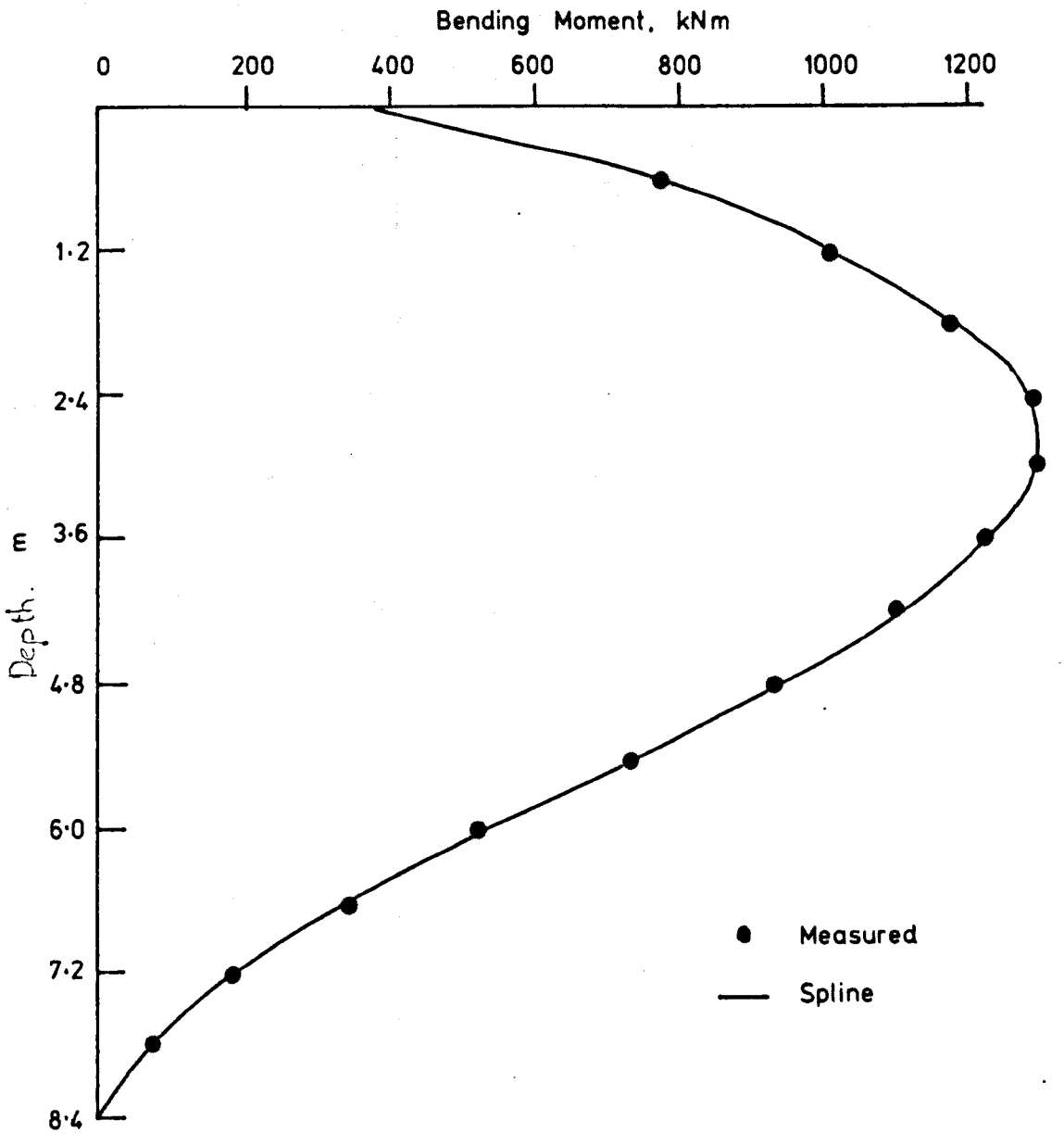

FIG. 4.9. BENDING MOMENT vs. DEPTH FOR ALL NUMBERS OF KNOTS FROM 8 TO 15 PILE No. 1
Experiment No. 1 Load = 469kN (e = 0·76m)

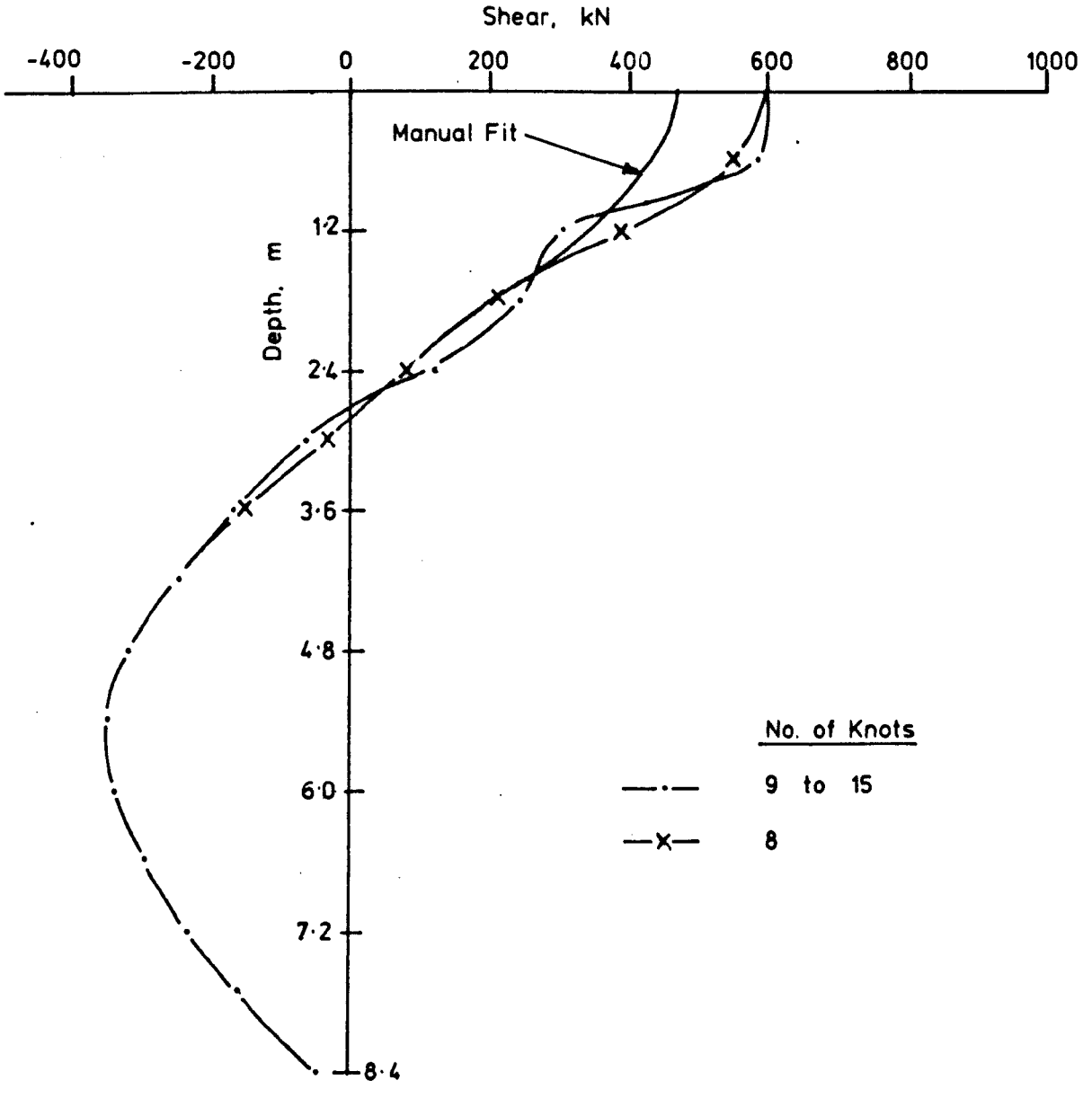

FIG. 4.10. SHEAR vs. DEPTH FOR VARIOUS NUMBER OF KNOTS. PILE No. 1

Experiment No. 1 Load = 469kNm
(e = 0·76m)

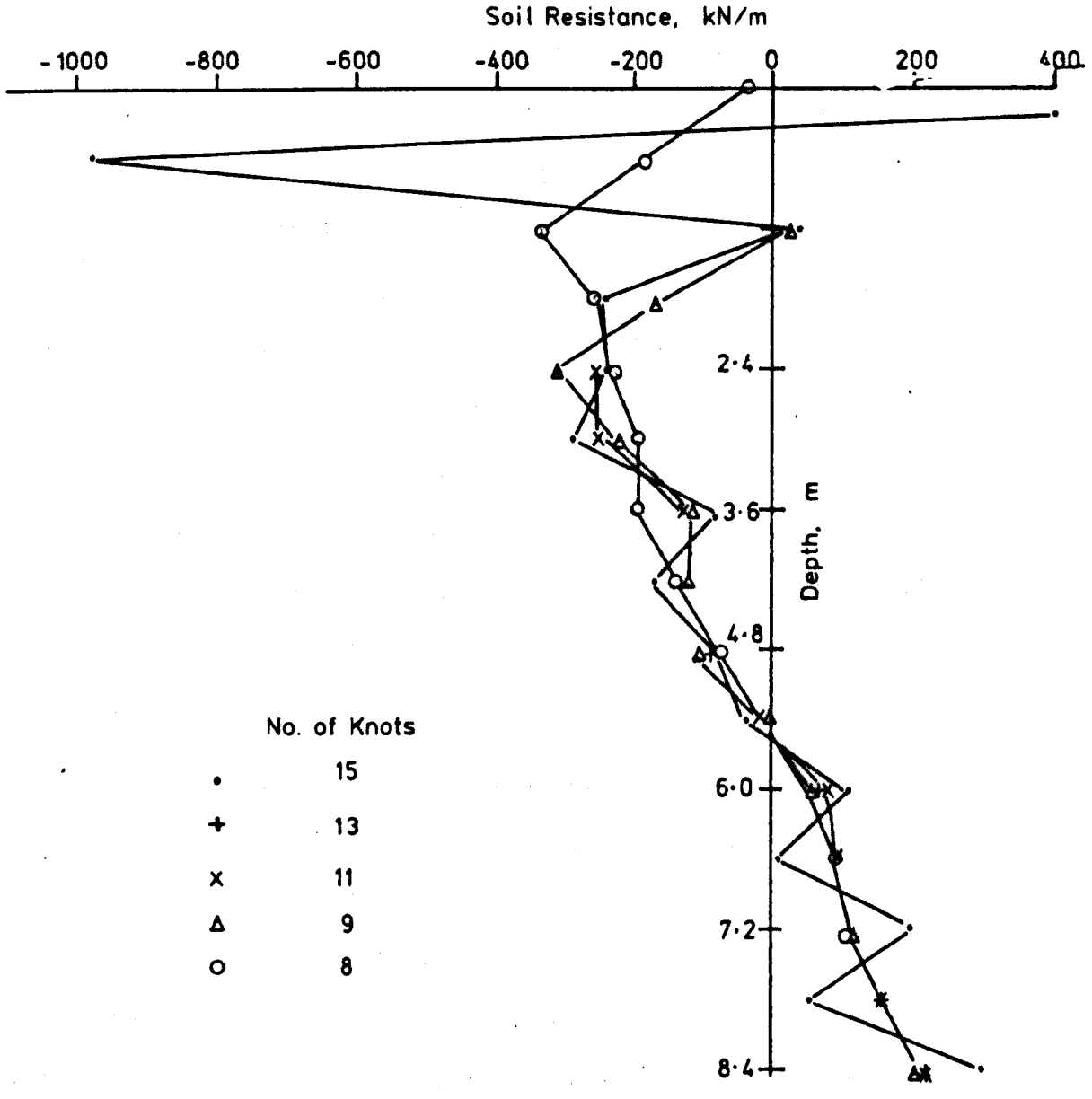

FIG. 4.11 SOIL RESISTANCE vs. DEPTH FOR VARIOUS NUMBERS OF KNOTS. PILE No. 1.

Experiment No. 1. Load = 469kN
(e = 0·76 m)

Figure 4.10 illustrates the shear distributions for the different numbers of knots. In common with the polynomial method, they show that it is not possible to model the complete shear distribution accurately. All the curves over-estimate the applied surface shear and the shear distribution towards the top of the pile is variable. However, all give similar distributions in the lower three quarters of the pile and knowing the applied horizontal load it is possible to adjust the distribution at the top of the pile manually.

Differentiating the cubic spline twice yields the series of straight lines shown in Fig. 4.11 to represent the soil resistance distribution. Although the lines tend towards a realistic distribution as the number of knots reduces, this is not necessarily a reliable indication of the true pressure distribution.

4.3.2 Discussion

It can be shown that the above trends are typical of every test performed and for more variations in the number and position of the knots than illustrated here.

Theoretically the best results should be produced by minimising the sum of the least squares. However, as shown in Figs. 4.9 to 4.11, this is not obvious and for this reason only a few examples of knot variations have been illustrated.

4.3.3 Conclusions

Comparing Figs. 4.1 to 4.8 with Figs. 4.9 to 4.11 the spline method of analysis produces bending moment and shear force distributions as good as, but not better than, the polynomial method, while the soil resistance distributions are inferior. The use of NAG subroutines limits the calculated distributions to bending moment, shear and soil resistance as displacements could not be calculated by the splines generated with these subroutines.

CHAPTER FIVE

THE RESULTS AND IMPLICATIONS OF THE CENTRIFUGE MODEL TESTS

5.1 INTRODUCTION

In this chapter the experimental results obtained from the tests described in Chapter 3 will be presented and discussed.

The series of centrifuge tests produced results which will be used to study the effect on the behaviour of the piles of variations in their length, diameter, flexural rigidity and the load eccentricity.

The particular results used to define the behaviour of the piles are the deflection at the soil surface and the magnitude and position of the maximum bending moment, calculated using the polynomial method described in Section 4.2.

5.2 RESULTS

5.2.1 Applied Horizontal Load and Pile Deflection at the Soil Surface

The relationship between applied horizontal load and pile deflection at the soil surface is illustrated in Figs. 5.1 to 5.9 for length, diameter, flexural rigidity and the load eccentricity variations. Figures 5.1 to 5.3 show the variations for each pile for various lengths and load eccentricities.

Figs. 5.4 to 5.6 illustrate the effect of load eccentricity by selecting two lengths and two eccentricities for each pile.

Figure 5.7 illustrates the effect of the diameter by considering pairs of piles of the same length and flexural rigidity.

Figures 5.8 and 5.9 illustrate the effect of flexural rigidity by considering pairs of piles of the same length and diameter.

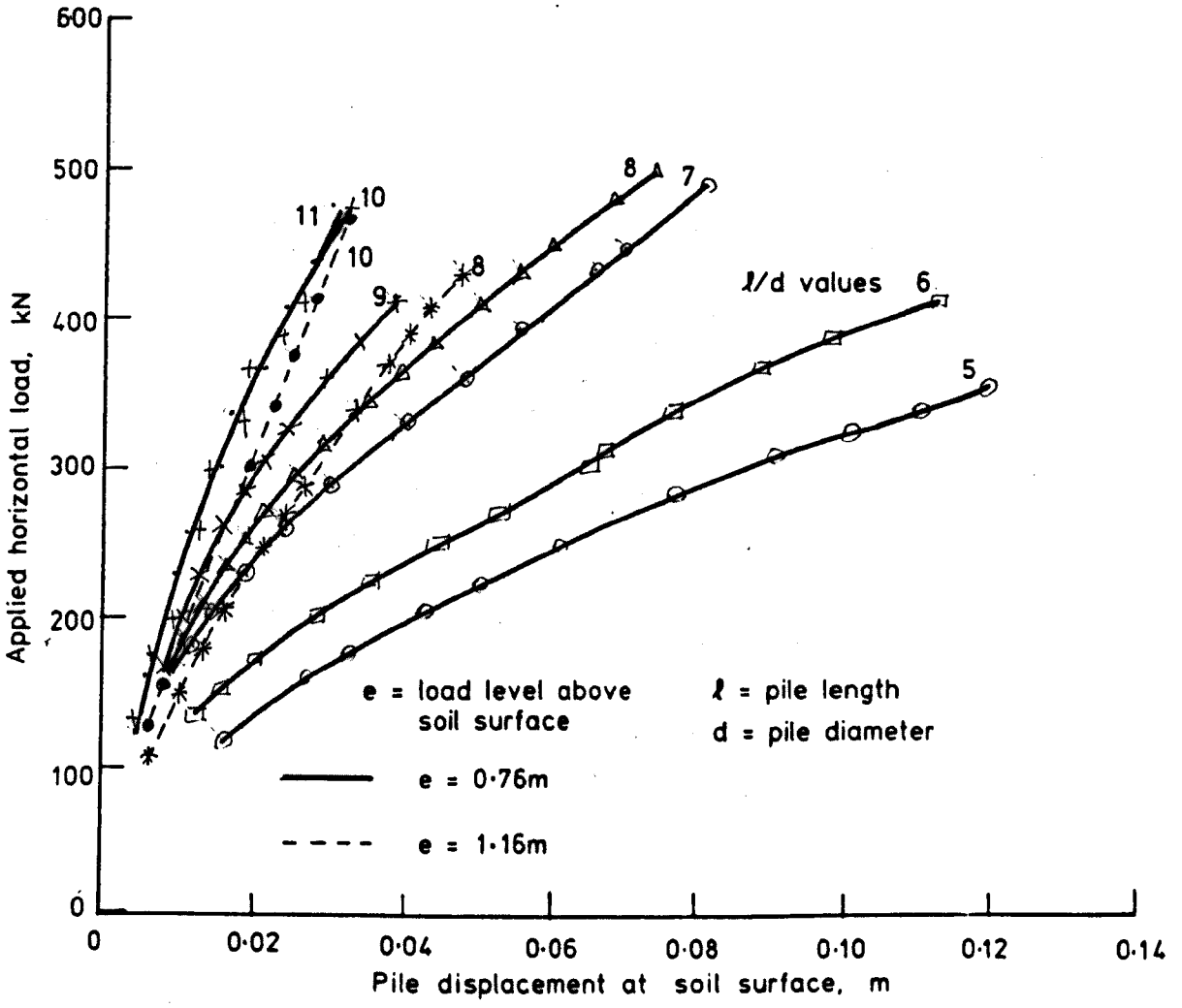

FIG. 5.1 APPLIED LOAD vs. PILE DISPLACEMENT AT SOIL SURFACE

PILE No. 1 ($d = 0{\cdot}76m$, $EI = 7{\cdot}73\ 10^5 kNm^2$)

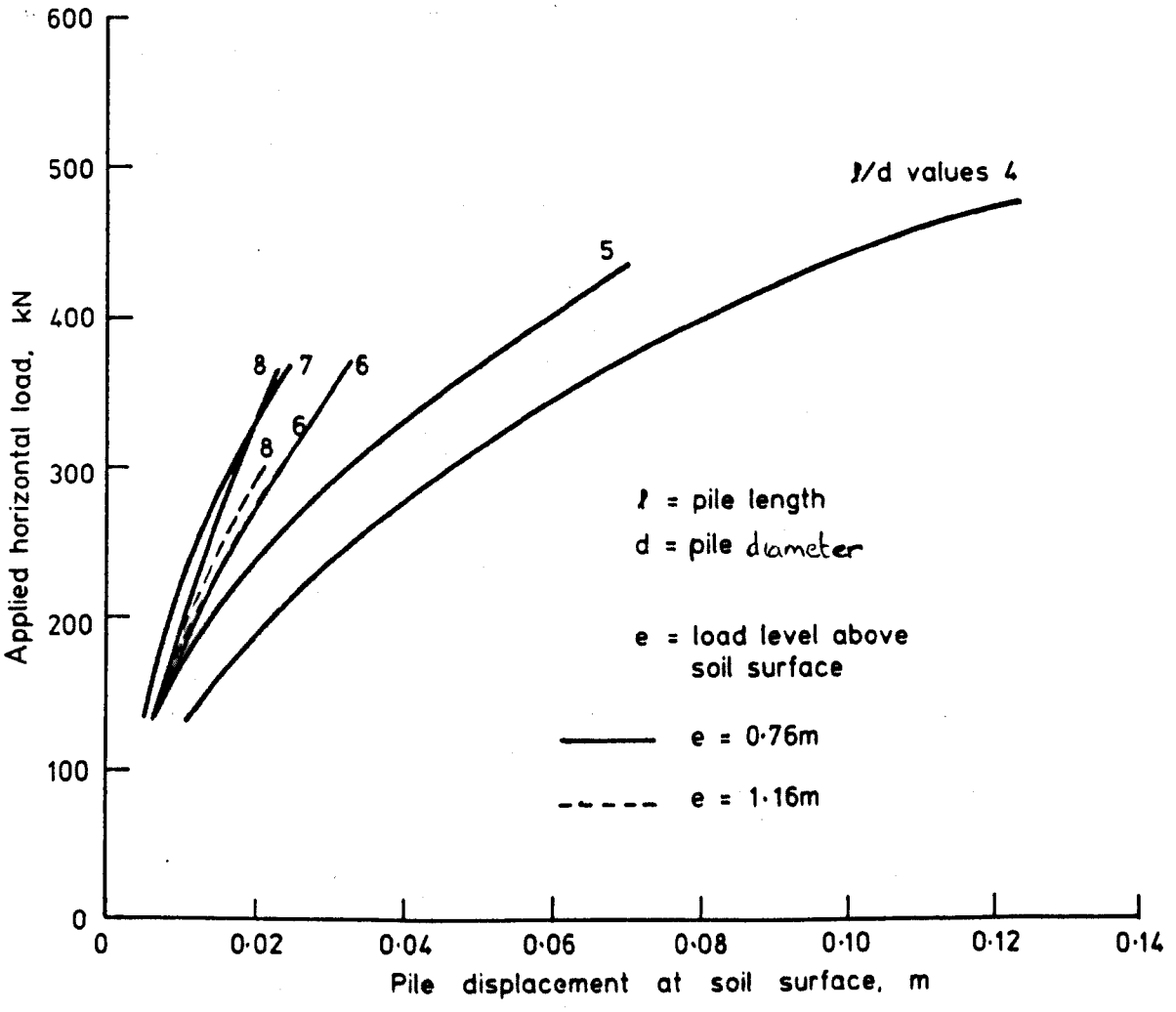

FIG. 5.2. APPLIED LOAD vs. PILE DISPLACEMENT AT SOIL SURFACE

PILE No. 2 (d= 0·98m, EI= 7·35 10^5kNm^2)

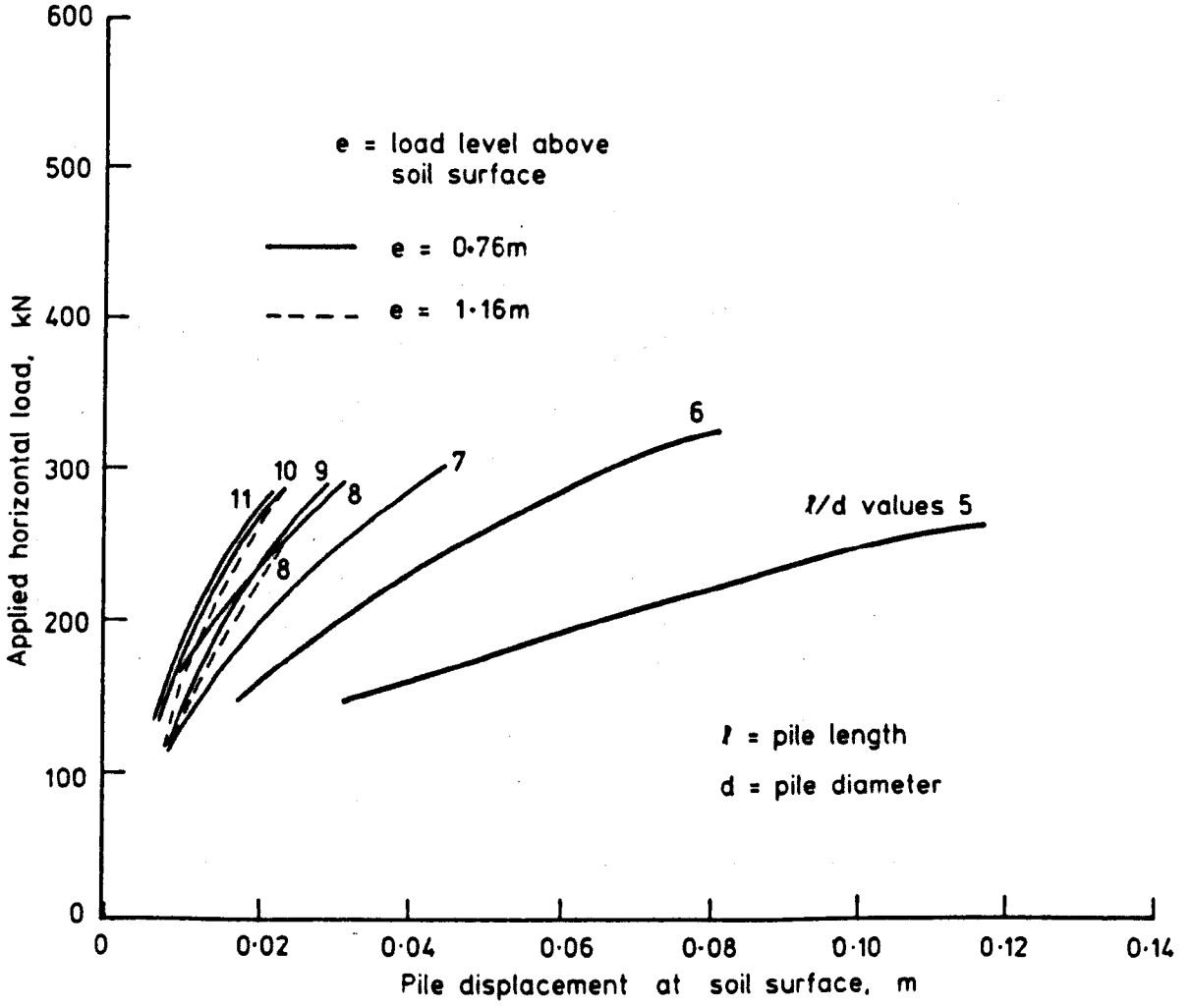

FIG. 5. 3. APPLIED LOAD vs. PILE DISPLACEMENT AT SOIL SURFACE

PILE No. 3 (d = 0·76m EI = 4·02 10^5kNm^2)

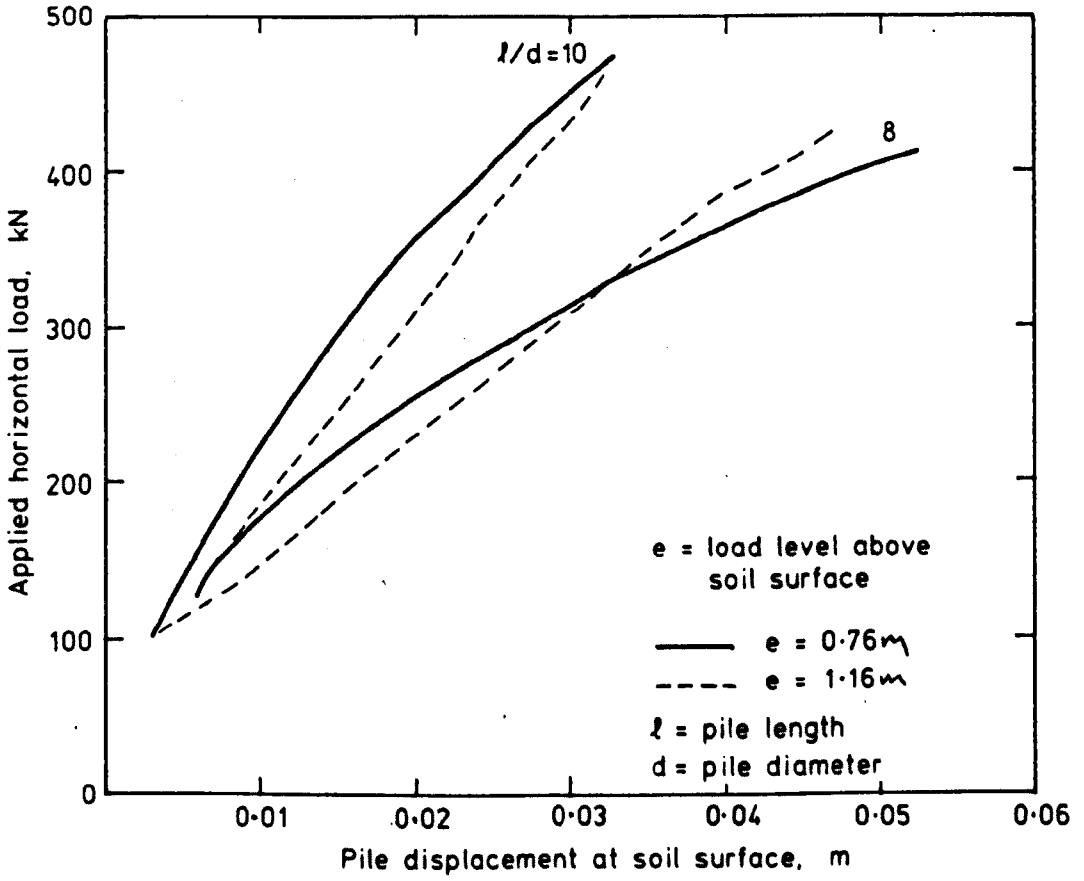

FIG. 5.4. COMPARATIVE INFLUENCE OF LOAD ECCENTRICITY ON PILE DEFLECTION. PILE No. 1

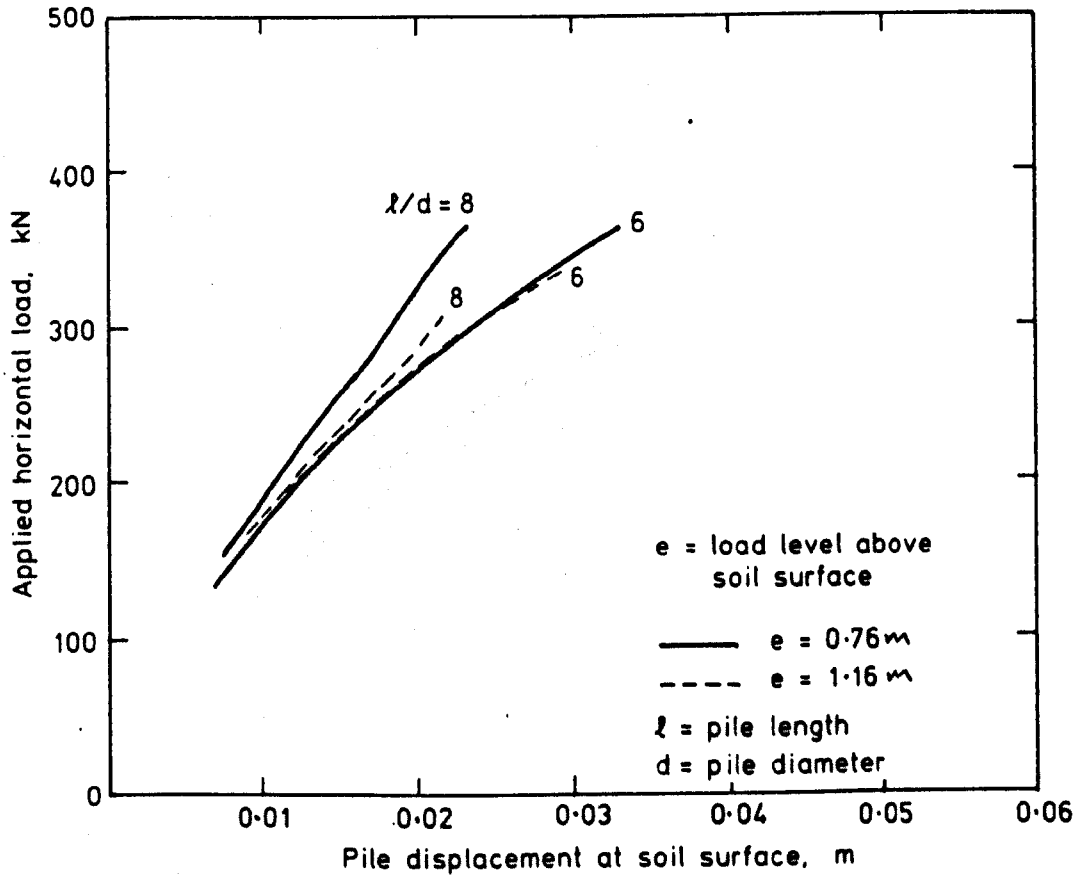

FIG. 5.5. COMPARATIVE INFLUENCE OF LOAD ECCENTRICITY ON PILE DEFLECTION PILE No. 2

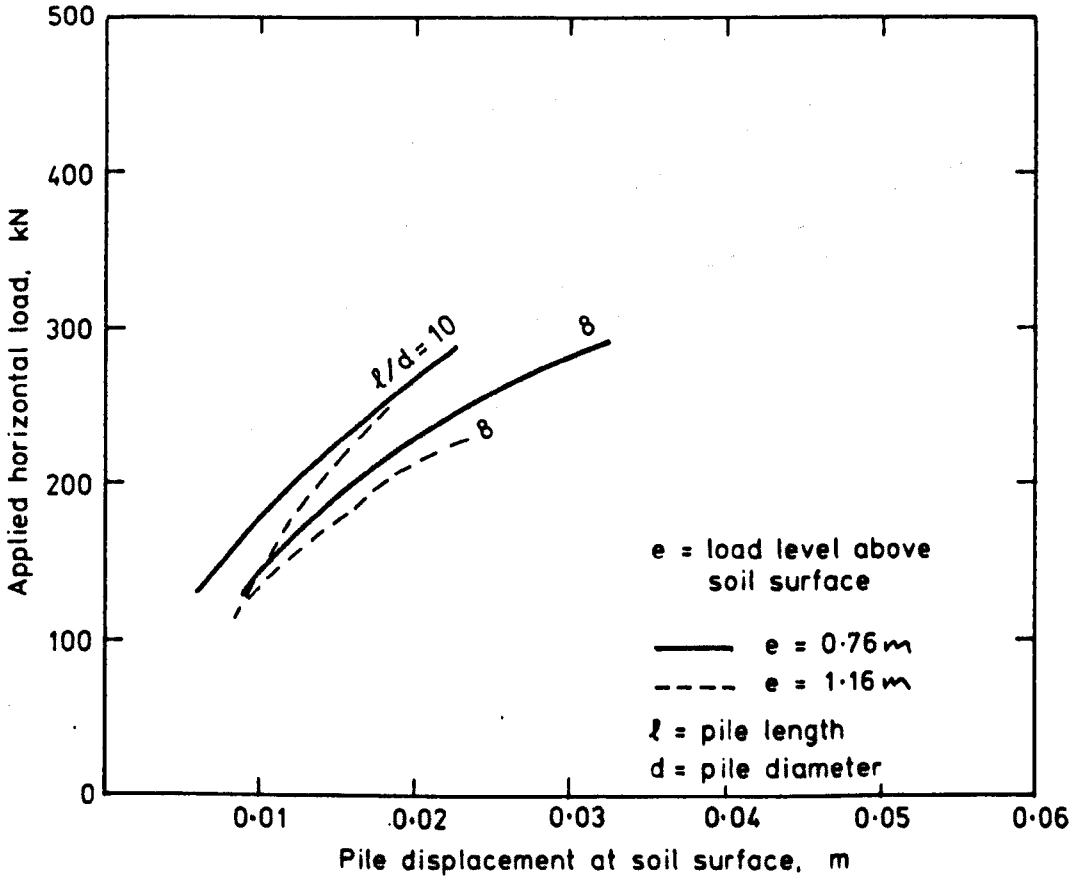

FIG. 5. 6. COMPARATIVE INFLUENCE OF LOAD ECCENTRICITY ON PILE DEFLECTION PILE No. 3

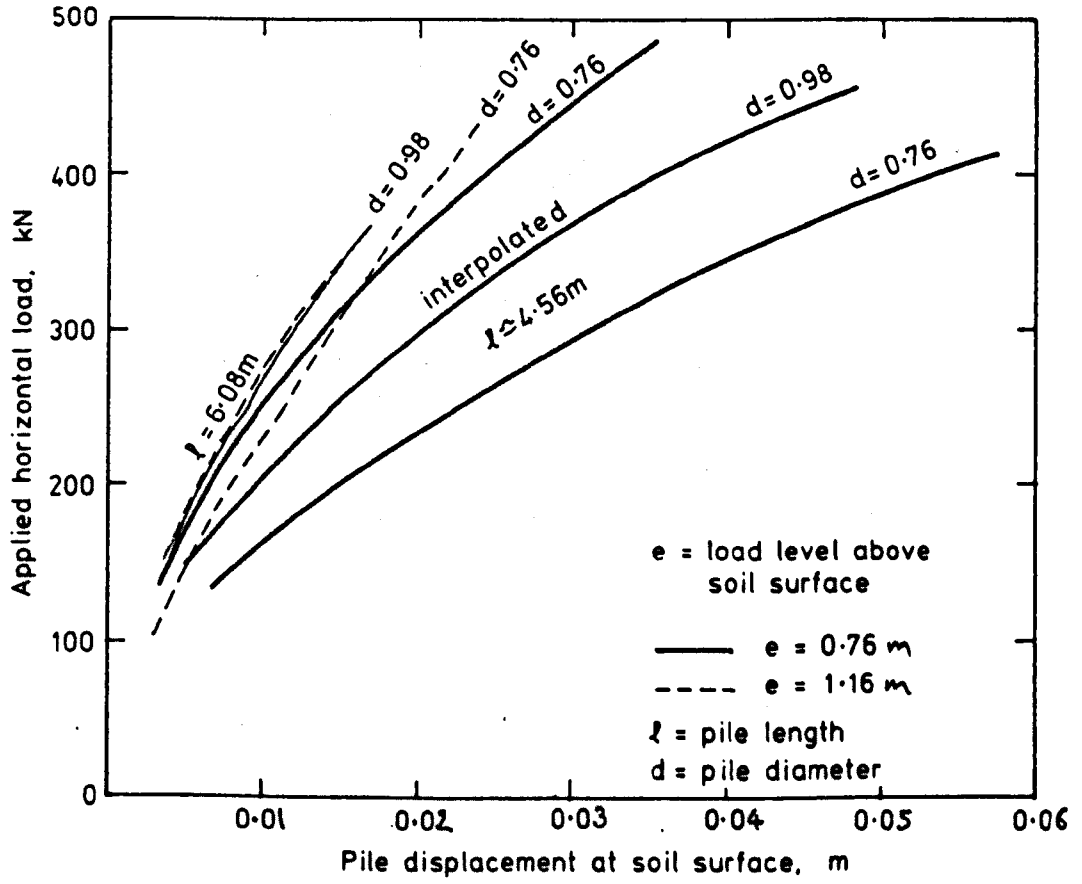

FIG. 5. 7. INFLUENCE OF PILE DIAMETER ON PILE DEFLECTION PILES No. 1 & 2

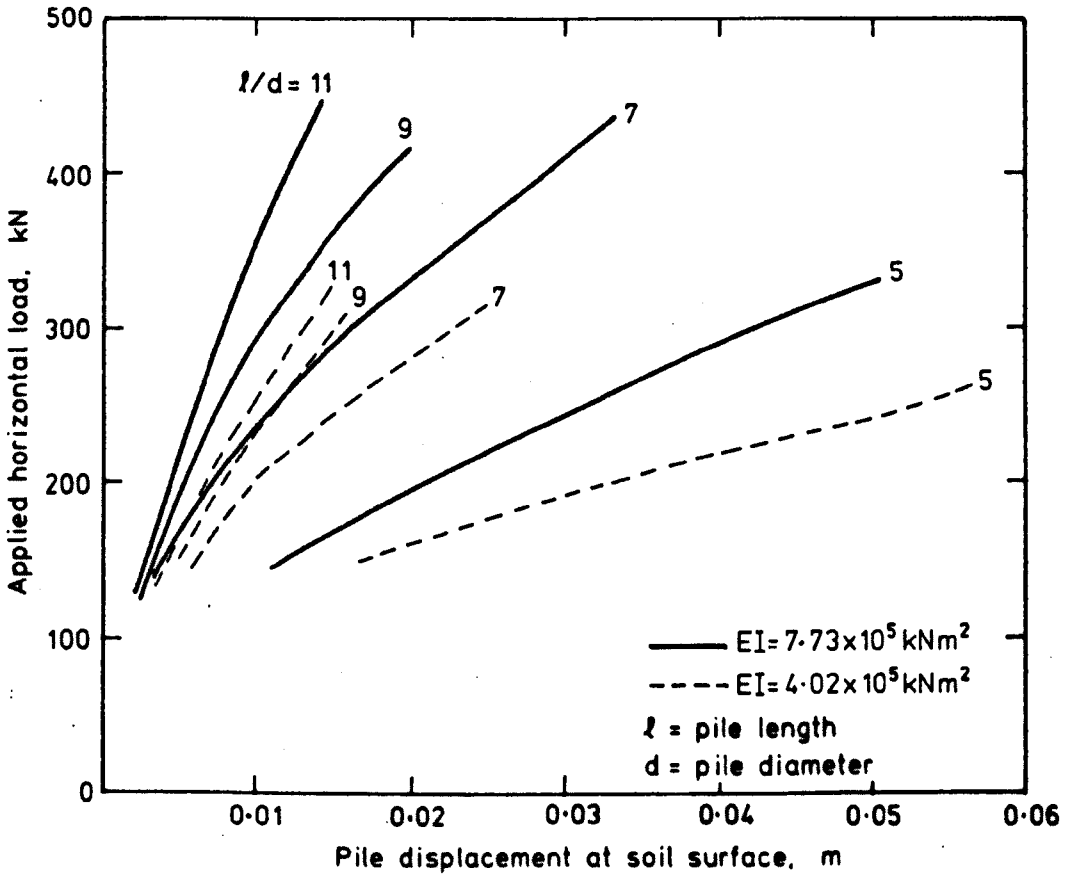

FIG. 5.8. INFLUENCE OF FLEXURAL RIGIDITY ON PILE DEFLECTION PILES No. 1 & 3 (e = 0·76)

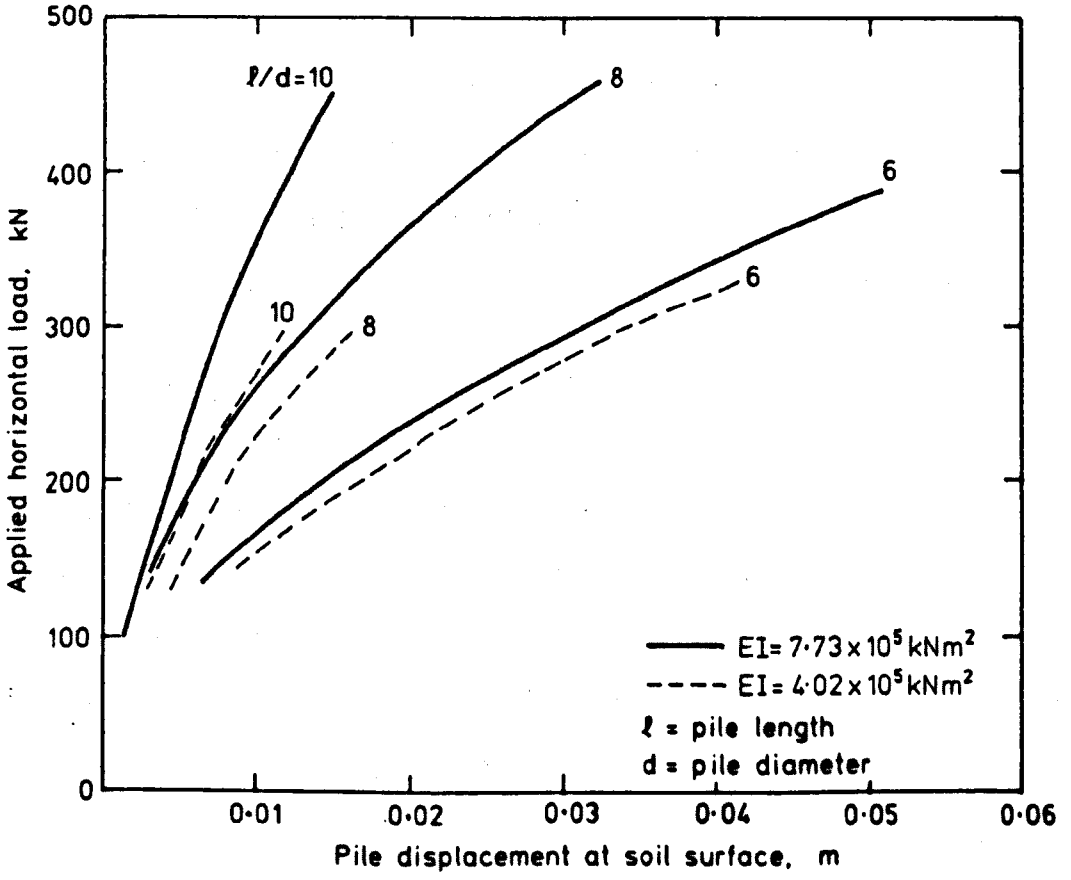

FIG. 5. 9. INFLUENCE OF FLEXURAL RIGIDITY ON PILE DEFLECTION PILES No. 1 & 3 (e = 0·76)

5.2.2 Applied Horizontal Load and Maximum Bending Moment

The relationship between applied horizontal load and the maximum bending moment is illustrated in Figs. 5.10 to 5.18 for length, diameter, flexural rigidity and load eccentricity variations.

Figures 5.10 to 5.12 show the variations for each pile for various lengths and load eccentricities.

Figures 5.13 to 5.15 illustrate the effect of load eccentricity by selecting two lengths and two eccentricities for each pile.

Figure 5.16 illustrates the effect of the diameter by considering pairs of piles of the same length and flexural rigidity.

Figures 5.17 and 5.18 illustrate the effect of flexural rigidity by considering pairs of piles of the same length and diameter.

5.2.3 Position of the Maximum Bending Moment

The position of the maximum bending moment varies with increasing applied horizontal load. This is illustrated for pile No. 1 in Fig. 5.19 which shows the depth of the maximum bending moment plotted against the maximum bending moment for increasing load and in Table 5.1 which shows the average value of the ratio of depth of maximum bending moment to pile length for each pile at various length to diameter ratios.

5.2.4 Influence of Pile Length on Pile Deflection at the Soil Surface

Fig. 5.20 shows the pile deflection plotted against the pile length at a constant applied horizontal load of 250 KN.

5.3 DISCUSSION

The purpose of the experimental work described in this chapter was to determine the principal factors governing the behaviour

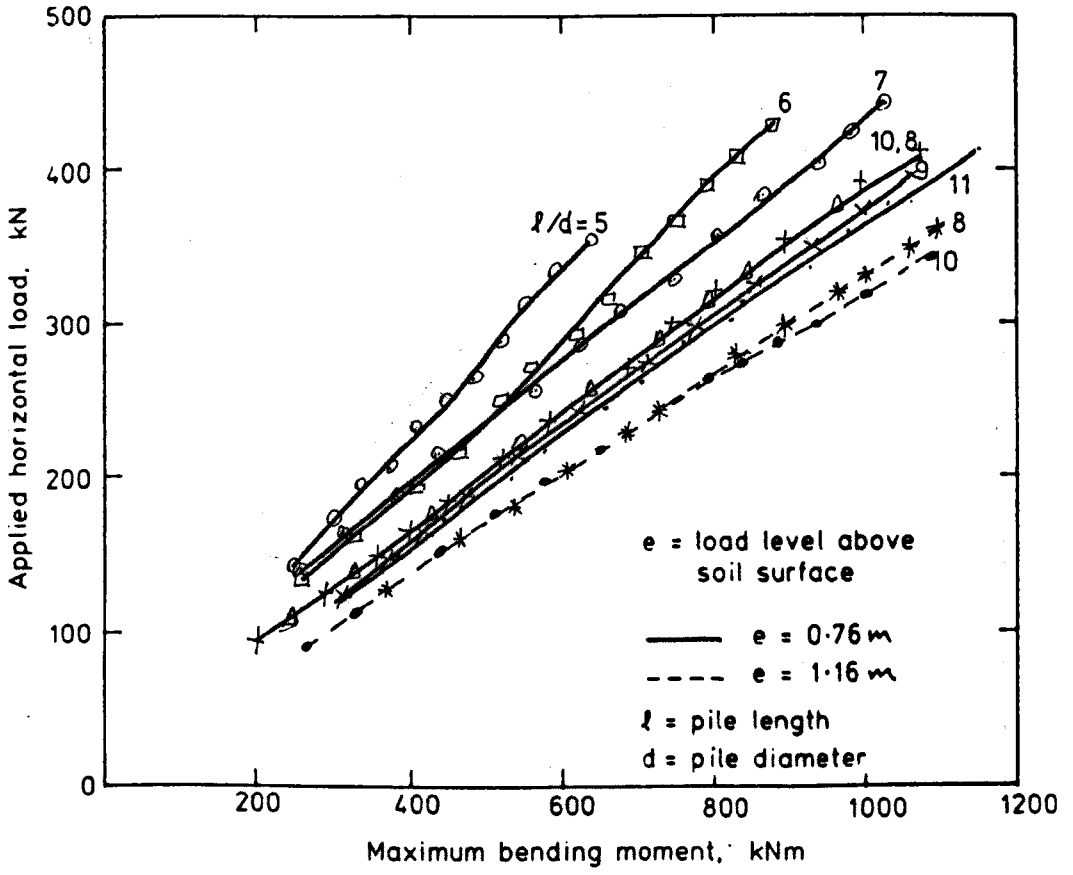

FIG. 5.10. APPLIED LOAD vs. MAXIMUM BENDING MOMENT

PILE No. 1

For long piles $\hat{M} = (e + 2)\,P$

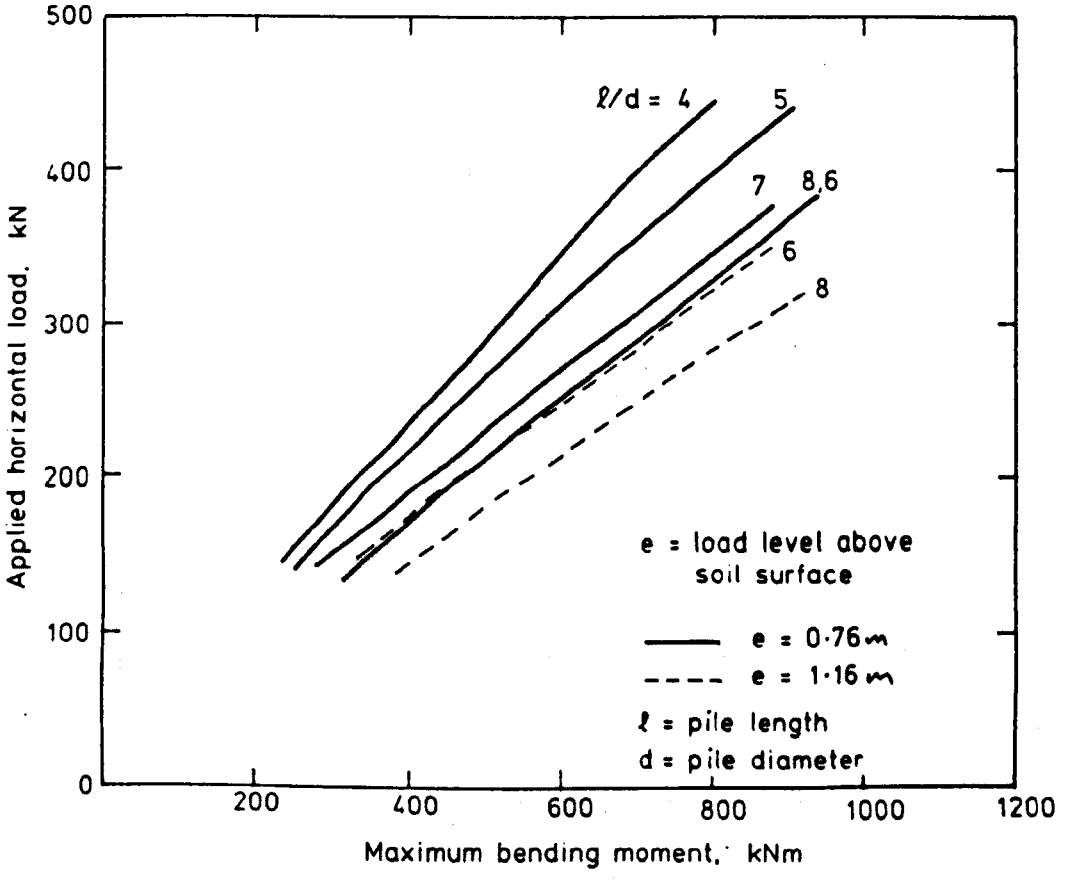

FIG. 5.11. APPLIED LOAD vs. MAXIMUM BENDING MOMENT

PILE No. 2

For long piles $\hat{M} = (e + 1{\cdot}8)\, P$

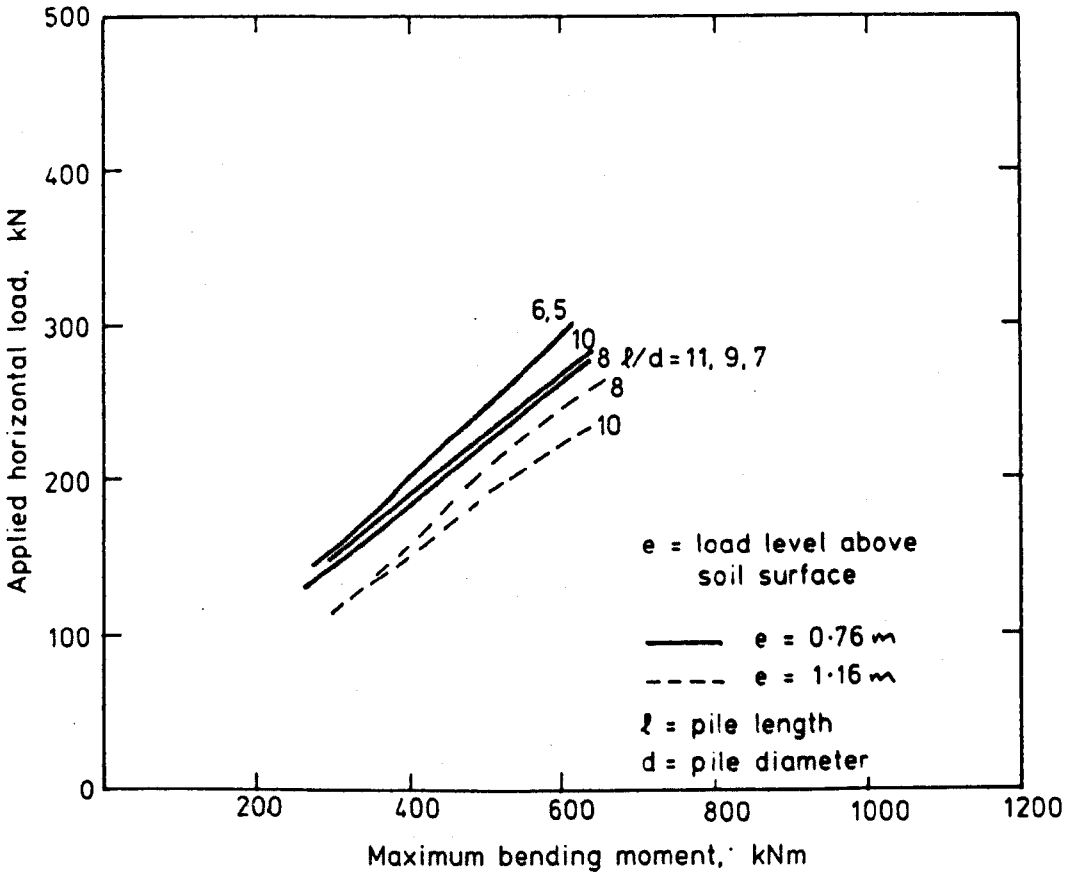

FIG. 5.12. APPLIED LOAD vs. MAXIMUM BENDING MOMENT

PILE No. 3

For long piles $M = (e + 1{\cdot}6)\,P$

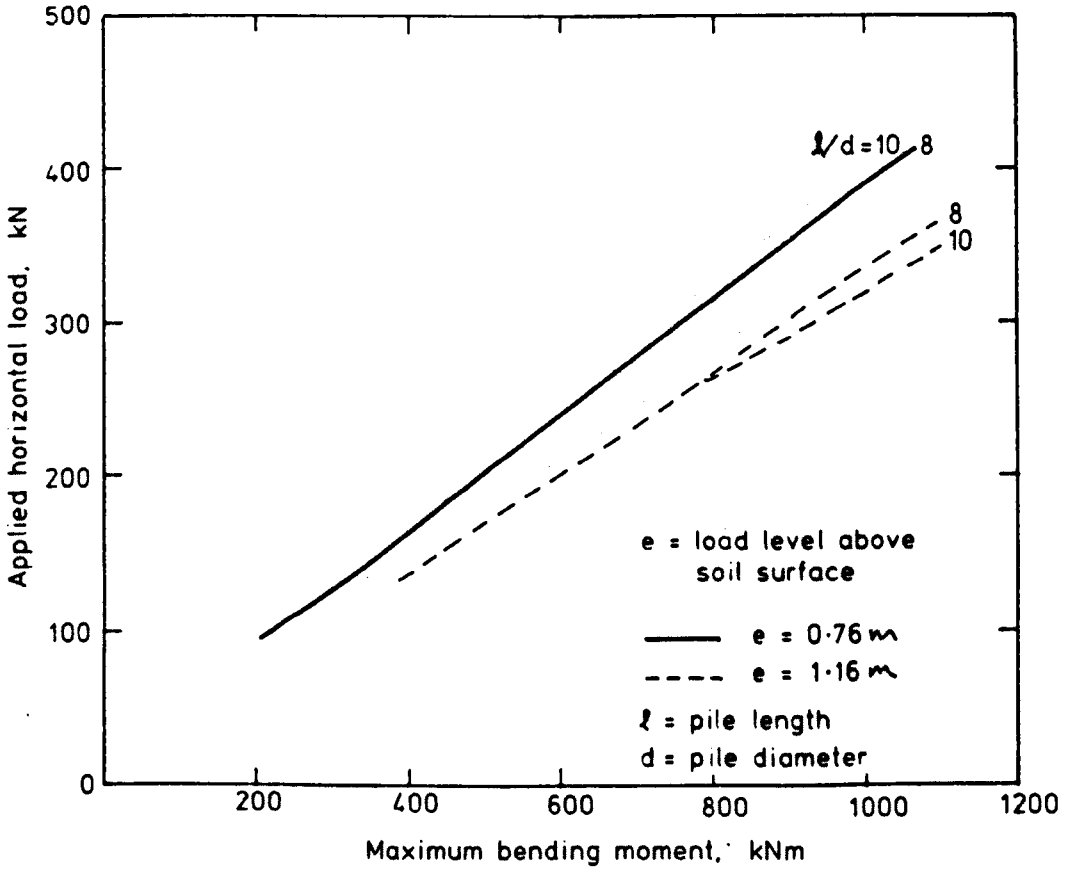

FIG. 5.13. COMPARATIVE INFLUENCE OF LOAD ECCENTRICITY ON THE MAXIMUM BENDING MOMENT

PILE No. 1

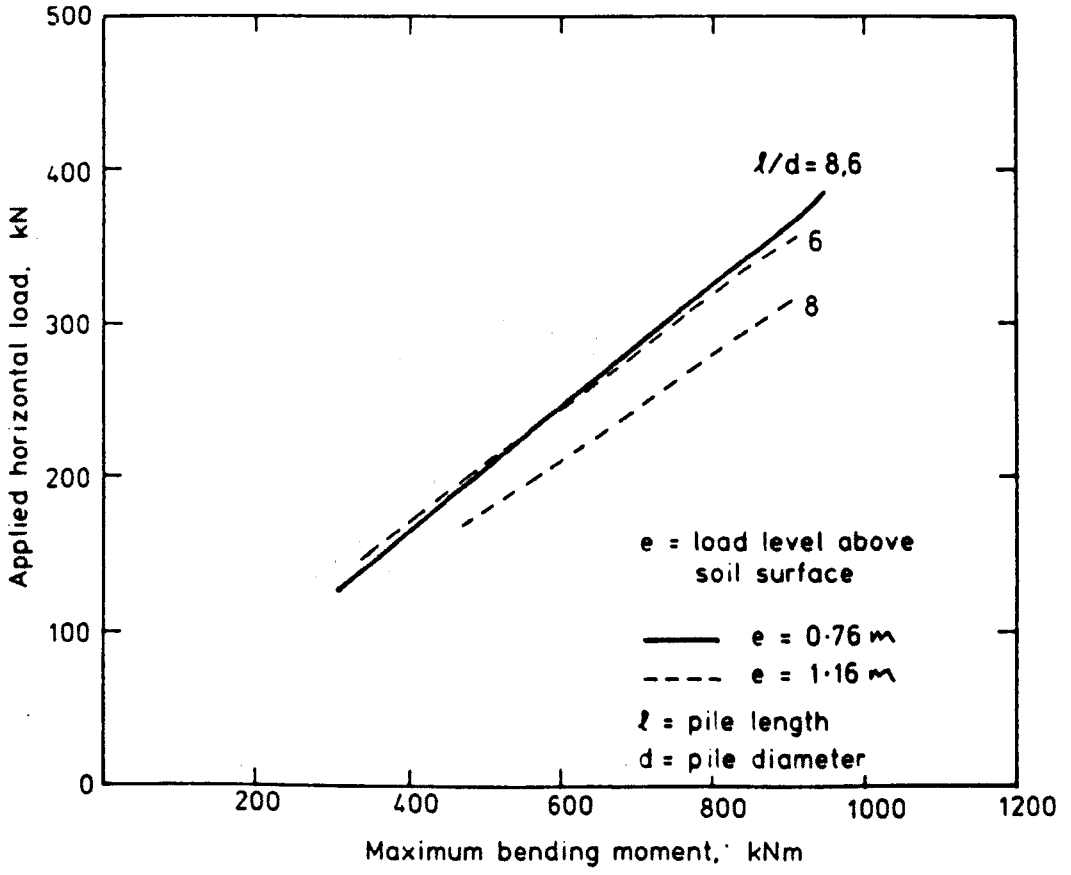

FIG. 5.14. COMPARATIVE INFLUENCE OF LOAD ECCENTRICITY ON THE MAXIMUM BENDING MOMENT

PILE No. 2

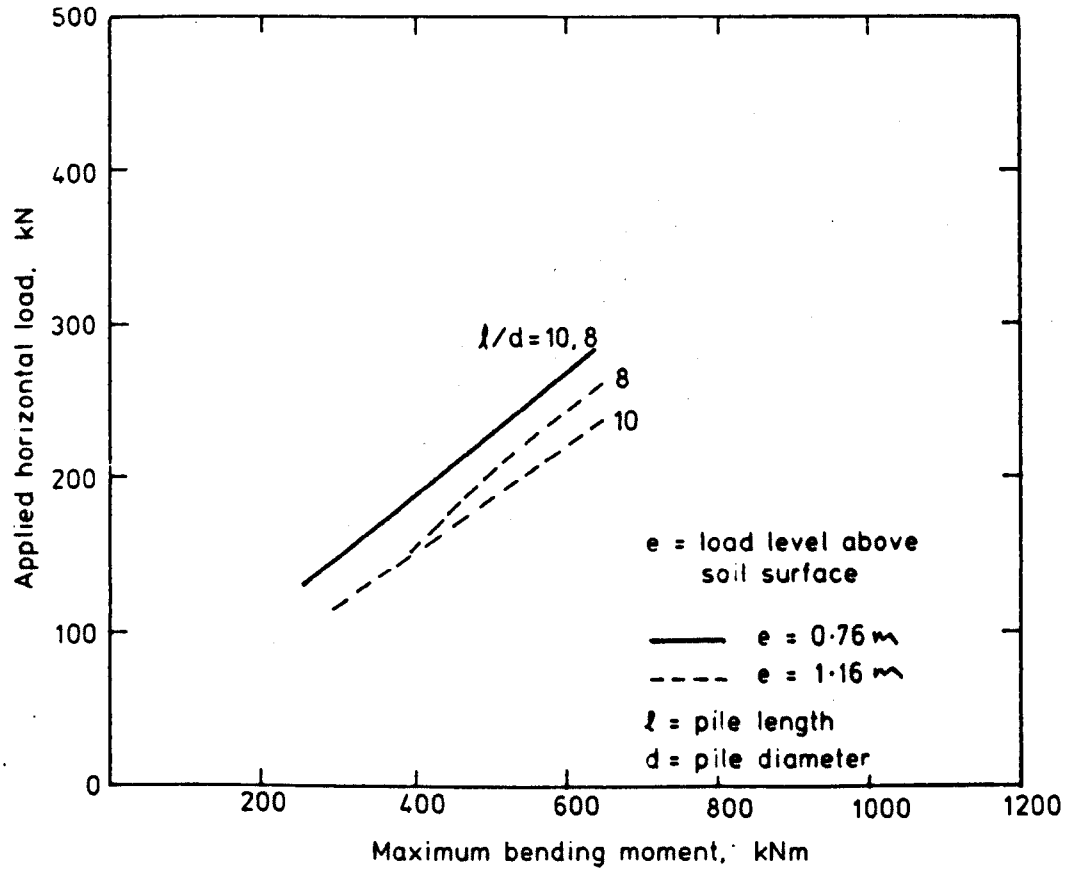

FIG. 5. 15. COMPARATIVE INFLUENCE OF LOAD ECCENTRICITY ON THE MAXIMUM BENDING MOMENT PILE No. 3

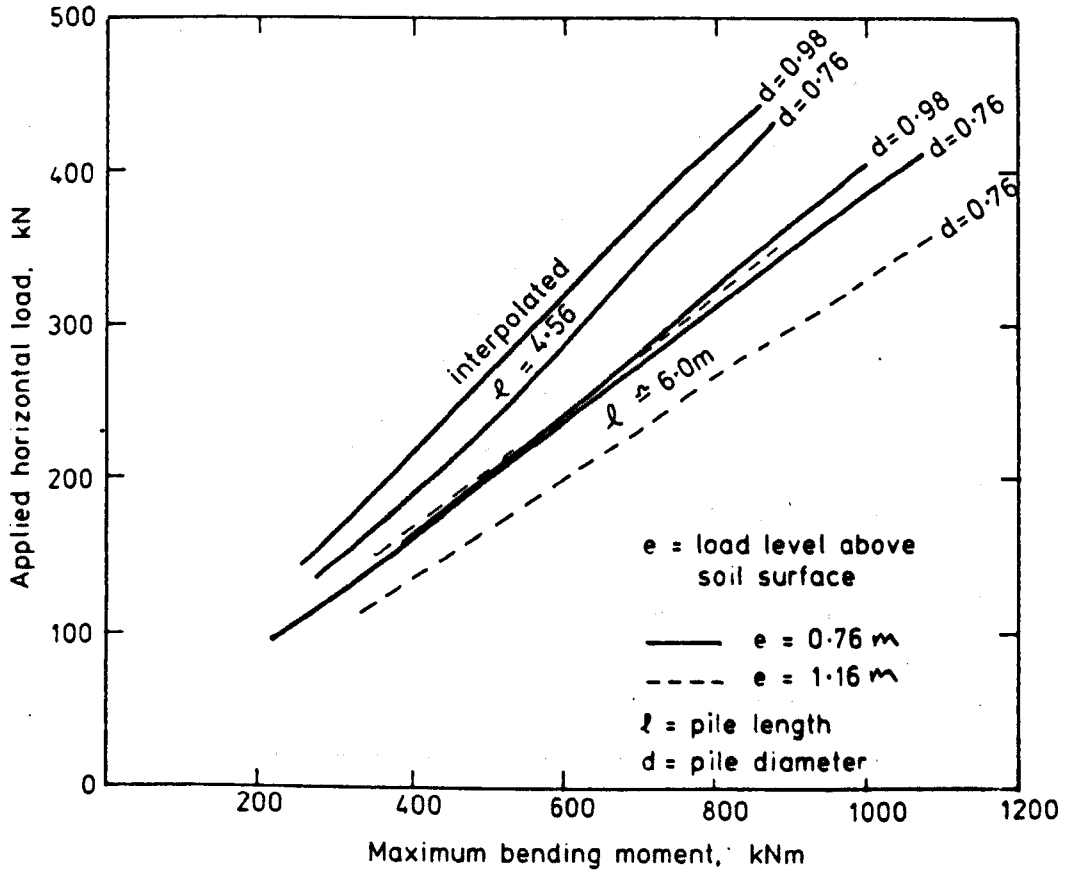

FIG. 5.16. INFLUENCE OF PILE DIAMETER ON THE MAXIMUM BENDING MOMENT. PILES No. 1 & 2

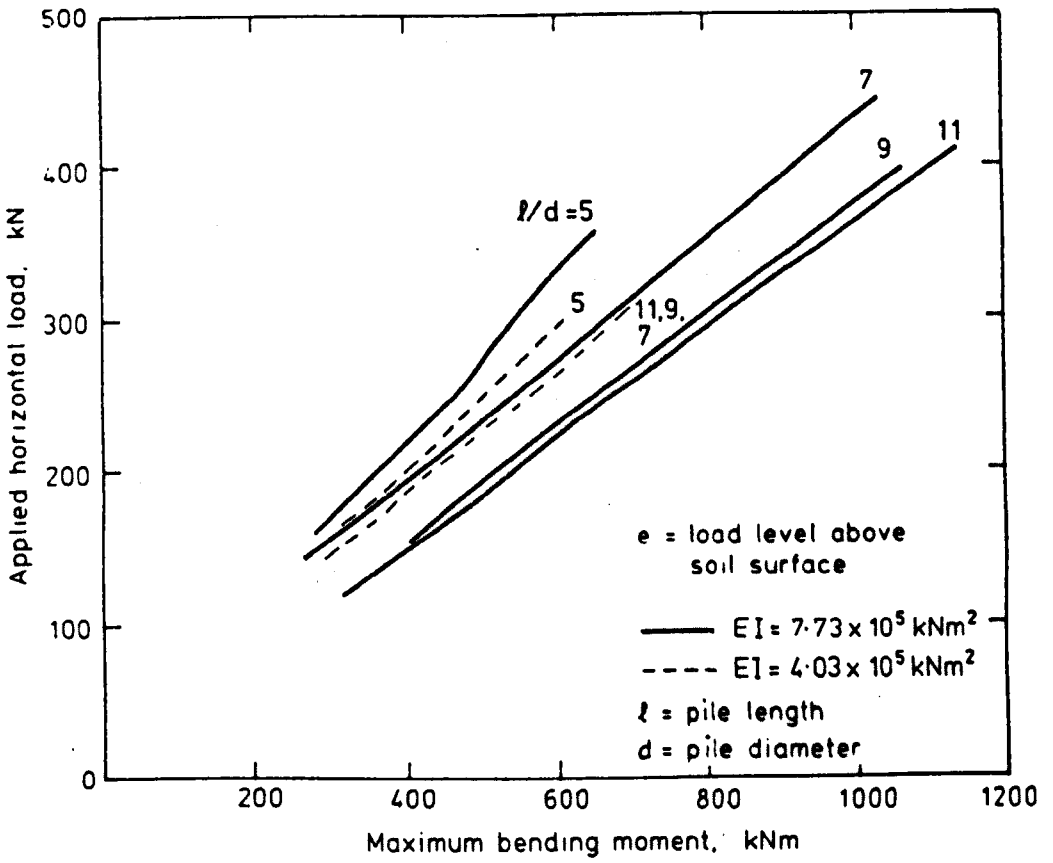

FIG. 5.17. INFLUENCE OF FLEXURAL RIGIDITY ON THE MAXIMUM BENDING MOMENT PILES No. 1 & 3 (e = 0·76)

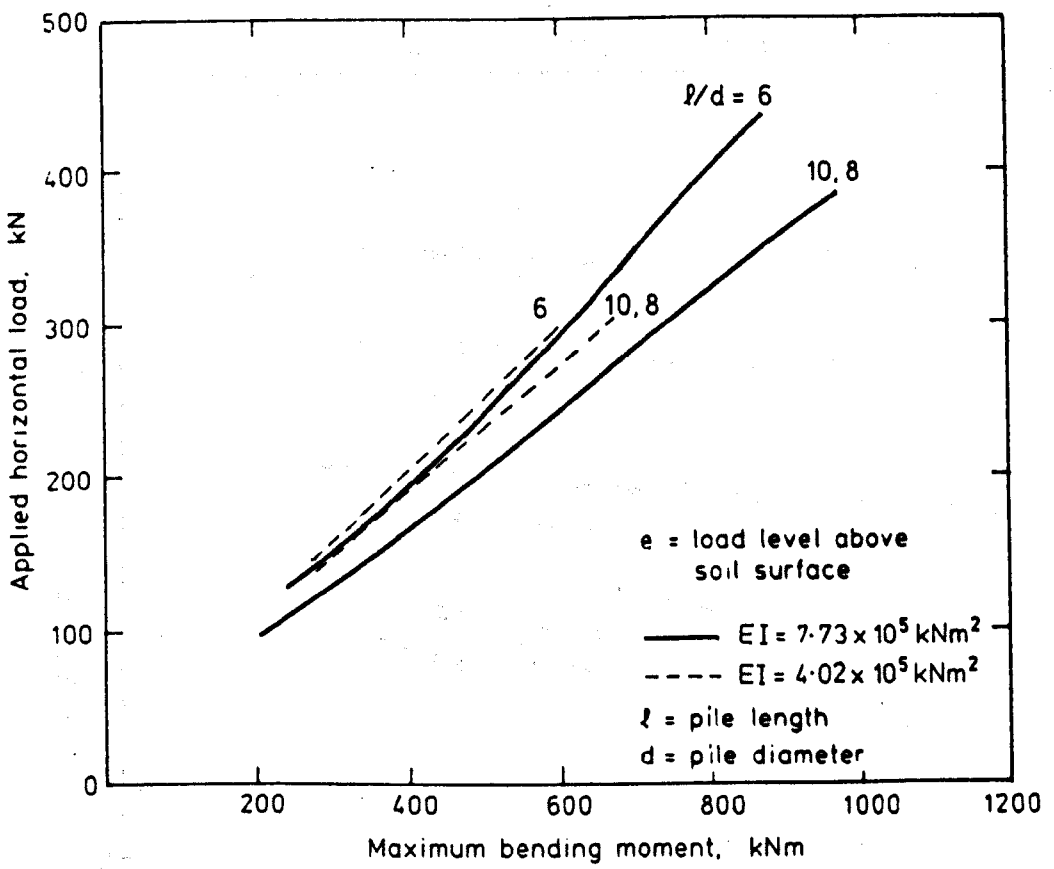

FIG. 5.18. INFLUENCE OF FLEXURAL RIGIDITY ON THE MAXIMUM BENDING MOMENT PILES No. 1 & 3 (e = 0·76)

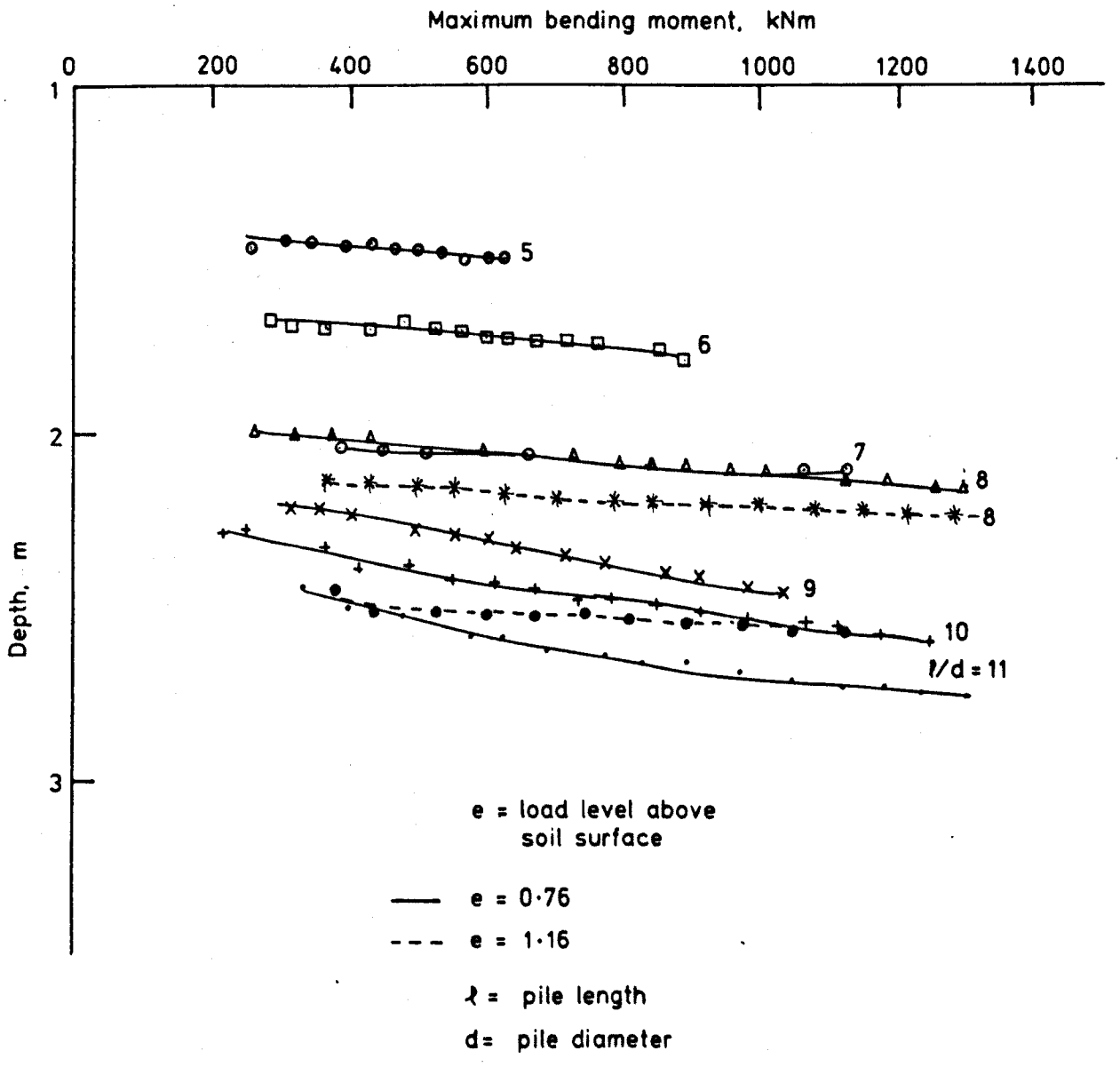

FIG. 5.19. MAGNITUDE vs. POSITION OF THE MAXIMUM BENDING MOMENT PILE No. 1 ($d = 0{\cdot}76m$, $EI = 7{\cdot}73 \times 10^5 kNm^2$)

	ℓ/d	Pile No.1 $\frac{z_{max}}{\ell_{max}}$	Pile No.2 $\frac{z_{max}}{\ell_{max}}$	Pile No.3 $\frac{z_{max}}{\ell_{max}}$
e = 0.76 m	11	0.31	-	0.30
	10	0.32	-	0.33
	9	0.34	-	0.34
	8	0.36	0.24	0.37
	7	0.39	0.31	0.39
	6	0.38	0.33	0.41
	5	0.39	0.39	0.42
	4	-	0.27	-
e = 1.16 m	10	0.33	-	0.26
	8	0.34	0.25	0.33
	6	-	0.32	-

Table 5.1 : Average ratio of (depth of Max BM/pile length) for each pile and various ℓ/d ratios.

Pile No. 1 d = 0.76 m, EI = 7.73×10^5 KNm^2

Pile No. 2 d = 0.98 m, EI = 7.35×10^5 KNm^2

Pile No. 3 d = 0.76 m, EI = 4.02×10^5 KNm^2

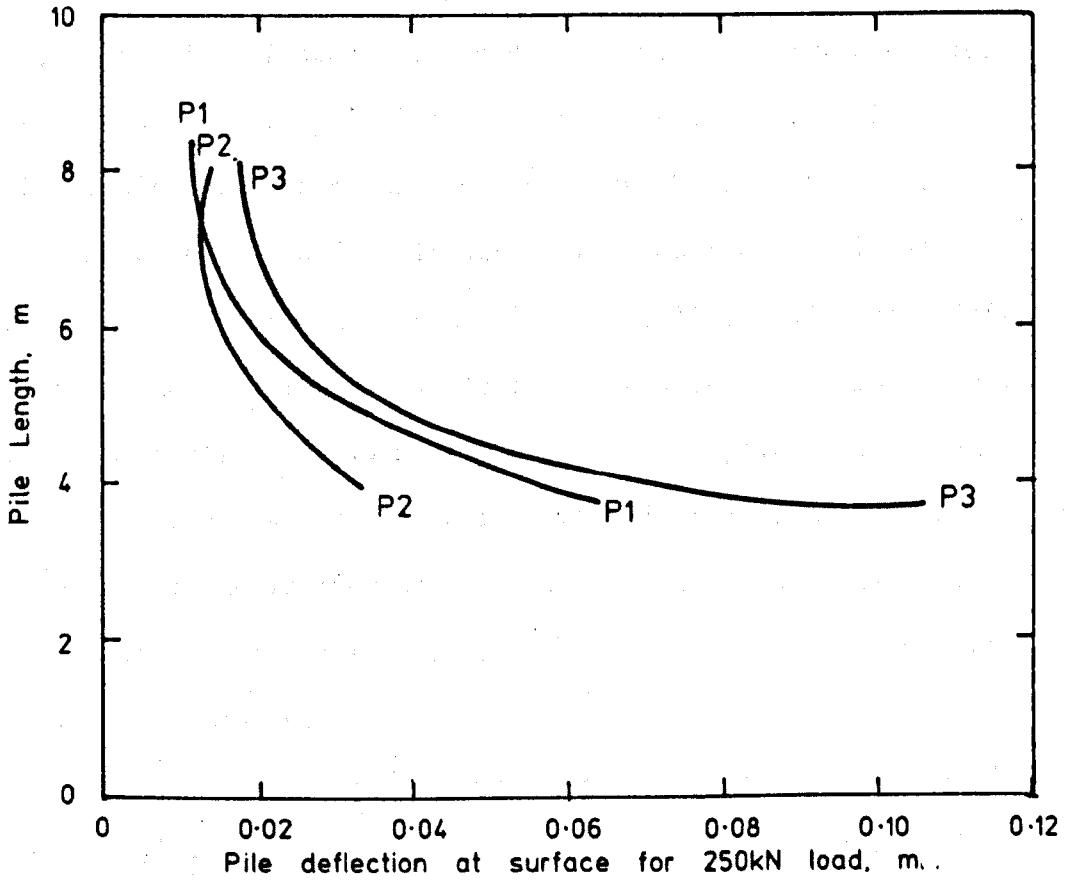

FIG. 5. 20. PILE LENGTH vs. PILE DISPLACEMENT AT SOIL SURFACE AT AN APPLIED HORIZONTAL LOAD. OF 250kN

of a laterally loaded pile in sand and will be discussed in this light.

5.3.1 Applied Horizontal Load and Pile Deflection at the Soil Surface

The effect of varying the length of pile is illustrated in Figs. 5.1 to 5.3. As expected a reduction in pile length results in an increase in deflection at any given load. The relationship is not linear, as the load increases, the displacement for any given load difference increases. This indicates the non-linearity of the soil behaviour, since the pile was never strained beyond its elastic limit.

Figures 5.4 to 5.6 illustrate that an increase in applied bending moment, due to an increase in the applied load eccentricity, produces an increase in pile deflection. However, this increase is small and the deflection is mostly due to the applied horizontal load.

Figure 5.7 shows that a reduction in pile diameter causes an increase in pile deflection at any given load. This is significant in that it is not accounted for in any of the theoretical approaches presented in Chapter 6.

Figures 5.8 and 5.9 show that reducing the flexural rigidity of the pile yields an increase in the pile deflection at any given load.

5.3.2 Applied Horizontal Load and Maximum Bending Moment

The effect of varying the pile length is illustrated in Figs. 5.10 to 5.12. They show that a reduction in pile length results in a reduction of the maximum bending moment. They also indicate a linear relationship between the applied horizontal load and the maximum bending moment.

Figures 5.13 to 5.15 show that increasing the load eccentricity and hence, the applied bending moment, increases the maximum bending

moment by the same amount.

Figure 5.16 shows that a reduction in pile diameter results in an increase in the maximum bending moment. Again, none of the theoretical approaches allow for this effect.

Figures 5.17 and 5.18 show that for the longer piles, reducing the flexural rigidity of the pile yields a reduction in the maximum bending moment.

5.3.3 Position of the Maximum Bending Moment

Figure 5.19 shows that as the applied horizontal load increases the depth of the maximum bending moment increases indicating a local plastic failure of the soil at ground level. In a purely elastic medium the depth of the maximum bending moment would remain constant. The same is true for all the piles tested.

Table 5.1, together with Fig. 5.19 shows that as the length of the pile increases, the depth of the maximum bending moment increases. Also, an increase in load eccentricity has little effect upon the depth of the maximum bending moment verifying that pile-soil interaction depends more upon the applied horizontal load.

A reduction in pile diameter causes an increase in the depth of the maximum bending moment. This is consistent with the observed increase in deflection since this would cause an increase in the depth to which the soil would fail plastically at the top of the pile, hence causing an increase in the depth of the maximum bending moment.

Also, from Table 5.1, reducing the flexural rigidity indicates a slight trend towards increasing the depth of the maximum bending moment.

5.3.4 Influence of Pile Length on Pile Deflection at the Soil Surface

This is shown in Fig. 5.20 which indicates that there is a length of pile over which any increase in length does not affect the pile displacement. This critical length is of the order of 9 to 10 m for the piles tested in this sand. This length is not significantly affected by diameter and flexural rigidity and does not conflict with theoretical predictions (Section 6.4).

However, more experiments are necessary with piles of smaller diameter and flexural rigidity to verify this observation.

5.4 CONCLUSIONS

The behaviour of laterally loaded piles in sand, as observed in centrifuge model tests, have been presented and discussed.

It has been shown that an increase in pile length, flexural rigidity and diameter reduce the deflections and the depth of the maximum bending moment. Also, the applied horizontal load has a greater relative effect upon the deflection than the applied bending moment.

The maximum bending moment has been found to increase with increase in pile length and flexural rigidity and reductions in pile diameter.

The difference between the maximum bending moment and the applied moment at the soil surface is mainly due to the applied horizontal load and for the longer piles the maximum bending moments can be expressed as $M_{max} = (e + \alpha)H$. For the pile tested, approximate values of α deduced from Figs. 5.10 to 5.12 are

Pile No.	1	2	3
α	2.0	1.8	1.6

There appears to be a critical length of pile above which the displacement is not effected, which is not significantly dependent on pile diameter and flexural rigidity.

CHAPTER SIX

AN ASSESSMENT OF THE MERITS OF SOME THEORETICAL APPROACHES

6.1 INTRODUCTION

There are two commonly adopted methods of calculating the deformations of a laterally loaded pile, based on either the assumption that the soil may be replaced by a Winkler spring medium, or by an elastic continuum.

In the Winkler spring method the laterally loaded pile is replaced by an elastic beam supported by a series of discrete springs acting along the length of the beam. The spring stiffness represents the stiffness of the soil and is generally referred to as the coefficient of subgrade reaction, Terzaghi[33].

Hetenyi[16] produced a series of closed form solutions for this method for a variety of loading conditions and end restraints on the pile.

This simple approach has been improved by allowing the coefficient of subgrade reaction to vary along the length of the pile.

Reese and Matlock[28] and Matlock and Reese[20] carried out a dimensional analysis of the problem and developed a series of equations, see Section 6.2.1, containing similar groups of parameters when the coefficient of subgrade reaction was either constant (homogeneous soil), or varied linearly with depth (non-homogeneous soil). These equations contain a set of coefficients, related to the lateral and moment loading, which can be obtained using the characteristic length defined in Eq. (6.2) from a series of graphs produced by Matlock and Reese[20].

The method has been furthered by Broms[5] for long flexible and short rigid piles and Davison and Gill[10] for a two-layer soil system.

A limitation of the Winkler model is that it does not represent a continuum and, therefore, does not permit transference of shear stress. This may lead to an over estimation of displacements.

A further development in the method was to replace the linear springs with non-linear p-y (soil-resistance-displacement) curves, Matlock[19], Reese, Cox and Koop[27], and Reese and Cox[26]. However using this method it is difficult to choose appropriate p-y curves for a given pile size and soil type. Therefore, pile tests are recommended to confirm pile behaviour.

The second method of analysis, for an elastic pile embedded in an elastic continuum, is based on the integration of Mindlin's solutions of the stresses caused by a point load acting within an isotropic elastic continuum.

This analysis is known as the elastic continuum or integral equation method.

Poulos[21,22] idealised the pile as an infinitely thin strip with the same width and bending rigidity as the prototype pile and used finite differences to solve the differential equations. He produced equations expressing surface deflection and rotation in terms of dimensionless influence factors which can be determined graphically using a dimensionless flexibility factor and the length to depth ratio of the pile, see Section 6.2.2.

The method was extended by Poulos[23] to allow for soil yielding and by Banerjee and Davies[2] to include a non-homogeneity index, namely the ratio of Young's modulus at the surface to that at the pile base.

Evangelista and Viggani[13] improved the accuracy of solutions given by Poulos' method by varying the size of the elements down the pile.

Randolph[24] carried out a series of finite element analyses, using the same method as that described in Chapter 2 but with triangular rather than rectangular elements, for homogeneous and non-homogeneous soils, and fitted empirical power law expressions to the lateral deflections and rotations at the ground line. He characterised the soil stiffness by the shear modulus rather than Young's modulus and only presents solutions for flexible piles which are longer than their critical length, and, therefore, independent of the embedded length. The critical length of a pile is the length beyond which any further increase has no effect upon the pile displacement or bending moments.

6.2 THEORETICAL SOLUTIONS

It is generally accepted that sand can best be modelled as a non-homogeneous soil. Therefore, only the theoretical solutions for soil modulus increasing linearly with depth are presented here.

6.2.1 The Solution of Matlock and Reese[20]

This solution is based on the Winkler spring model. The equations for the non-homogeneous soil are:-

$$y = \frac{H_o T^3}{E_p I_p} A_y + \frac{M_o T^2}{E_p I_p} B_y$$

$$\theta = \frac{H_o T^2}{E_p I_p} A_s + \frac{M_o T}{E_p I_p} B_s$$

$$M = H_o T A_m + M_o B_m \qquad (6.1)$$

$$V = H_o A_v + \frac{M_o}{T} B_v$$

$$p = \frac{H_o}{T} A_r + \frac{M_o}{T^2} B_r$$

where y, θ, M, V and p are the displacement, slope, bending moments

shear force and pressure respectively, E_p is the Young's Modulus and I_p is the second moment of area of the pile.

The A and B coefficients relate to lateral and moment loading respectively and T is the characteristic length of the pile defined by:-

$$T = 5\sqrt{\frac{E_p I_p}{n_h}} \qquad (6.2)$$

where n_h is the rate of increase of the coefficient of horizontal sub-grade reaction with depth.

The charts for determining the coefficients A and B are reproduced in Fig. 6.1, they can be used to calculate the distributions of displacement down a pile. Similar charts are available for the calculation of slope, bending moment, shear force and pressure distributions, Figs. 6.2 and 6.3.

6.2.2 The Solution of Poulos[23]

This solution is based on the elastic continuum approach. The expressions for displacement and slope for the non-homogeneous soil are respectively

$$y_o = \frac{H_o}{N_h L^2} \left(I'_{\rho H} + \frac{e}{L} I'_{\rho m} \right) / F'_{\rho} \qquad (6.3)$$

$$\theta_o = \frac{H_o}{N_h L^3} \left(I'_{\theta H} + \frac{e}{L} I'_{\theta m} \right) / F'_{\theta}$$

where y_o and θ_o are the deflection and slope at the ground line and e is the eccentricity of the load, L is the length of the pile and N_h is the rate of increase of the Young's modulus with depth.

$I'_{\rho H}$ and $I'_{\rho m}$ are dimensionless elastic-influence factors for displacement caused by horizontal load and moment respectively. Similarly $I'_{\theta H}$ and $I'_{\theta m}$ are influence factors for slope.

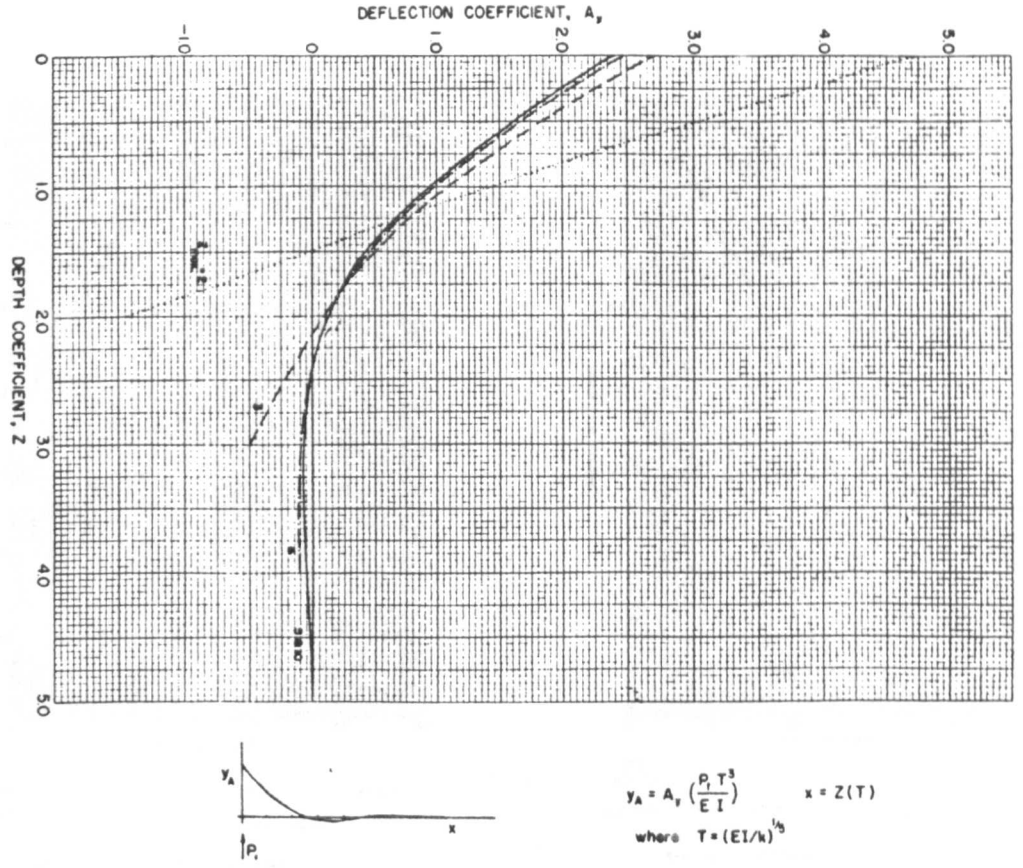

Pile deflection produced by lateral load

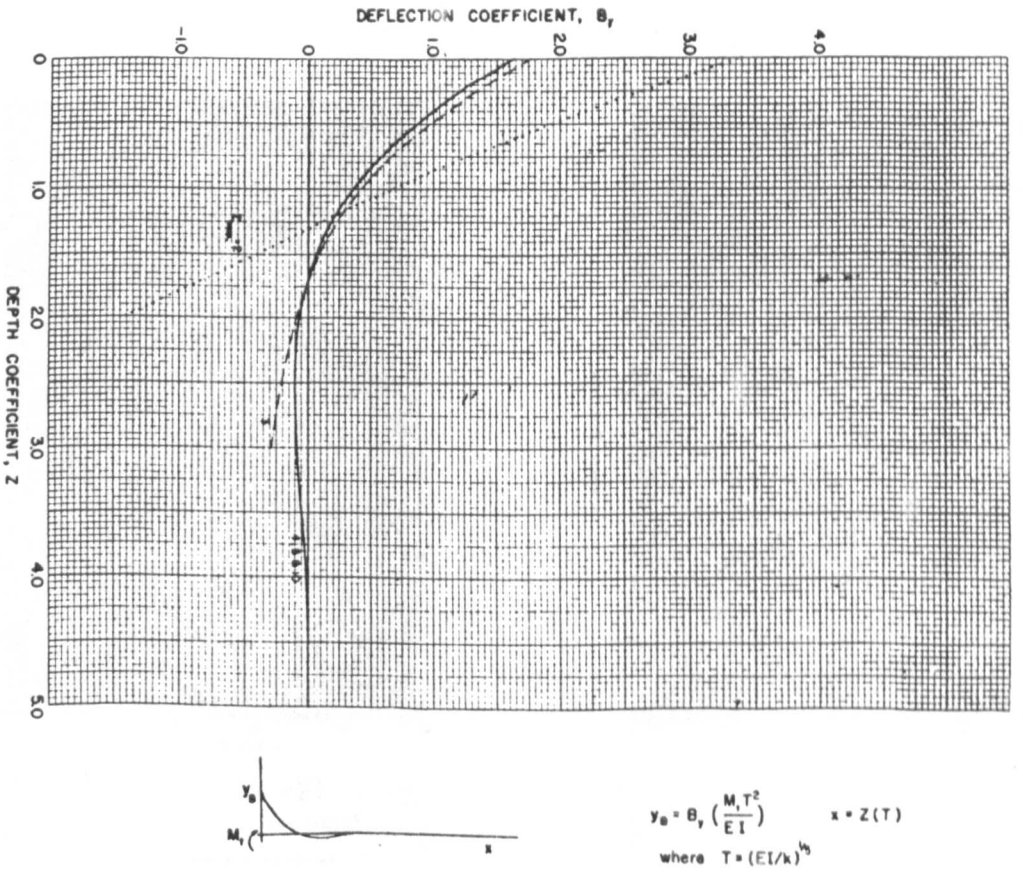

Pile deflection produced by moment applied

FIG. 6. 1.

NON-DIMENSIONAL SOLUTION CHARTS FOR LATERALLY LOADED PILES IN SOIL WITH LINEARLY INCREASING MODULUS. (MATLOCK AND REESE)

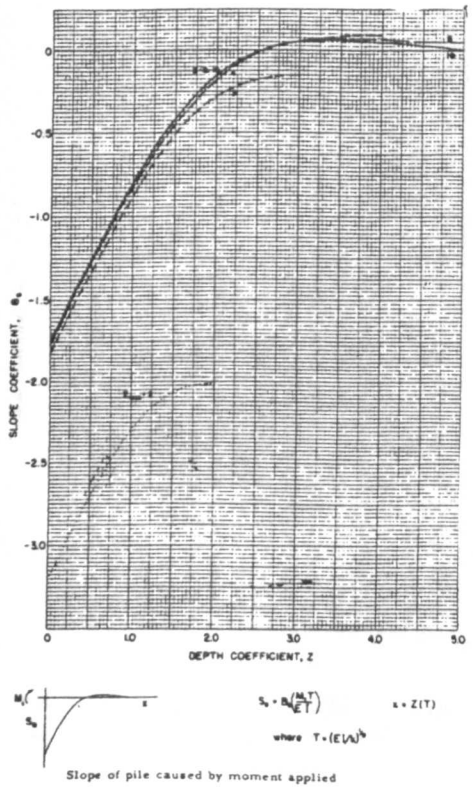

Slope of pile caused by moment applied

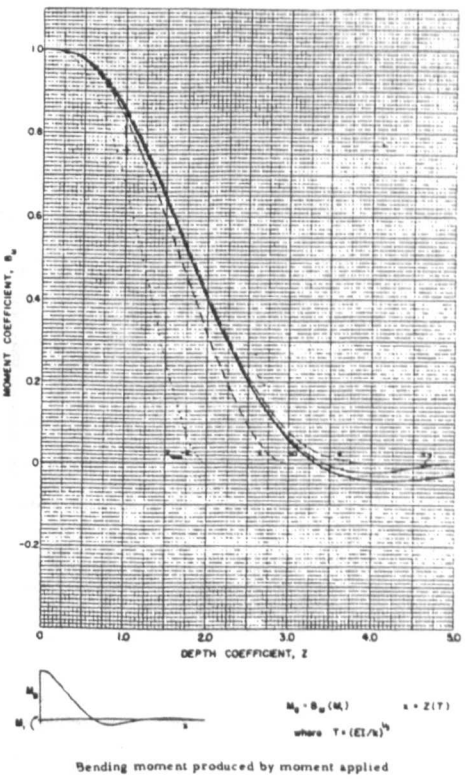

Bending moment produced by moment applied

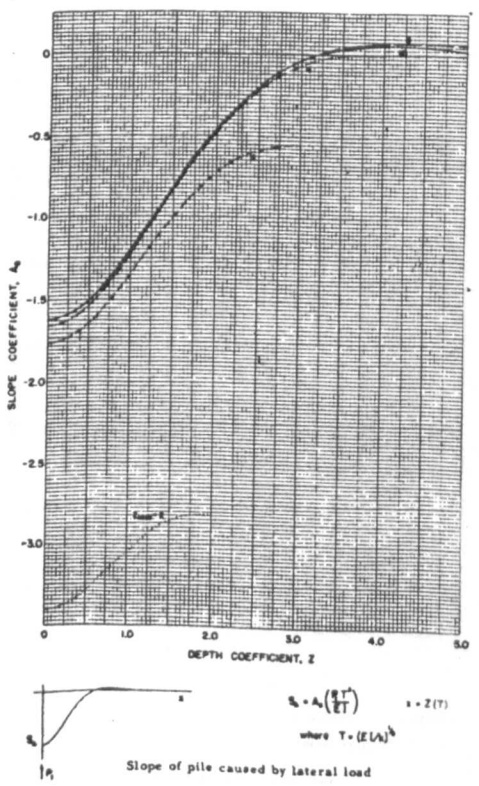

Slope of pile caused by lateral load

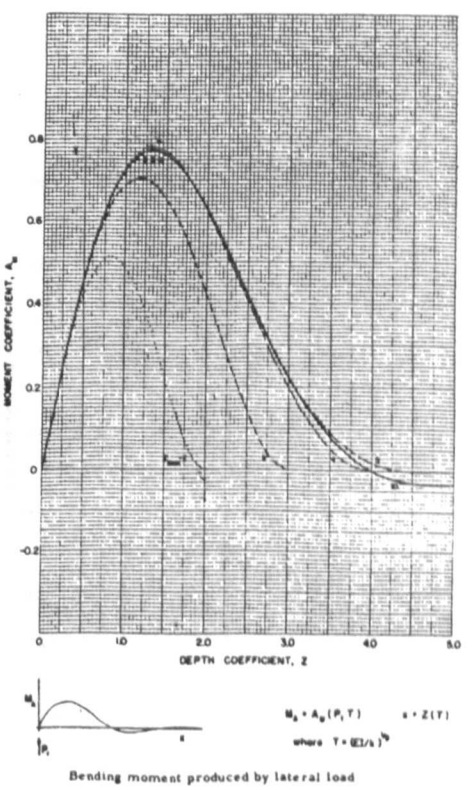

Bending moment produced by lateral load

FIG. 6. 2.

NON-DIMENSIONAL SOLUTION CHARTS FOR LATERALLY LOADED PILES IN SOIL WITH LINEARLY INCREASING MODULUS (MATLOCK AND REESE)

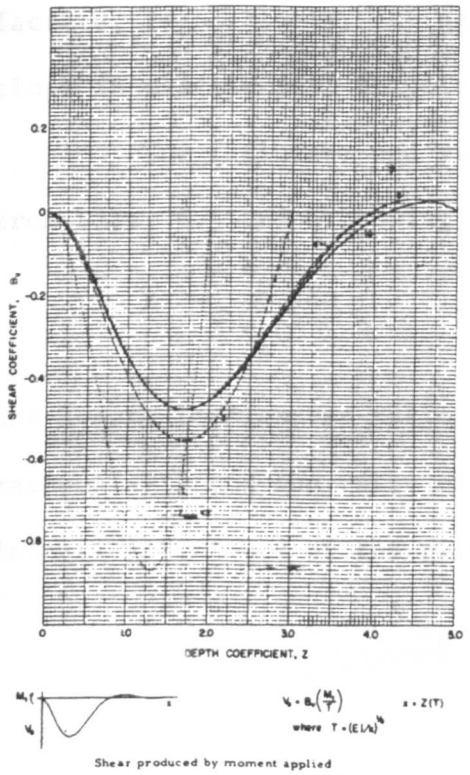

Shear produced by moment applied

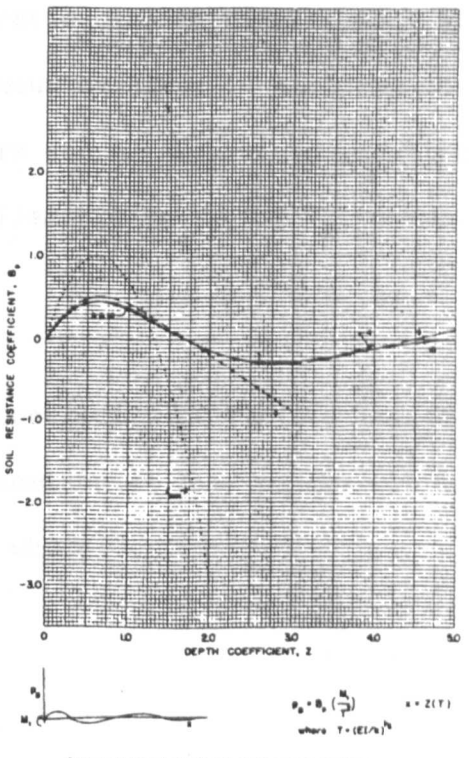

Soil resistance produced by moment applied

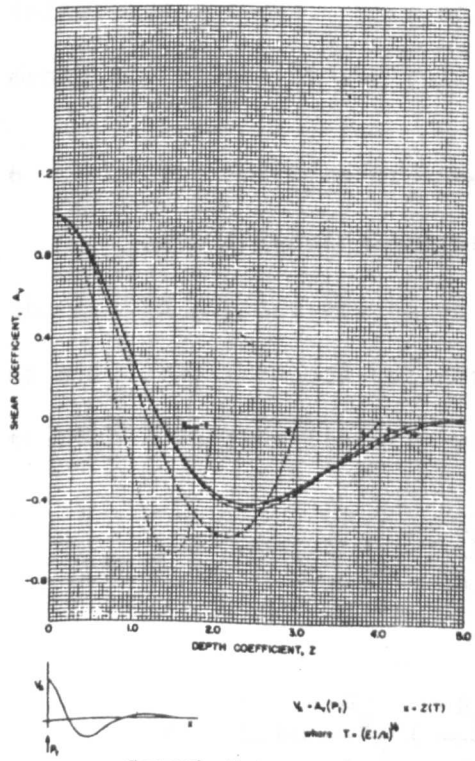

Shear produced by lateral load

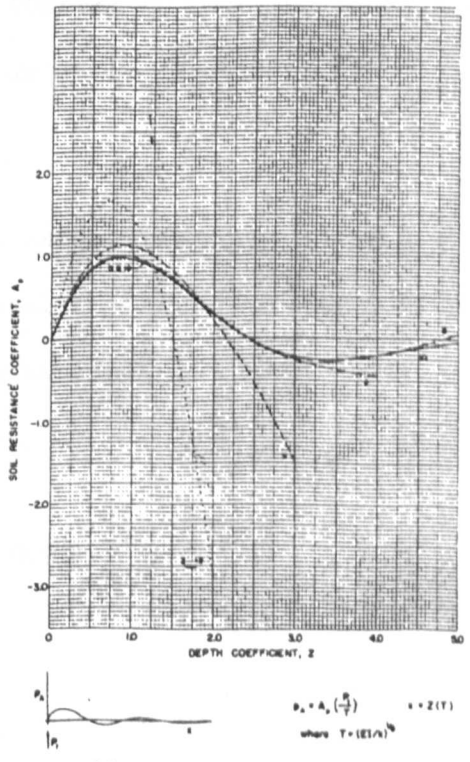

Soil resistance produced by lateral load

FIG. 6.3.

NON-DIMENSIONAL SOLUTION CHARTS FOR LATERALLY LOADED PILES IN SOIL WITH LINEARLY INCREASING MODULUS (MATLOCK AND REESE)

F'_ρ and F_θ are yield-displacement and slope-displacement factors, respectively, defined as the ratio of pile displacement or slope in elastic soil to pile displacement or slope in yielding soil.

The influence and yield factors can be determined graphically from Figs. 6.4 and 6.5 using the pile flexibility factor K_N, where

$$K_N = \frac{E_p I_p}{N_h L^5} \tag{6.4}$$

the length to diameter ratio (L/d), eccentricity of load to length ration (e/L) and the ratio of applied horizontal load to the ultimate lateral resistance of the pile (H_o/H_u) where

$$H_u = \frac{0.5\,\gamma\, d\, L^3\, K_p}{e + L} \tag{6.5}$$

in which γ is the bulk density of the soil, d is the diameter of the pile and K_p is the coefficient of passive earth pressure, $(1 + \sin \phi')/(1 - \sin \phi')$, and ϕ' is the angle of internal friction (effective stress). This solution is limited in that only displacements and slopes at the soil surface can be evaluated.

6.2.3 The Solution of Randolph[24]

The following expressions for deflection y and slope θ at the ground surface are based on the results of finite element studies of a laterally loaded cylindrical pile embedded in elastic soil with stiffness varying linearly with depth

$$y = 0.54 \frac{H_o}{m^* r_o^2} \left(\frac{E_p}{m^* r_o}\right)^{-3/9} + 0.60 \frac{M_o}{m^* r_o^3} \left(\frac{E_p}{m^* r_o}\right)^{-5/9} \tag{6.6}$$

$$\theta = 0.60 \frac{H_o}{m^* r_o^3} \left(\frac{E_p}{m^* r_o}\right)^{-5/9} + 1.13 \frac{M_o}{m^* r_o^4} \left(\frac{E_p}{m^* r_o}\right)^{-7/9}$$

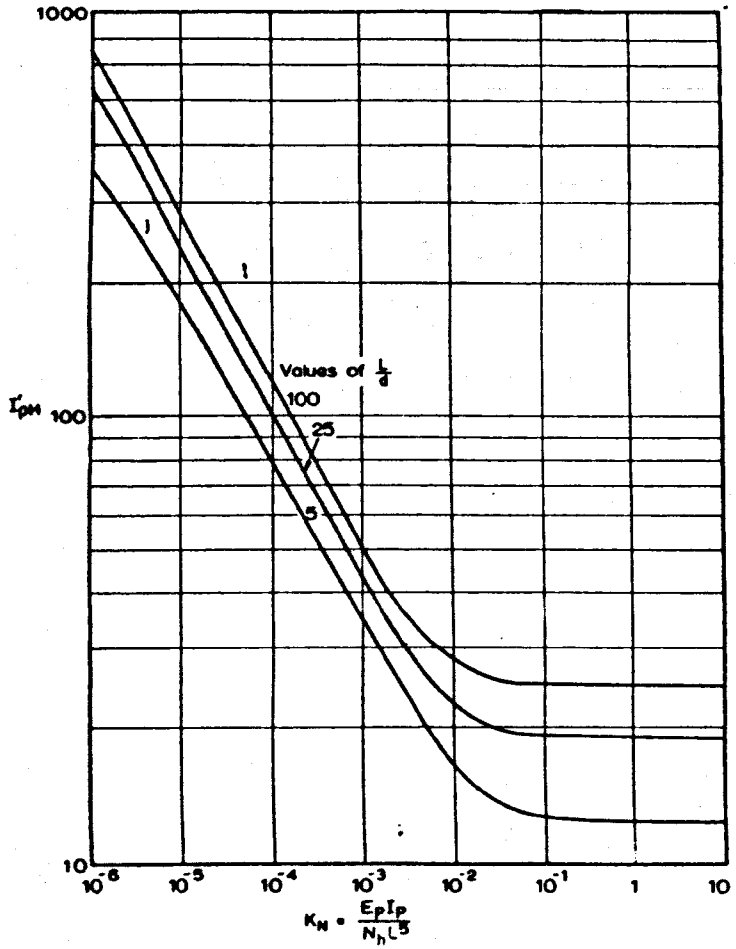

Values of $I'_{\rho H}$–free-head floating pile, linearly-varying soil modulus.

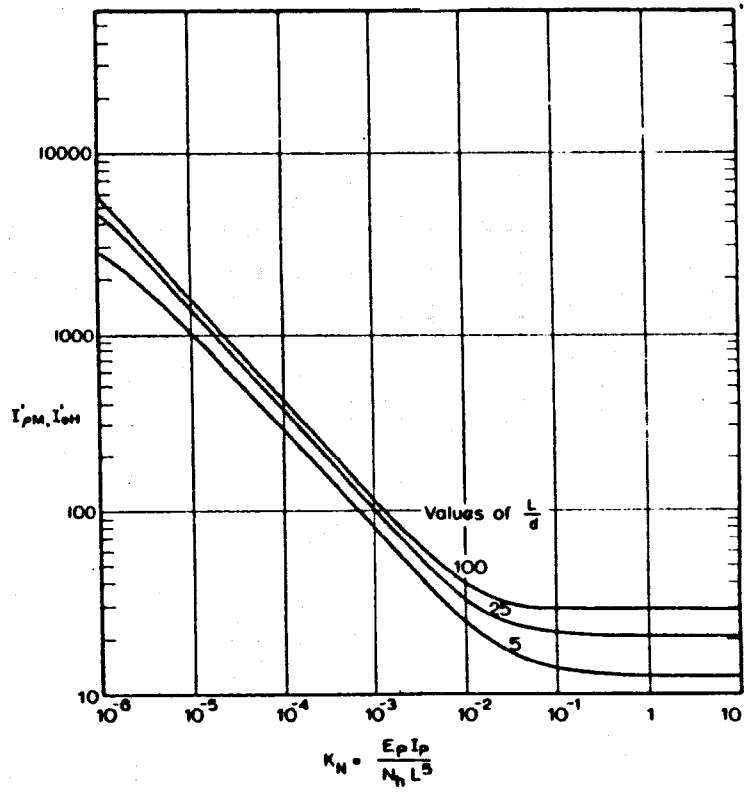

Values of $I'_{\rho M}$ and $I'_{\theta H}$–free-head floating pile, linearly-varying soil modulus.

FIG. 6.4. SOLUTION CHARTS FOR LATERALLY LOADED FREE-HEAD PILES IN SOIL WITH LINEARLY INCREASING MODULUS

(POULOS)

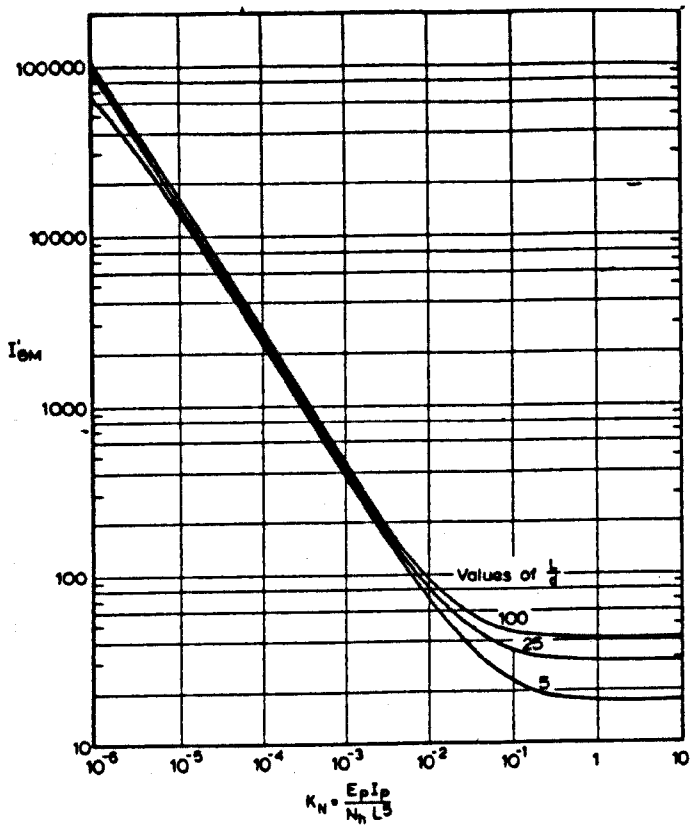

Values of $I'_{\theta M}$–free-head floating pile, linearly-varying soil modulus.

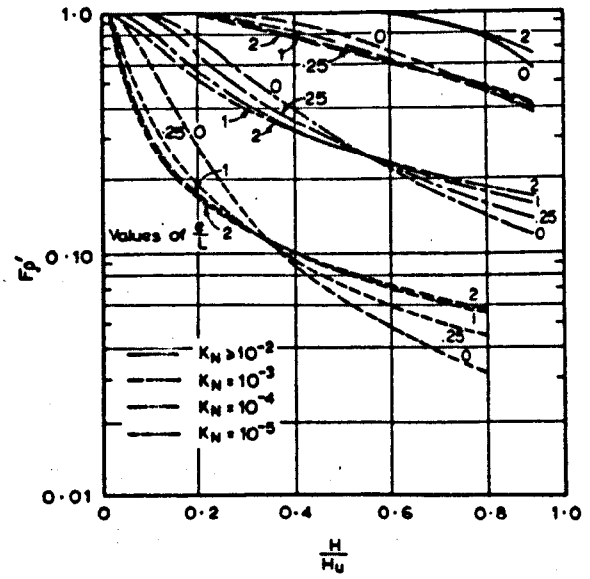

Yield-displacement factor F'_p–free-head floating pile, linearly-varying E_s and p_y.

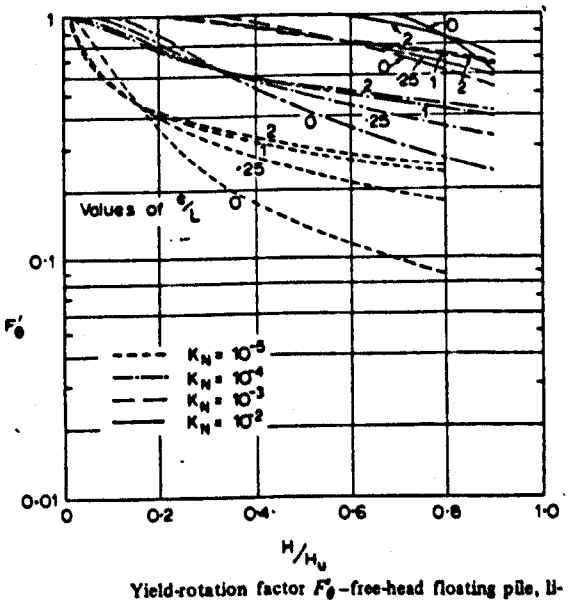

Yield-rotation factor F'_θ–free-head floating pile, linearly varying E_s and p_y.

FIG. 6.5. SOLUTION CHARTS FOR LATERALLY LOADED FREE-HEAD PILES IN SOIL WITH LINEARLY INCREASING MODULUS

(POULOS)

where r_o is the radius of the pile, E_p is the effective Young's modulus of the pile defined as

$$E_p = (EI)_p/(\pi r_o^4/4) \qquad (6.7)$$

in which $(EI)_p$ is the flexural rigidity of the pile and

$$m^* = m(1 + 3\nu/4) \qquad (6.8)$$

where m is the rate of increase of soil shear modulus with depth and ν is Poisson's ratio. This solution is also limited to evaluation of the deflection and slope at the soil surface.

6.2.4 Relationships Between the 'Soil' Moduli used in the Theories

In Randolph's solution the shear modulus

$$G = mz = \frac{m^*}{(1 + 3\nu/4)} \cdot 2$$

and in Poulos' solution Young's modulus

$$E_s = N_h z$$

Since $G = E_s/2(1 + \nu)$

$$\frac{m^*}{N_h} = \frac{(1 + 3\nu/4)}{2(1 + \nu)} \qquad (6.9)$$

The parameter n_h in Matlock and Reese's solution represents a variation of modulus of subgrade reaction with depth and cannot be related implicitly to N_h (or m*). Moreover the modulus of subgrade reaction

$$K_h = n_h z$$

is a function of pile diameter d, and spring characteristic K, whereas the soil elastic moduli are independent of pile width. Since $K_h = kd$ and $p = ky$, K_h has the same units as E_s (or G) and, possibly

for no other reason, n_h and N_h have sometimes been considered equivalent. Some empirical justification can be found by considering the settlement of a rectangular footing on the surface of an elastic homogeneous medium

$$y = pd \frac{(1 - \nu^2)}{E_s} I \qquad (6.10)$$

where y is the settlement, p is the average contact pressure, d is the breadth, I is an influence factor which depends upon the length/breadth ratio and flexibility of the footing, ν is Poisson's ratio and E_s is the Young's modulus of the soil.

For a long rigid strip footing I = 1.26 and Eq. (6.10) becomes

$$pd = \left(\frac{E_s}{(1 - \nu^2)1.26} \right) y = K_h y \qquad (6.11)$$

now for $\nu = 0$, $K_h = 0.85 E_s$ and for $\nu = 0.5$ $K_h = 1.06 E_s$ and therefore for this example K_h and E_s are roughly comparable.

The CIRIA report 103[38] also suggests that for single piles in homogeneous soil, Young's modulus E_s and the subgrade reaction modulus K_h are roughly equal and that for single piles in non-homogeneous soil N_h and n_h are roughly equal.

6.3 APPLICATION OF THE THEORIES

The results from the centrifuge model tests, reported in Chapter 5, were used to consider the relative merits of the three theoretical solutions summarised above. The p-y curve method of analysis, mentioned in Section 6.1, was not taken further for the following reasons.

The derivation of p-y curves is an empirical technique which requires a large number of measured, calculated and graphically

estimated values. It is recommended that pile tests are carried out in which bending moments are measured down the pile. The p-y curves are then constructed by integrating and differentiating the bending moment distribution. Integration and differentiation of bending moment distributions has been discussed in Chapter 4. The resulting displacements and soil resistance distributions were found to be unrealistic and inconsistent because of inaccuracies in measuring the experimental data. Therefore, p-y curves obtained in this way could not be relied on.

The solutions given in Section 6.2 can be used to calculate the deflection at the ground surface for any applied horizontal load and bending moment for known properties of pile and soil. While the properties of the model pile are known quite reliably, those of the soil are not.

If the soil is assumed to have moduli increasing linearly from zero at the top of the pile, substitution of the known values of displacement from the centrifuge tests, into the theoretical expressions enables n_h, N_h and m* to be evaluated.

(The expressions for the rotation have not been used because values recorded from the centrifuge test were not considered sufficiently accurate.)

6.3.1 Variation of Parameter n_h (Matlock and Reese)

Values of n_h obtained by back-analysis, see Appendix (C), have been plotted against the displacement at the soil surface in Fig. 6.6 for pile No. 1. The variations of n_h with displacement at the soil surface and with the ratio of this displacement to pile diameter for all the piles are shown in Figs. 6.7 and 6.8.

Polynomial curves were fitted to the data, in Fig. 6.8, by the method of least squares in an attempt to produce a relationship

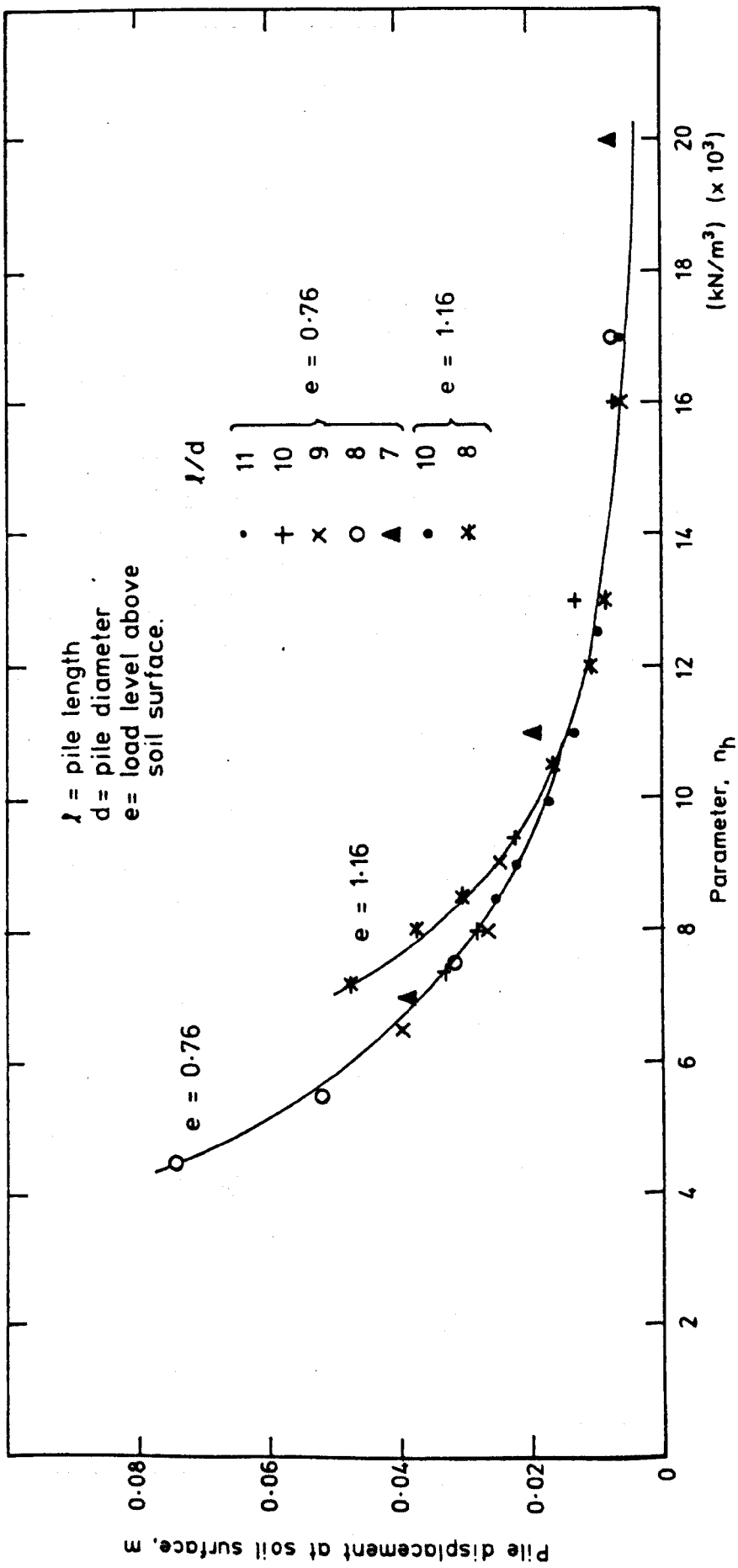

FIG.6.6. PILE No. 1 ($l/d \geq 7$)

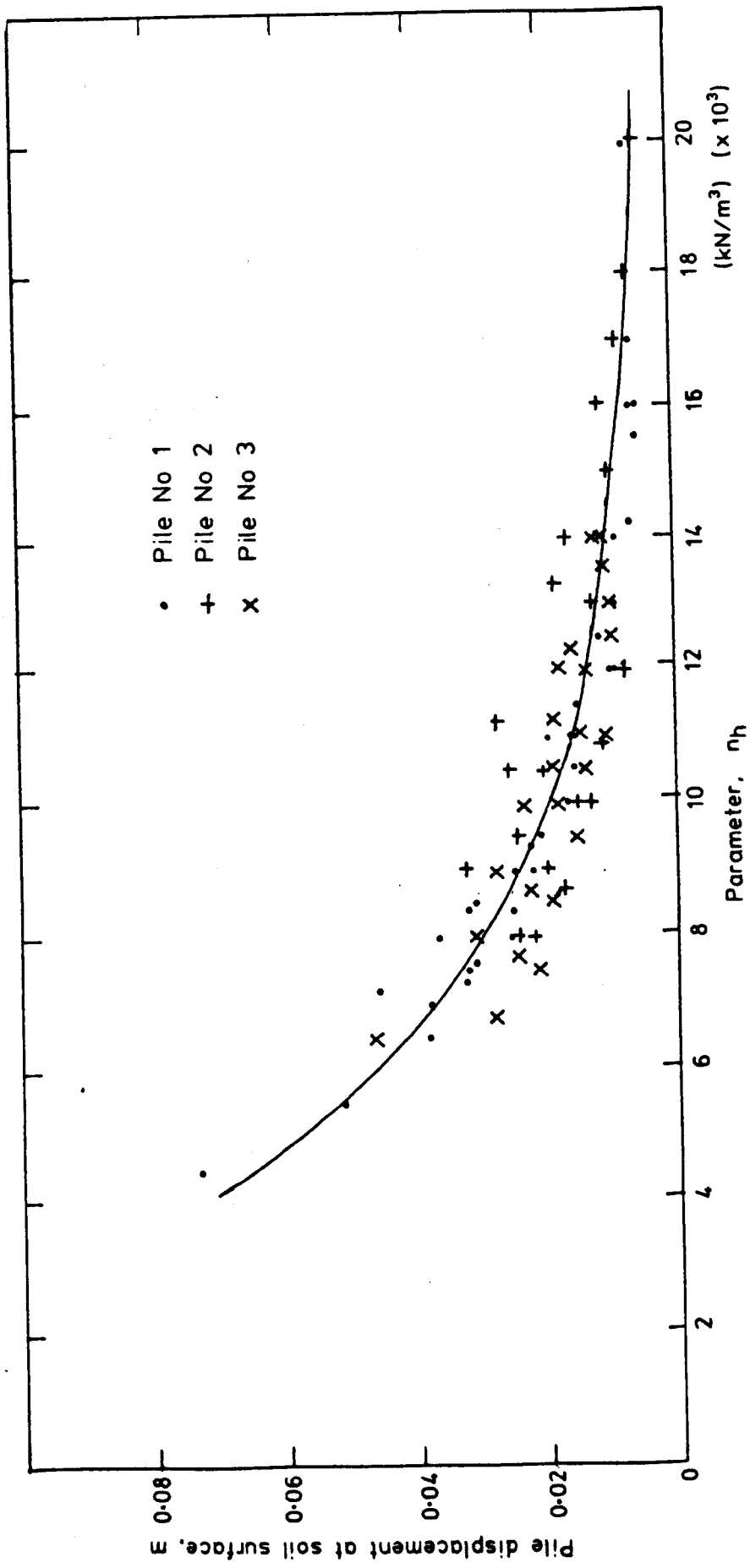

FIG. 6.7. PILE No 1, 2 AND 3 ($\ell/d \geq 7$)

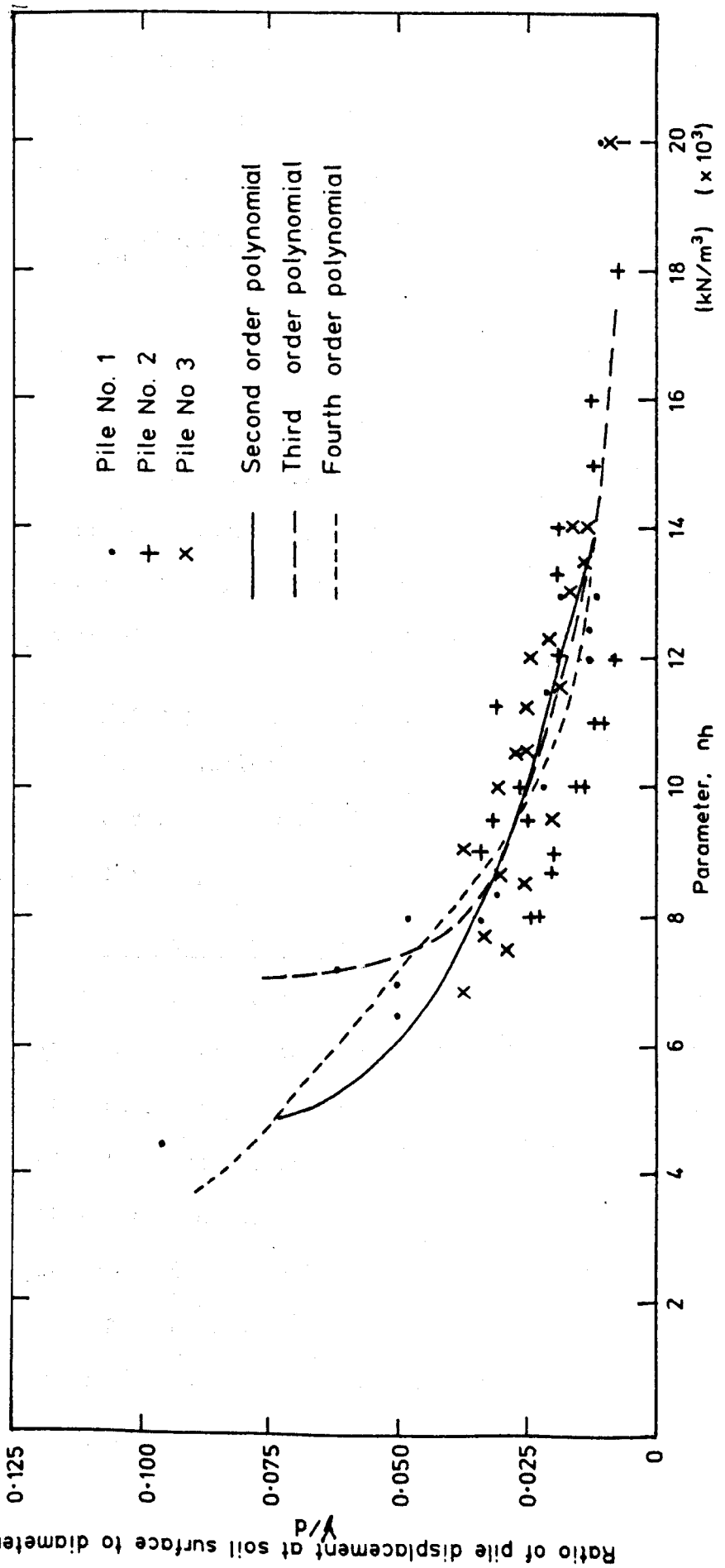

FIG. 6.8. PILE No 1, 2 AND 3 ($\ell/d \geq 7$)

between n_h and the deflection/diameter ratio.

The fourth order polynomial is the best fit mathematically. The others behave erratically for high values of Y/d. The equation for the fourth order polynomial is

$$n_h = 2.274 \times 10^4 - 1.046 \times 10^6(Y/d) + 2.938 \times 10^7 (Y/d)^2 - 3.763 \times 10^8(Y/d)^3 + 1.699 \times 10^9(Y/d)^4 \quad (6.12)$$

6.3.2 Variation of Parameter N_h (Poulos)

The variation of parameter N_h with the displacement at the soil surface, obtained by back-analysis, see Appendix (C), is shown for pile No. 1 in Fig. 6.9 and for all the piles with $l/d > 7$ in Fig. 6.10.

6.3.3 Variation of Parameter m* (Randolph)

The variation of parameter m* with the displacement at the soil surface, obtained by back-analysis, see Appendix (C), is shown for pile No. 1 in Fig. 6.11.

6.3.4 Variation of Parameter N (F.E. Method)

In the elastic finite element analysis used in Chapter 2, Young's modulus was allowed to vary with depth so that $E_s = Nz$ and the best fit to the experimental results obtained by comparing the linear load-displacement relationship from the finite element method with the non-linear load-displacement relationship from the experimental results and hence obtaining the best fit by eye.

The vertical lines in Fig. 6.10 compare values of N with N_h and those in Fig. 6.11 compare $m^* = (1 + 3\nu/4)N/2(1 + \nu)$ (see Eq. (6.9)) with m*, with $\nu = 0.3$.

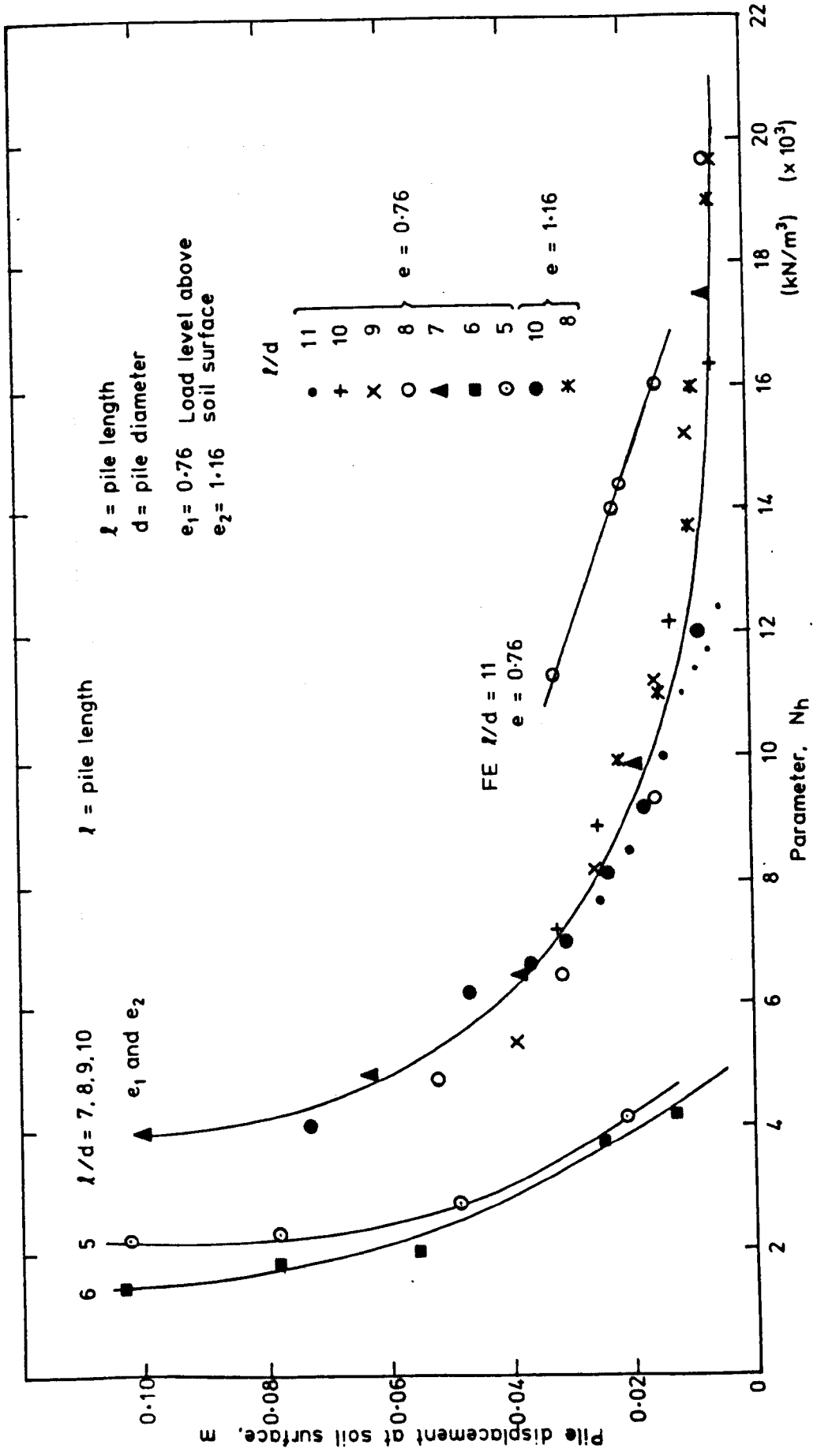

FIG. 6. 9. PILE No. 1

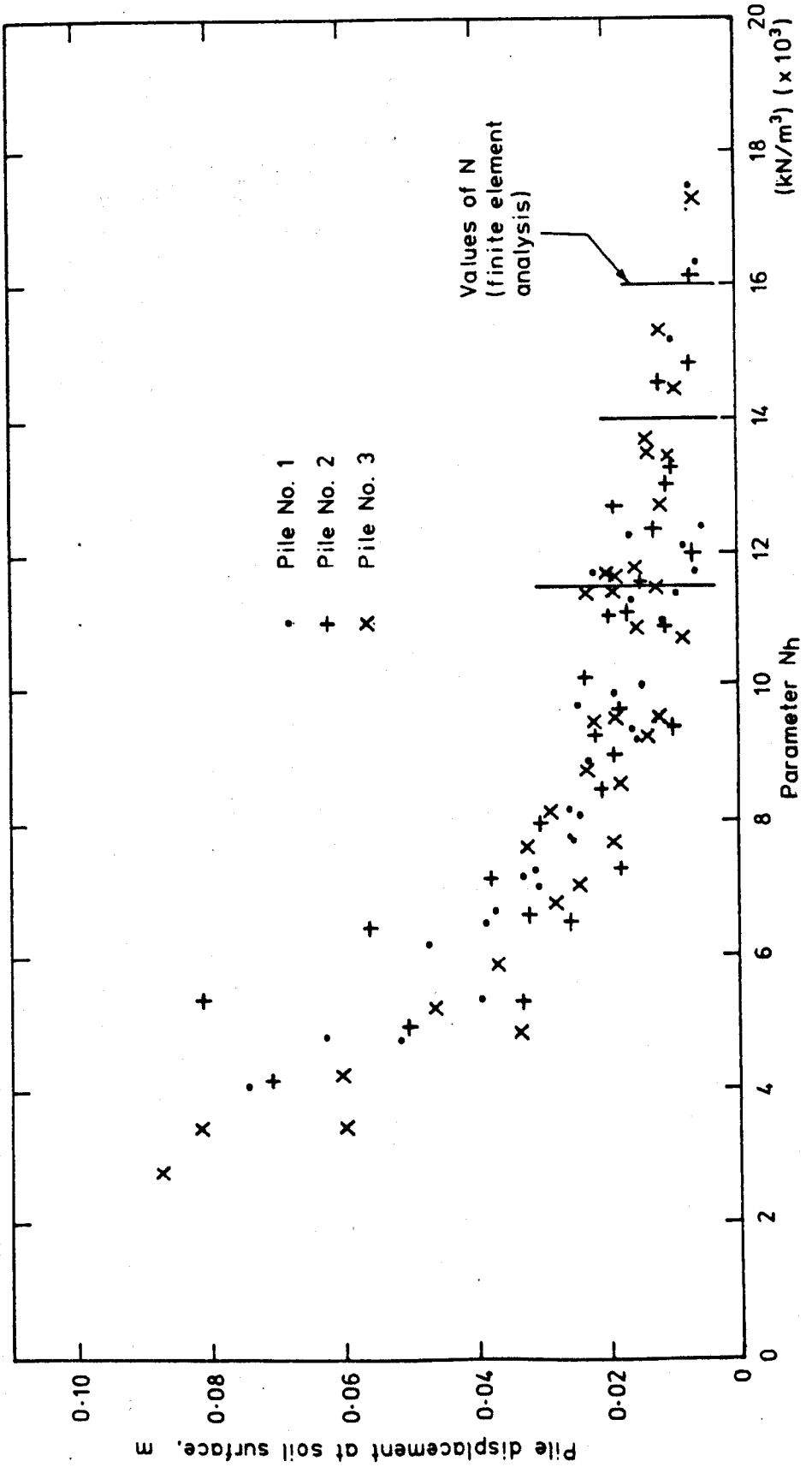

FIG.6.10 PILE Nos. 1, 2 AND 3 (l/d > 7)

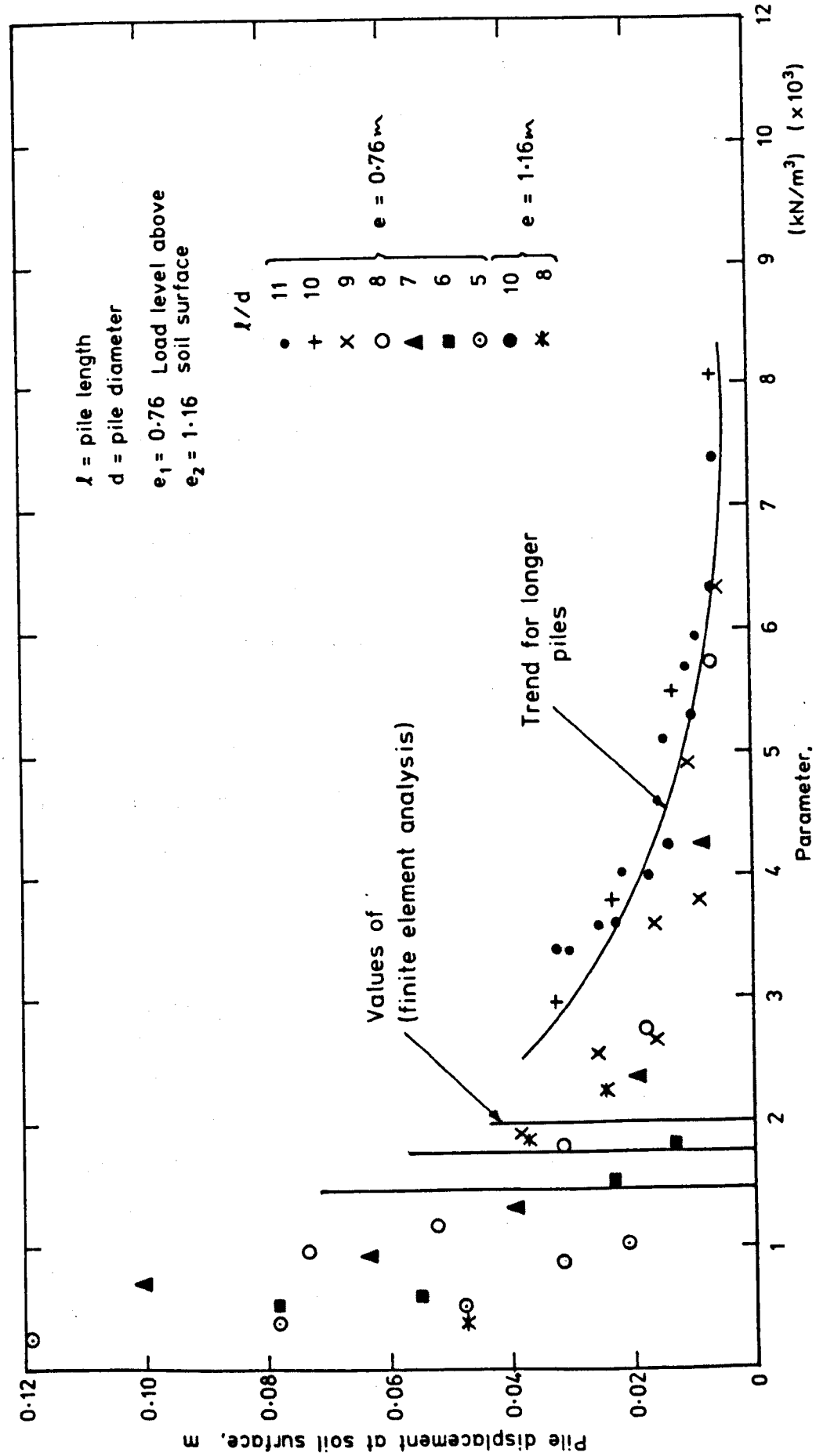

FIG. 6 11 PILE No. 1

6.4 DISCUSSION

The three solutions for predicting pile displacements have been shown in Figs. 6.6 to 6.11 to be inadequate for predicting real behaviour because the various soil parameters employed are by no means constant.

These elastic solutions are not able to account for variations in soil stiffness as pile displacement and soil yielding take place.

Concentrating on the practical aspects of pile design, where the deflection at the ground surface may be limited to 0.05 times the pile diameter, small changes in this deflection produce the largest variations in the parameters.

In Fig. 6.8 a fourth order polynomial has been fitted to the variation of parameter n_h obtained using the Matlock and Reese method. This indicates that it is possible to generate a relationship between n_h and Y/d for increasing displacement. The relationship would have to be obtained experimentally from centrifugal models or full-scale tests for any soil type. However, the value of n_h obtained may not be representative of the soil properties at various depths, being merely a parameter which gives the correct deflections at the soil surface.

The theories of Matlock and Reese and Poulos produce values of n_h and N_h of similar magnitude, for piles with $\ell/d \geq 7$, suggesting that coefficients of horizontal subgrade reaction are of the same order as values of Young's modulus.

Randolph's method yields values of m^* of the same order as values of m^* computed from N_h using Eq. (6.9) for the longer piles (e.g. with $N_h = 16 kN/m^3$ and $\nu = 0.3$, $m^* = 66 kN/m^3$). It is only strictly valid for piles longer than their critical length.

Matlock and Reese's solutions show that piles behave as long piles when $\ell > 4T$.

If parameter n_h and N_h are considered equivalent, then for long piles Poulos' parameter $K_N < (1/4)^5 = 10^{-3}$. This is not in conflict with the behaviour shown in Fig. 6.4.

The elastic parameters n_h and N_h determined by back-analysis lie in the range 5 to 20 MNm^{-3}. Thus piles 1 and 2 with EI $\doteqdot$ 750 MNm^{-2} could be considered long when $\ell > 10.90$ m or $\ell > 8.26$ m at the ends of the range. The corresponding lengths for pile 3 with EI = 400 MNm^{-3} are 9.60 m and 7.62 m respectively.

These values do not conflict with the experimental observations reported in Chapter 5.

In Fig. 6.9, using the Poulos solution, curves where $\ell/d \lesssim 6$ were included. Curves for similar values of ℓ/d could not be produced in Figs. 6.6 to 6.8 using the Matlock and Reese solution, because the value of z_{max} (= L/T) was less than 2.

6.5 CONCLUSIONS

The experimental results, produced in Chapter 5, have been used to evaluate the parameters required in three existing theoretical solutions for predicting pile displacements.

It has been shown that these parameters are not constant but vary appreciably with pile displacement.

Relationships between the parameters evaluated by back-analysis and displacements at the soil surface can be obtained experimentally, but these may not really represent soil properties at depth.

It has also been shown that the rate of increase of Young's modulus, N_h, and the rate of increase of horizontal subgrade reaction, n_h, with depth are similar for a single pile in dry sand even though they are not constant.

CHAPTER SEVEN

CONCLUSIONS AND FURTHER WORK

7.1 CONCLUSIONS

The problem of a laterally loaded pile in sand has been approached in three different ways, centrifugal modelling, finite element analysis and existing theories.

Centrifugal modelling is a well established and documented technique and therefore in the absence of scale field tests, the results produced from experiments can be considered as an accurate and realistic measurement of pile - soil interaction.

The measured bending moment distributions were interpreted using either polynomials or cubic splines. The polynomial method was shown to be superior and a fourth order polynomial generally found to give the best results.

Increases in pile length, flexural rigidity and diameter reduced the pile displacement at the soil surface and the depth of the maximum bending moment. The applied load had a greater effect upon the displacement at the soil surface than the applied bending moment.

The maximum bending moment was increased by increases in pile length and flexural rigidity and reductions in pile diameter.

The difference between the maximum bending moment and the applied bending moment at the soil surface is mainly due to the applied horizontal load and for the longer piles, with $\ell/d \geq 7$, it can be expressed as $M_{max} = (e + \alpha)H$ (Section 5.4).

There appears to be a critical length of pile (of the order of 9 m for piles close to 1 m in diameter) above which the displacement is not effected, which is not significantly dependent on the pile diameter and flexural rigidity.

The evaluation of the parameter used in three existing theories,

by back-analysis of the experimental results, showed that the parameters n_h, N_h and m* are not constant but vary appreciably with pile displacement.

The two parameters n_h and N_h, the rates of increase of horizontal subgrade reaction modulus and Young's modulus with depth, are of similar magnitude for a single pile in dry sand even though they are not constant.

An attempt has been made to apply a finite element method using Fourier series to represent the non-axisymmetric loads and displacements. The technique utilises the axysmmetric geometry and material properties of the problem. By comparing the experimental observations with the results produced using this finite element method, the technique has been shown to have the same limitations as other elastic solutions. For a purely elastic problem in which the material properties vary only radially and vertically, and not circumferentially, the technique is, without doubt, a very useful method of numerical analysis, saving cost, time and storage on the computer. However, for a soil behaving plastically, the method is of limited use in its form presented in this thesis.

7.2 FURTHER WORK

Although a limited parameter study of a laterally loaded pile in dry sand has been attempted in this work, there is still considerable scope for further testing in a centrifuge. Studies are required using:

(i) more flexible piles;

(ii) smaller diameter piles hence higher ℓ/d values and with (i) to attempt to obtain a relationship between the parameter α and the pile diameter and flexural rigidity for long piles;

(iii) piles of different cross-sections;

(iv) a variety of soil densities and grain sizes to include the

effects of pore pressures in clays;

(v) more loading conditions:- vertical load, compressive and tensile, zero applied bending moment and pile head and/or pile toe restraints;

(vi) cyclic loading to model wave action on an offshore structure and the dynamic effects of earthquakes;

(vii) pile groups with all the above experimental conditions;

(viii) a method of driving the pile whilst the centrifuge is running model the effect of pile driving.

As for the finite element analysis, the Fourier series technique cannot be taken any further for this problem without access to cheaper, more powerful computing facilities. However, further research can be done using two and three dimensional models into the effects of

(i) stress - strain relationships for soil,

(ii) cyclic and dynamic loading,

and (iii) pile groups.

With the obvious limitation of plane strain when using two-dimensional models and size and cost when using three-dimensional models.

By using the results from the series of tests described in this thesis and extending them, as indicated above, it should be possible to establish definitions for rigid and flexible piles and critical length in various soil types and hence to formulate useful empirical solutions. Since an engineer is interested in the displacement and rotation at soil surface and the position and magnitude of the maximum bending moments, these solutions need only be for these values.

APPENDIX (A)

Centrifugal modelling scaling laws

Quantity	Model	Prototype
Linear dimension	1	N
Acceleration	N	1
Area	1	N^2
Volume	1	N^3
Second moment of area	1	N^4
Velocity	1	1
Mass	1	N^3
Force	1	N^2
Bending moment	1	N^3
Stress	1	1
Density	1	1

APPENDIX (B)

Stress Distribution between Model and Prototype

This following analysis is similar to that given by Schofield[30].

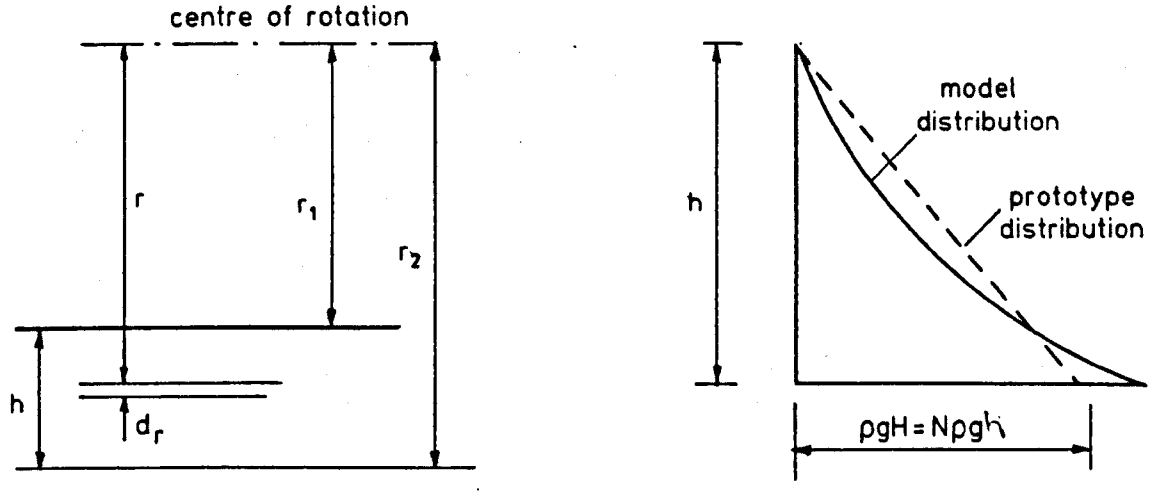

a) Centrifuge model distributions

b) Stress distributions

Fig. B.1

Consider a model constructed of height h to represent a homogeneous stratum of depth H in the field, the scaling factor is $N = H/h$.

When the model is spun with angular velocity ω, the vertical stress at radius r, see Fig. B.1(a), is

$$\sigma = \rho \omega^2 \int_{r_1}^{r} r \, dr = \rho \frac{\omega^2}{2} (r^2 - r_1^2) \qquad (B.1)$$

and thus the model and prototype stresses distributions, see Fig. B.1(b), match at the top where $r = r_1$ and at one other position $r = r_o$.

For equal stresses at r_o

$$\rho \frac{\omega^2}{2} (r_o^2 - r_1^2) = \rho g N(r_o - r_1) .$$

Therefore

$$\omega^2 = 2\,Ng/(r_o + r_1) \tag{B.2}$$

The error at other positions is given by

$$\varepsilon = N\rho g(r - r_1) - \rho \frac{\omega^2}{2} (r^2 - r_1^2)$$

$$= N\rho g(r - r_1) - N\rho g(r^2 - r_1^2)/(r_o + r_1) \tag{B.3}$$

For a mathematical maximum $d\varepsilon/dr = 0$ and therefore $r = (r_o + r_1)/2$. For another practical maximum $r = r_2$ the best approximation is obtained when the maximum percentage errors are equal, therefore,

$$\frac{((\frac{r_o + r_1}{2}) - 1)\ N\rho g - ((\frac{r_o + r_1}{2})^2 - r_1^2)\ \frac{N\rho g}{(r_o + r_1)}}{((\frac{r_o + r_1}{2}) - r_1)\ N\rho g}$$

$$= \frac{(r_2^2 - r_1^2)\ \frac{N\rho g}{(r_o + r_1)} - (r_2 - r_1)\ N\rho g}{(r_2 - r_1)\ N\rho g} \tag{B.4}$$

therefore

$$1 - \frac{(r_o + r_1)/2 + r_1}{(r_o + r_1)} = \frac{r_2 + r_1}{r_o + r_1} - 1 \tag{B.5}$$

therefore

$$r_o = r_1 + \frac{2}{3}(r_2 - r_1) \tag{B.6}$$

i.e. at a 1/3 rd of the depth up from the base.

From Eq. (B.2)

$$\bar{r} = \frac{Ng}{\omega^2} = \frac{r_o + r_1}{2} = r_1 + \frac{h}{3} \tag{B.7}$$

i.e. the optimum scaling radius is at h/3 from the top. The maximum errors are, from Eq. (B.5)

$$\varepsilon = \frac{r_2 - r_o}{r_o + r_1} = \frac{h/3}{2\bar{r}} = \frac{h}{\bar{r}} \tag{B.8}$$

For example, in the Liverpool University centrifuge r_1 = 1.07 m, r_2 = 1.31 m, h = 0.24 m and $\bar{r}$ = 1.15 m, therefore ε = 3.48 %.

Note, the optimum speed is calculated as

$$\bar{\omega} = \frac{N_R}{\bar{r}} \qquad (B.9)$$

APPENDIX C

C1 Sample back-analysis calculations

Sample back-analysis calculations for each of the three theoretical solutions, presented in Chapter 5, are given below using the following data:-

Flexural rigidity, EI, = 7.7312×10^3 KNm^2

Diameter, d = 0.76 m

Eccentricity, e , = 0.76 m

Applied Horizontal Load, H, = 469.92 KN

Measured displacements, y, = 0.03077 m

Length, L, = 8.39 m

Angle of internal function $\phi' = 49.5^o$

Bulk density, γ, = 16.616 KN/m^3

C2 Matlock and Reese

From Equations (6.1)

$$y = \frac{H_o T^3}{E_p I_p} A_y + \frac{M_o T^2}{E_p I_p} B_y$$

substituting the above values and re-arranging

$$y = 6.078 \times 10^4 \, T^2 \, (T A_y + 0.76 B_y) \qquad (C.1)$$

Now

$$T = 5 \sqrt{\frac{EI}{n_h}}$$

therefore by guessing a value of n_h, and calculating values for T and $z_{max} = L/T$ the coefficients A_y and B_y can be determined from Figs. 6.1 and 6.2 respectively. The required displacement is found by trial and error. With n_h = 7600, T = 2.52 and z_{max} = 3.33. Therefore A_y = 2.65 and B_y = 1.7. Substituting into Eq. (C.1) gives

$y = 6.078 \times 10^4 \ (2.52)^2(2.52 \ . \ 2.65 + 0.76.1.7) = 0.03076$ m

which is close enough for these purposes.

C3 Poulos

From equations (6.3)

$$y = \frac{H_o}{N_h L^2} \left(I'_{\rho H} + \frac{e}{L} I'_{\rho m} \right) / F\dot{\rho} \qquad (C.2)$$

Using

$$K_N = \frac{E_p I_p}{N_h L^3} \quad \text{and} \quad H_u = \frac{0.5 \ \gamma \ d L^3 K_p}{e + L}$$

Coefficients $I'_{\rho H}$, $I'_{\rho m}$ and F_ρ' can be found from Figs. 6.3 and 6.4 after guessing a value of N_h. The values of N_h which yield the required displacement is found by trial and error.

The ultimate lateral resistance of the pile, H_u, is 3000 KN hence $H/H_u = 0.157$ and $e/\ell = 0.09$ with $N_h = 7250$, $K_N = 2.564 \times 10^{-3}$. Therefore from Fig. 6.4, $F_\rho' = 1.0$ and Eq. (6.2) becomes

$$y = \frac{H_o}{N_h L^2} \left(I'_{\rho H} + \frac{e}{L} I'_{\rho m} \right) \qquad (C.3)$$

with $L/d = 11$, from Fig. 6.3 $I'_{\rho H} = 28$ and $I'_{\rho m} = 60$. Substituting into Eq. (C.3) gives

$$y = \frac{469.92}{7250.(8.39)^2} \left(28 + \frac{0.76}{8.39} \ 60 \right) = 0.03078 \text{ m}$$

which is close enough for this purpose.

C4 Randolph

From equations (6.6)

$$y = 0.54 \ \frac{H_o}{m^* r_o^2} \left(\frac{E_p}{m^* \ r_o} \right)^{-3/9} + 0.60 \ \frac{M_o}{m^* r_o^3} \left(\frac{E_p}{m^* r_o} \right)^{-5/9}$$

(C.4)

Now

$$E_p = (EI)_p/(\pi r_o^4/4)$$

with $r_o = d/2 = 0.38$, $E_p = 4.652 \times 10^7$ KN/m^2 .

Using guessed values for m* the required displacement is found by trial and error.

With m* = 1600, substituting into Eq. (C.4) yields

$$y = \frac{0.54.469.92}{1600(0.38)^2}\left(\frac{4.652 \times 10^7}{1600.0.38}\right)^{-3/9} + \frac{0.60.357.14}{1600(0.38)^3}\left(\frac{4.652 \times 10^7}{1600.0.38}\right)^{-5/9}$$

$$= 0.0306 \text{ m}$$

which again is close enough.

From Figs. 6.6 to 6.11 it is possible to see how variations in the various moduli affect the y/d ratio.

REFERENCES

1. AVGHERIONOS, P.J. and SCHOFIELD, A.N.,
Drawdown Failure of Centrifugal Models: Int.Conf.Soil Mech.Fdn. Eng., Proc. 7th Conf., 1969, Vol. 2.

2. BANERJEE, P.K. and DAVIS, T.G.,
The Behaviour of Axially and Laterally Loaded Single Pile Embedded in non-homogeneous Soils: Geotechnique, 1978, Vol. 28, No. 3, pp.309-326.

3. BARTON, Y.O.,
Laterally Loaded Model Piles In Sand: Ph.D. thesis; 1982, Cambridge University.

4. BELYTSCHKO, T.,
Finite Elements for Axisymmetric Solids under Arbitrary Loadings with Nodes on Origin: AIAA, Nov. 1972, Vol.10, No.11, pp.1532-1533.

5. BROMS, B.B.,
Lateral Resistance of Pile in Cohesionless Soil: ASCE J. Soil Mech. Fd. Div., May 1964, Vol. 90, No.SM3, part 1, pp. 123-156.

6. CHEUNG, Y.K.,
Finite Strip Method in Structural Analysis, Pergamon, 1976.

7. COOK, R.D.,
Concepts and Applications of Finite Element Analysis: 1974, John Wiley and Sons Inc.

8. COPE, R.J., SAWKO, F. and TICKELL, R.G.,
Computer Methods for Civil Engineers: 1982, McGraw-Hill.

9. CRAIG, W.H. and ROWE, P.W.,
Operation of a Geotechnical Centrifuge from 1970 to 1979: Geo. Testing, Jou., March 1981, Vol. 4, No. 1, pp.19-25.

10. DAVISSON, M.T. and GILL, H.L.
Laterally Loaded Piles in a Layered Soil System: ASCE J. Soil. Mech. Fdn. Div., May 1963, Vol. 89, No. SM3.

11. DE BOOR, C.,
On Calculating with B-Splines: J.Approx.. Theory, 1972, Vol.6, pp. 50-62.

12. DESAI, C.S. and ABEL, J.F.,
Introduction to the Finite Element Method: 1972, New York, Van Nostrand Reinhold Company.

13. EVANGELISTA, A. and VIGGIANI, C.,
Accuracy of Numerical Solutions for Laterally Loaded Piles in Elastic Half-space: ASCE Num.Meth.Geomech. 2nd. Conf., 1976 (ed. Desai, C.S.), Vol. 3, pp. 1367-1370.

14. GOODMAN, R.E., TAYLOR, R.L. and BREKKE, T.L.,
A Model for the Mechanics of Jointed Rock: ASCE J. Soil Mech. Fdn. Div., 1968, Vol. 94, No. SM3, pp. 637-659.

15. GROSE, J.G.,
Stress Analysis of Axisymmetric Solids with Asymmetric Properties: AIAA, July 1972, Vol. 10, No. 7, pp. 866-871.

16. HETENYI, M.,
Beams on Elastic Foundations:, 1946, University of Michigan Press.

17. JANBU, N.,
Soil Compressibility as Determined by Oedometer and Triaxical Tests: 1963, European Conf. Soil Mech.Fnd.Eng., Wiesbaden, Vol. 1, pp.19-25.

18. KING, G.J.N., DICKIN, E.A. and LYNDON, A.,
The Development of a Medium Si-e Centrifuge Testing Facility: App.Cent.Mod.Geot. Design, Univ. Manchester Eng. Dept., 16-18 April, 1984, pp.25-46.

19. MATLOCK, H.,

Correlations for Design of Laterally Loaded Piles in Soft Clay: Proc. Offshore Tech. Conf., 2nd. Conf., 1970, Vol. L, pp.577-594.

20. MATLOCK, H. and REESE, C.C.

Generalised Solutions for Laterally Loaded Piles: ASCE J. Soil Mech. Fdn. Div., Oct. 1960, Vol. 80, No. SM5, part 1, pp.63-91.

21. POULOS, H.G.,

Behaviour of Laterally Loaded Piles - I single, - II Pile Groups: ASCE, J.Soil Mech. Fdn. Div., May 1971, Vol. 97, No. SM3, pp.711-751.

22. POULOS, H.G.,

Behaviour of Laterally Loaded Piles-III Socketed Piles: ASCE J. Soil Mech. Fdn. Div., 1971, Vol.98, No. SM4, pp.341-360.

23. POULOS, H.G.,

Load Deflection Prediction for Laterally Loaded Piles: Australian Geomech., 1973, J.G.3, No. 1, pp.1-8.

24. RANDOLPH, M.F.,

The Response of Flexible Piles to Lateral Loading: Geotechnique, 1981, Vol. 31, No. 2, pp. 247-259.

25. REESE, L.C.,

Laterally Loaded Pile Program Documentation: ASCE J.Geo. Eng. Div., April 1977, Vol. 103, No.GT4, pp.287-305.

26. REESE, L.C. and COX, W.R.,

Soil Behaviour from Analysis of Tests of Uninstrumented Piles Under Lateral Loading: ASTM 1968, Special Test Pub. 444, pp.160-176.

27. REESE, L.C., COX, W.R. and KOPP, F.P.,

Analysis of Laterally Loaded Piles in Sand: Proc. Offshore Tech. Conf., 5th Conf., 1974, Paper OTC 2080, pp.473-483.

28. REESE, L.C. and MATLOCK, H.,

Non-dimensional Solutions for Laterally Loaded Piles with Soil

Modulus Propertional to Depth: Proc. 8th. Texas Conf. Soil Mech. Fdn. Eng., pp.1-41.

29. ROWE, P.W.,
Application of Centrifugal Models to Geotechnical Structures: Sym. Recent Devel. Soil Mech., 1975, pp.1-25.

30. SCHOFIELD, A.N.,
Cambridge Geotechnical Centrifuge Operations: Geotechnique, 1980, Vol. 30, No.3, pp.227-268.

31. SCHOFIELD, A.N. (eds. George, P. and Wood, D.)
General Principles of Centrifuge Model Testing and a Review of ome Testing Facilities, pp.328-339 and The Role of Centrifuge Modelling, pp.341-350. Offshore Soil Mech., Lloyds Register of Shipping and Cambridge Univ. Eng. Dept.

32. STRICKLIN, J.A. et al.
Non-linear Analysis of Shells of Revolution by the Matric Displacement Method: AIAA, Dec. 1968, Vol. 6, No.12, pp.2306-2312.

33. TERZAGHI, K.,
Evaluation of Coefficients of Subgrade Reaction: Geotechnique, 1955, Vol. 15, pp.297-327.

34. WILSON, E.L.,
Structural Analysis of Axisymmetric Solids: AIAA, Dec. 1965, Vol. 3, No. 12, pp.2269-2274.

35. WINWICK, L.A. and ZIENKIEWICZ, O.C.,
Plastic (or Visco-Plastic) Behaviour of Axisymmetric Bodies Subjected to Non-symmetric loading - Semi Analytical Finite Element Solution, Int.N.Num. Meth.Eng., 1979, Vol. 14, pp.1399-1412.

36. ZIENKIEWICZ, O.C.,
The Finite Element Method: Third Edition, 1977, McGraw-Hill.

37. ZIENKIEWICZ, O.C. and TOO, J.J.M.,

The Finite Prism in Analysis of Thick Simply Supported Bridge Boxes: Proc.Inst.Civ.Eng., 1972, Part 2, No. 53, Paper No. 7450, pp. 147-172.

38. ELSON, W.K.,

Design of Laterally-Loaded Pile: CIRIA Report No. 103, 1984.

BIBLIOGRAPHY

BARTON, Y.O.,

Lateral Loading of Model Piles in the Centrifuge: M.Phil., 1979, Cambridge University.

BARTON, Y.O.,

Response of Pile Groups to Lateral Loading in the Centrifuge: App.Cent.Mod.Geot.Design, Univ. of Manchester Eng. Dept., 16-18 April 1984, pp. 456-472.

BARTON, Y.O. and PANDE, G.N.,

Laterally Loaded Pile in Sand: Centrifuge Tests and Finite Element Analysis: Int.Sym.Num.Mod.Geomech., Zurich, Sept. 1984, pp. 249-258.

BROMS, B.B.,

Lateral Resistance of Piles in Cohesive Soil: ASCE J.Soil.Mech. Fdn. Div., March 1964, Vol. 90, No. SM2, Part 1, pp.27-64.

BROMS, B.B.,

Design of Laterally Loaded Piles, ASCE J.Soil.Mech. Fdn.Div., May 1964, Vol. 91, No. SM3, pp.79-64.

MATLOCK, H. and REESE, L.C.

Foundation Analysis of Offshore Pile Supported Structures: Int. Conf. Soil. Mech. Fdn. Eng., Proc. 5th Conf., 1962, Vol. 2.

POULOS, H.G.,

Lateral Load-Deflection Prediction for Pile Groups: ASCE J. Geo. Eng. Div., Jan. 1975, Vol. 101, GT1, pp.19-34.

POULOS, H.G.,

The Influence of Shaft Length on Pile Load Capacity in Clays: Geotechnique, 1982, Vol. 32, No. 2, pp. 145-148.

POULOS, H.G. and DAVIS, G.H.,

Pile Foundation Analysis and Design: 1980, John Wiley and Sons.

RANDOLPH, M.F.,

A Theoretical Study of the Performance of Piles: Ph.D., 1977, Cambridge University.

REESE, L.C., COX, W.R. and KOOP, R.D.,

Field Testing and Analysis of Laterally Loaded Piles in Stiff Clay: Proc. Offshore Tech. Conf., 7th Conf. 1975, Vol. 2, pp. 671-690.

STRICKLIN, J.A., DE ANDRADE, J.C., STEBBINS, F.J. and CWIETNY Jr., A.J.,

Linear and Nonlinear Analysis of Shells of Revolution with Asymmetrical Stiffness Properties: Proc. 2nd. Conf. Matrix. Meth. Struct. Mech., Wright-Patterson A.F. Base Ohio, 1968, pp.1231-1251.

TERZAGHI, K.

Theoretical Soil Mechanics: 1943, John Wiley and Sons Inc.

ZIENKIEWICZ, O.C. and CORMGAU, I.C.,

Visco-plasticity-plasticity and Creep in Elastic Solids. A Unified Numerical Solution Approach: Int.J.Num.Meth.Eng., 1974, Vol. 8, pp.821-845.

KING, G.J.W. and FULTHORPE, J.N.

Centrifuge Model Tests on Laterally Loaded Single Piles: Proc. 3rd. Indian Conf. on Offshore Eng., Bombay, Dec. 1986.

DESAI, I.D. AND CHANDRASEKARAN, V.S.

Displacements of Laterally Loaded Circular Wells: Conf. Geotec. Eng., 'GEOTECH 80', Bombay, 1980, V/2, pp.165-170.